

Novel Optical Access Network Architectures and  
Transmission System Technologies for Optical  
Fiber Communications

WANG Zhaoxin

A Thesis Submitted in Partial Fulfillment  
of the Requirements for the Degree of  
Doctor of Philosophy

in

Information Engineering

©The Chinese University of Hong Kong

September 2006

The Chinese University of Hong Kong holds the copyrights of this thesis. Any person(s) intending to use a part or whole of the materials in the thesis in a proposed publication must seek copyright release from the Dean of the Graduate School.

UMI Number: 3254556

### INFORMATION TO USERS

The quality of this reproduction is dependent upon the quality of the copy submitted. Broken or indistinct print, colored or poor quality illustrations and photographs, print bleed-through, substandard margins, and improper alignment can adversely affect reproduction.

In the unlikely event that the author did not send a complete manuscript and there are missing pages, these will be noted. Also, if unauthorized copyright material had to be removed, a note will indicate the deletion.

**UMI**<sup>®</sup>

---

UMI Microform 3254556

Copyright 2007 by ProQuest Information and Learning Company.

All rights reserved. This microform edition is protected against unauthorized copying under Title 17, United States Code.

ProQuest Information and Learning Company  
300 North Zeeb Road  
P.O. Box 1346  
Ann Arbor, MI 48106-1346

# Abstract

Currently, optical communications plays an important role in the transmission aspect of backbone fiber networks. However, there still remain two challenges in this field: one is the bottleneck between high-capacity local area networks (LANs) and the backbone network, where the answer is the broadband optical fiber access networks; the other is the bottleneck of low-speed electrical signal processing in high capacity optical networks, where one possible solution is all-optical nonlinear signal processing. This thesis will cover both of the two topics. In the first topic, the emphasis will be put on the novel optical access network infrastructure design to improve the access network reliability and functionality as well as the reduction of system complexity. In the second topic, the focus is how to utilize the newly-emerging photonic devices or newly-designed configurations to improve the performance of current optical signal processing subsystems for applications in lightwave transmission systems.

In the area of broadband optical fiber access networks, two aspects are considered: survivability and monitoring function. For the first part, several new network protection schemes among various access network topologies (i.e. tree and ring) are proposed and experimentally demonstrated, which could reduce the access network cost and simplifying the operation of the access network. For the second part, an interesting in-service fault surveillance scheme in the current TDM-PON is proposed via analyzing the composite radio-frequency (RF) spectrum of the common supervisory channel at the central office (CO). Experiment proves its effectiveness with negligible influence on the signal channels. In addition, a system demonstration of the WDM-based optical broadband access network with automatic optical protection function is presented, showing the potential of WDM technologies in the broadband optical access networks.

In the area of nonlinear optical signal processing, the technology innovation is in two areas: new architecture design and the new photonic devices. For the issue of architecture design, the focus is on the Nonlinear Optical Loop Mirror (NOLM) structure. A new polarization-independent OTDM demultiplexing scheme is proposed and demonstrated by incorporating a polarization-diversity loop into a conventional NOLM, which offers stable operation using the conventional components without sacrificing the operation speed or structural simplicity. In another study the design of a novel OFSK transmitter based on phase-modulator-embedded NOLM is conceived and implemented, which features data-rate transparent, continuous tuning of the wavelength spacing and stable operation. For the aspect of new photonic devices, this thesis focuses on the applications of photonic crystal fibers (PCF). In one work, a relatively short-length of dispersion-flattened high-nonlinearity PCF ( $\gamma=11.2 \text{ (W}\cdot\text{km)}^{-1}$ ,  $D<-1 \text{ ps/nm/km@1500-1600 nm}$ ,  $S<1\times 10^{-3} \text{ ps/km/nm}^2$ ) is integrated into a dispersion-imbalanced loop mirror (DILM) to form a nonlinear

intensity discriminator and its application in the nonlinear suppression of the incoherent interferometric crosstalk has been successfully demonstrated. The special characteristics of the PCF ensure a broadband signal quality improvement and make the DILM more compact and stable. In the other work, the small birefringence of this PCF helps to simply achieve the polarization-insensitive wide-band wavelength converter based on four-wave-mixing in PCF.

In summary, this thesis introduces a series of novel optical access network architecture designs and transmission system technologies for optical fiber communications and discusses their feasibilities in practice from the research perspective. We hope that these proposed technologies can contribute to the further developments in this field.

# 摘要

目前，光纖通信在骨幹網絡中發揮了重要的作用。但是，仍然有兩個問題需要解決：一個是存在于高速局域網和骨幹網絡之間的瓶頸，其解決方案為寬帶的光纖接入網絡；另一個則是緩慢的電信號處理速度和高速大容量的光傳輸網絡之間的矛盾，其可能的解決方案為基于非線性效應的全光信號處理。本論文將圍繞這兩個課題展開討論。在第一個課題中，其重點為通過新型網絡構架的設計，達到增強網絡功能，降低系統複雜度的目的。在第二個課題中，將集中于討論如何利用新型結構和新型器件改善目前的全光信號處理系統的性能。

在寬帶光纖接入網絡這一課題中，本文主要考慮兩個方面：如何實現網絡的保護和監控。具體的工作有以下幾項：首先，針對幾種目前常用的光纖接入網絡的拓撲結構，設計了幾種新穎的保護方案以達到降低網絡成本，簡化網絡操作的目的，並在實驗上驗證了其可行性。其次，針對目前使用的無源光網絡，提出了一種在線監控機制，並通過實驗證明了該方案的有效性。最後，本文將給出一個帶有自動保護功能，基于波分複用技術的寬帶光纖接入網絡的系統演示，其目的在于展示波分複用技術在寬帶光纖接入網絡的巨大應用潛能。

在全光非線性信號處理這一課題中，首先將介紹兩種新型的光纖環鏡結構的應用。一項工作是 8 字型的非線性光纖環鏡結構，它可以用于實現偏振無關的光時分複用系統的解複用器。另一項工作是光頻率（波長）鍵控發射機的設計，該發射機可以通過將一個相位調制器置于光纖環鏡中實現，具有對速率透明，波長間隔連續可調等特點。另外，本文還討論了具有高非線性和色散平坦性質的光子晶體光纖在全光非線性信號處理系統中的應用。將一小段具備該性質的光子晶體光纖置于一個色散非均衡的非線性光纖環鏡中，可以實現具有寬調諧波段以及穩定工作的光信號再生器。如果再結合利用該種光纖在制作時產生的殘余雙折射，則能夠實現偏振無關，並具有寬調諧波段的基于四波混頻效應的波長轉換器。

# Acknowledgement

First of all, I would like to express my gratitude to my thesis supervisor, Prof. Chinlon Lin, who helped me to build a comprehensive view on the field. He gave me a lot of suggestions in selecting the research topics for this thesis. He also discussed extensively with me about most of the details in this thesis, through which he helped me understand the merits and importance of these works. Whenever I met difficulties in the work, he gave me suggestions according to his abundant experience or introduced other experts who could help.

I would also like to thank my thesis co-supervisor Prof. Chun-Kit Chan. Discussions with him were always fruitful and had inspired many research ideas which eventually led to this thesis. Especially, he proposed many potential challenges which forced me to comprehend more on the works, and resulted in more in-depth ideas. His critical reading and refinement on each paper I finished always made the paper more fluent. Appreciations should also be given to Prof. Lian-Kuan Chen for his useful suggestions and discussions on some of my work.

My deep appreciation also goes to those past and present colleagues. Dr. Li Huo had many discussions with me about most of my work and assisted me in the broadband access testbed project. Mr. Xiaofeng Sun was in cooperation with me on the work of broadband access network and he gave me many good suggestions to refine my ideas related to this part. Mr. Ning Deng and Mr. Jam Ku also offered many advices and helps in some of the experimental works. Dr. K. K. Chow provided many feasible suggestions in the experimental work related to PCF. Within limited space, I can not express my full gratitude to many other friends and colleagues. Although their names do not appear here, I am equally indebted to them.

I am grateful to Mr. K. K. Choy for his technical assistance and advices in the broadband access testbed project and Mr. W. H. Siu for his support in the fabrication of electronics and hardware.

Last, but not the least, I am deeply indebted to my families for their long-term support, tolerance and encouragement. This thesis is dedicated to them.

# Table of Contents

Chapter 1	Introduction.....	1
1.1	Current Challenges in Optical Fiber Networks.....	1
1.1.1	Broadband Optical Fiber Access Network.....	2
1.1.2	All-Optical Nonlinear Signal Processing.....	5
1.2	Major Contributions of This Thesis.....	6
1.3	Outline.....	8
Chapter 2	Broadband Optical Fiber Access Network Architecture Design .....	9
2.1	Introduction on Broadband Optical Fiber Access Network.....	9
2.1.1	Three Current Optical Access Technologies .....	9
2.1.2	TDM-PON .....	10
2.1.3	WDM-PON.....	12
2.1.4	Broadband Optical Access Network Deployment in Industry.....	15
2.2	Automatic Optical Protection Schemes in WDM-Based Broadband Access Network.....	20
2.2.1	Centrally Controlled Protection Scheme in AWG-Based WDM-PON	20
2.2.1.1	Introduction.....	21
2.2.1.2	Principle of Operation.....	24
2.2.1.3	Experimental Demonstration .....	26
2.2.1.4	An Improved Network Architecture Design.....	29
2.2.1.5	Discussion.....	31
2.2.1.6	Summary .....	31
2.2.2	Survivable “Broadcast and Select” WDM-PON.....	31
2.2.2.1	Introduction.....	31
2.2.2.2	Principle of Operation.....	32
2.2.2.3	Experimental Demonstration .....	35
2.2.2.4	Discussions .....	36
2.2.2.5	Summary .....	37
2.2.3	Single-Fiber Self-Healing CWDM Metro/Access Ring Network with Unidirectional OADM .....	37
2.2.3.1	Introduction.....	37

2.2.3.2	Principle of Operation.....	38
2.2.3.3	Experimental Demonstration .....	40
2.2.3.4	Discussion .....	42
2.2.3.5	Summary .....	43
2.3	In-Service Fault Surveillance Scheme in the Current TDM-PON.....	44
2.3.1	Introduction.....	44
2.3.2	Principle of Operation.....	44
2.3.3	Experimental Demonstration .....	46
2.3.4	Discussion .....	49
2.3.5	Summary .....	49
2.4	System Demonstration of the WDM-Based Optical Broadband Access Network.....	50
2.4.1	Introduction.....	50
2.4.2	Emerging Broadband Services.....	50
2.4.3	Testbed Description .....	52
2.4.4	Summary and Future Work.....	55
2.5	Summary .....	55
Chapter 3	All-Optical Nonlinear Signal Processing Technologies .....	56
3.1	NOLM Structure Design and Its Application .....	56
3.1.1	Introduction on NOLM.....	56
3.1.2	Polarization-Independent NOLM Using Polarization-Diversity Loop 60	
3.1.2.1	Introduction.....	60
3.1.2.2	Principle of Operation.....	61
3.1.2.3	Experimental Demonstration .....	62
3.1.2.4	Summary .....	65
3.1.3	OFSK Transmitter Based on Phase-Modulator-Embedded NOLM ..	65
3.1.3.1	Introduction.....	66
3.1.3.2	Principle of Operation.....	66
3.1.3.3	Experimental Demonstration .....	67
3.1.3.4	Summary .....	71
3.2	Nonlinear Optical Signal Processing Systems Based on PCF .....	71
3.2.1	Introduction on PCF Development .....	71
3.2.1.1	Photonic Crystal Bandgap.....	72

3.2.1.2	Principles and Applications of PCF .....	72
3.2.1.3	Fabrication of PCF .....	75
3.2.1.4	Outlook .....	76
3.2.2	A Nonlinear Intensity Discriminator with a Wavelength-Tunable DILM Based on Dispersion-Flattened High-Nonlinearity PCF .....	76
3.2.2.1	Introduction.....	76
3.2.2.2	Experimental Demonstration .....	77
3.2.2.3	Experimental Results and Discussions .....	78
3.2.2.4	Summary .....	82
3.2.3	Polarization-Insensitive Wide Band Wavelength Converter Using PCF with Small Birefringence .....	83
3.2.3.1	Introduction.....	83
3.2.3.2	Principle of Operation.....	83
3.2.3.3	Experimental Demonstration .....	85
3.2.3.4	Summary .....	88
3.3	Summary .....	88
Chapter 4	Summary and Conclusion .....	89
4.1	Summary of the Thesis .....	89
4.2	Conclusion .....	91
4.3	Suggestions for Future Work .....	92

# List of Figures

Fig 1.1	Global undersea optical fiber networks. TAT: Trans-Atlantic Telecommunications; TPC: Trans-Pacific Cable; FLAG: Fiber Link Around Globe (courtesy of lecture notes from IEG 4030, CUHK) .....	2
Fig 1.2	Backbone network infrastructures of (a) United States and (b) Mainland China (courtesy of lecture notes from IEG 4030, CUHK) .....	2
Fig 2.1	Architecture of TDM-PON and the corresponding wavelength assignment	11
Fig 2.2	Three possible topologies for WDM-PON: (a) tree; (b) ring; (c) branch....	12
Fig 2.3	CWDM wavelength grid specified by ITU-T G.694.2.....	14
Fig 2.4	Network architecture of WDM-PON with centralized light source .....	15
Fig 2.5	Verizon FTTP Network [30] .....	16
Fig 2.6	SBC FTTH broadband access network (in Greenfield areas) [31].....	17
Fig 2.7	SBC FTTN broadband access network (in Brownfield/overbuild areas) [31] .....	18
Fig 2.8	Broadband access demand in Japan [32].....	18
Fig 2.9	NTT FTTx network architectures [32] .....	19
Fig 2.10	(a) Schematic network architecture using the group protection principle based on the periodical properties of AWG; (b) corresponding wavelength assignment; (c) ONU group details in normal state (left) and protection state (right) [33].....	22
Fig 2.11	(a) Schematic network architecture using the group protection principle based on the cyclic properties of AWG; (b) corresponding wavelength assignment [34].....	23
Fig 2.12	(a) Schematic network architecture using centrally controlled protection scheme; (b) corresponding wavelength assignment; (c) ONU group details in normal state (left) and protection state (right) .....	26
Fig 2.13	Experimental setup of the centrally controlled protection scheme.....	28
Fig 2.14	BER measurements under normal mode and protection mode. Inset shows the switching time during traffic restoration.....	28
Fig 2.15	An improved network architecture based on centrally controlled protection scheme.....	29

Fig 2.16	Proposed broadcast and select WDM-PON network architecture with eight ONUs .....	33
Fig 2.17	ONU design: (a) normal mode; (b) protection mode: bold lines show the active fibers for data communication. B/D filter: Broadcast/Dedicated band filter.....	34
Fig 2.18	BER measurements of the dedicated traffics under normal and protection modes .....	35
Fig 2.19	BER measurements of the broadcast traffics under normal and protection modes; inset shows the protection characteristics by monitoring the received power of the downstream signals.....	36
Fig 2.20	(a) Proposed single-fiber self-healing ring network architecture; (b) Structure of AN2 in the normal state: solid and dash arrows show the routing paths of the downstream and upstream traffic of AN2 respectively; both of the traffic for AN2 will pass through the left hand fiber, so AN2 can receive/send data from/to the hub through the CCW/CW direction.....	39
Fig 2.21	(a) Network structure in case of fiber cut between AN2 and AN3; (b) Structure of AN2 in the protection state: solid and dash arrows show the routing paths of the downstream and upstream traffic of AN2 respectively; both of the traffic for AN2 will pass through the right hand fiber, so AN2 can still communicate with the hub via the other direction of the ring without interrupting other in-service data streams.....	40
Fig 2.22	Experimental setup of the proposed single-fiber self-healing CWDM metro/access ring network .....	41
Fig 2.23	BER measurements under normal and protection modes: (a) AN1; (b) AN2 .....	42
Fig 2.24	Measured protection characteristics by monitoring the received power of the downstream signals: (a) AN1; (b) AN2 .....	42
Fig 2.25	(a) Configuration of monitoring light source; (b) Generated RF frequency cavity modes .....	45
Fig 2.26	Network architecture of the proposed monitoring scheme; $\lambda_{\text{data-down}}$ : downstream data channel; $\lambda_{\text{data-up}}$ : upstream data channel; $\lambda_{\text{m}}$ : monitoring channel .....	46
Fig 2.27	Operating principle of the proposed monitoring scheme .....	46

Fig 2.28 RF spectrum of the monitoring channel: (a) healthy state; (b) fiber branch B2 is broken .....	47
Fig 2.29 Corresponding FFT output: (a) healthy state; (b) fiber branch B2 is broken, where F2 is absent.....	48
Fig 2.30 BER performance with and without proposed monitoring module.....	48
Fig 2.31 Testbed setup .....	53
Fig 2.32 Schematic diagram of the Hub .....	54
Fig 2.33 Schematic diagram of the Access Node (AN).....	54
Fig 3.1 Basic NOLM structure.....	56
Fig 3.2 Structure of NALM and the operation principle.....	58
Fig 3.3 Structure of DILM and the operation principle .....	58
Fig 3.4 Principle of two-wavelength operation of NOLM.....	59
Fig 3.5 Proposed PI-NOLM and operation principle.....	62
Fig 3.6 Experimental setup for polarization-independent OTDM demultiplexer....	63
Fig 3.7 Eye diagrams of the switched 10.61-Gb/s signal pulses from 42.44-Gb/s OTDM signals: (a) and (b) show the best and worst cases of the conventional NOLM; (c) and (d) show the best and worst cases of PI-NOLM .....	64
Fig 3.8 BER performance of the 10.61-Gb/s demultiplexed data from 42.44-Gb/s OTDM signals in various situations.....	64
Fig 3.9 BER performance of the four 10.61-Gb/s demultiplexed channels from the 42.44-Gb/s OTDM signals in the worst case when the proposed PI-NOLM was used .....	65
Fig 3.10 Proposed OFSK transmitter design and operation principle .....	67
Fig 3.11 Experimental setup of the proposed OFSK transmitter: left inset shows the spectrum at the transmitter output; right inset shows the waveform of the OFSK signal after transmission .....	68
Fig 3.12 Measured waveforms of individual wavelengths and the composite OFSK signal .....	69
Fig 3.13 BER measurements of 10 Gb/s ASK and demodulated OFSK signal before and after transmission .....	69
Fig 3.14 Power penalties for different wavelength spacing of the demodulated OFSK signal.....	70
Fig 3.15 Receiver sensitivity comparisons of ASK and demodulated OFSK signal at various data-rates .....	71

Fig 3.16	SEM image of the end of the endlessly single-mode PCF .....	73
Fig 3.17	SEM images of the end of several kinds of high nonlinearity PCF.....	74
Fig 3.18	SEM images of the end of air-guiding PCF.....	75
Fig 3.19	Experimental setup. MZM: Mach-Zender modulator; ATT: Attenuator. .	78
Fig 3.20	(a) Transfer characteristics of DILM and (b) BER measurements w/o DILM in case of no noise loading.....	79
Fig 3.21	Eye diagram measured (a) before and (b) after the DILM in case of -10dB crosstalk level at 1550nm.....	80
Fig 3.22	(a) Power penalty measurements at various crosstalk levels for 1550 nm without time delay; (b) Power penalty measurements at 1550 nm with -10 dB crosstalk for various time delays and (c)Power penalty measurements at -10 dB crosstalk for various wavelengths without time delay .....	82
Fig 3.23	Schematic operation principle: the circle shows the cross section of PCF with birefringence; S, P and C represent the signal, pump and converted signal respectively .....	84
Fig 3.24	Experimental setup .....	85
Fig 3.25	Output spectrum of 12-nm up-conversion.....	86
Fig 3.26	Converted signal power vs. the input signal polarization.....	86
Fig 3.27	Eye diagrams (after preamplifier before the photodetector) corresponding to (a) the largest and (b) the smallest output power when the input signal polarization is changed .....	87
Fig 3.28	Output conversion efficiency vs. the converted wavelength.....	87
Fig A.1	Setup at the Hub.....	102
Fig A.2	Configuration inside the rack at the Hub.....	103
Fig A.3	Setup at the Access Node (AN) .....	104
Fig A.4	Configuration inside the rack at the Hub.....	105
Fig A.5	Screen display of the HD video streaming .....	106
Fig A.6	Screen display of the 3D video streaming .....	107
Fig A.7	Screen display of the real-time video streaming.....	108

# List of Acronyms

3DTV: three-dimensional television  
ADSL: asymmetric digital subscriber line  
AN: access node  
APD: avalanche photo-diode  
APON: asynchronous transfer mode (ATM) passive optical network  
ASE: amplified spontaneous emission  
ASK: amplitude-shift-keying  
AWG: array waveguide grating  
BADM: bi-directional add/drop multiplexer  
BER: bit-error-rate  
BPON: Broadband passive optical network  
CATV: community antenna television  
CCW: counter-clockwise  
CLS: centralized light sources  
CO: central office  
CW: clockwise  
CWDM-PON: coarse wavelength-division-multiplexing passive optical network  
DCF: dispersion-compensation fiber  
DFB: distributed feedback  
DFF: dispersion-flattened fiber  
DI: delay interferometer  
DILM: dispersion-imbalanced loop mirror  
DPSK: differential phase shift keying  
DSF: dispersion-shifted fiber  
DSL: digital subscriber line  
DV: digital video  
DWDM: dense wavelength division multiplexing  
EAM: electro-absorption modulator  
EDFA: Erbium-doped fiber amplifier  
EPON: Ethernet passive optical network  
FFT: Fast Fourier Transform  
FP: Fabry-Perot  
FSR: free spectral range  
FTTB: fiber to the building  
FTTC: fiber to the home

FTTN: fiber to the node  
FTTP: fiber to the premise  
FWM: four-wave-mixing  
GbE: Gigabit Ethernet  
GPON: Gigabit passive optical network  
HDTV: high-definition television  
HFC: hybrid fiber coax  
IP: Internet protocol  
IR: infrared  
LAN: local area networks  
LCD: liquid-crystal display  
MAC: media access control  
MC: media converter  
MLFL: mode-locked fiber ring laser  
MLSL: mode-locked semiconductor laser  
MSK: minimum-shift-keying  
M-TIR: modified total internal reflection  
MZM: Mach-Zehnder modulator  
NALM: nonlinear amplifying loop mirror  
NOLM: nonlinear optical loop mirror  
NRZ: non-return-to-zero  
OA&M: operation, administration and management  
OADM: optical add-drop multiplexer  
OADM: optical time-division-multiplexing  
OBPF: optical band-pass filter  
OEO: optical-electrical-optical  
OFSK: optical frequency-shift-keying  
OLT: optical line terminal  
ONU: optical network unit  
OTDR: optical time domain reflectometer  
P2P: point-to-point  
PBS: polarization beam splitter  
PC: polarization controller  
PCF: photonic crystal fibers  
PI-NOLM: polarization-independent nonlinear optical loop mirror  
PLC: planar lightwave circuit  
PMF: polarization-maintaining fiber  
PON: passive optical network

PRBS: pseudo-random binary sequence  
QoS: quality of service  
RF: radio-frequency  
RN: remote node  
RZ: return-to-zero  
SAI: serving access interface  
SDV: switched digital video  
SEM: scanning electron microscope  
SFP: small form pluggable  
SLA: service level agreements  
SOA: semiconductor optical amplifier  
SOP: state of polarization  
SPM: self-phase-modulation  
SSMF: standard single mode fiber  
TDMA: time division multiple access  
TDM-PON: time-division-multiplexing passive optical network  
TFF: thin film filter  
TOAD: terahertz optical asymmetric demultiplexer  
VOD: video on demand  
WC: wavelength coupler  
WDMA: wavelength division multiple access  
WDM-PON: wavelength-division-multiplexing passive optical network  
XPM: cross-phase-modulation

# Chapter 1 Introduction

## 1.1 Current Challenges in Optical Fiber Networks

The physical infrastructures of the communication networks around the world consist of a backbone network connecting various central offices, enterprises and high capacity hubs, and meshes of local access networks serving the end users. Among them, long-haul applications—often known as backbone networks—connecting large population centers across distances of hundreds of kilometers or more can be viewed as the major "highways" of communication networks. In this area, optical fiber [1, 2] has been the dominant media for long distance high-speed transmission systems. The rapid advances in transmission technology, especially the invention of Erbium-doped fiber amplifier (EDFA) [3] and the concept of dense-wavelength division multiplexing (DWDM), have helped the backbone network to gradually evolve from the early phase of replacing electrical cables between repeaters by optical fibers to a new phase of transmitting very-high-capacity multiple wavelength signals over a much longer distance without any electronic amplification.

Currently, the worldwide backbone network has been well built. It includes the global undersea optical fiber networks to connect the different continents (Fig 1.1) and the terrestrial lightwave systems to connect various cities and regions in each country. Fig 1.2 (a) and (b) illustrates the backbone network infrastructures of United States and Mainland China, respectively.

Despite of the great success of fiber-optics in the telecommunication networks, there still remain two challenges: one is the bottleneck between high-capacity local area networks (LANs) and the backbone network, which triggers the development of the broadband optical fiber access networks; the other is the bottleneck of low-speed electrical signal processing in high speed and high capacity optical networks, where an alternative solution is to use the all-optical nonlinear signal processing.

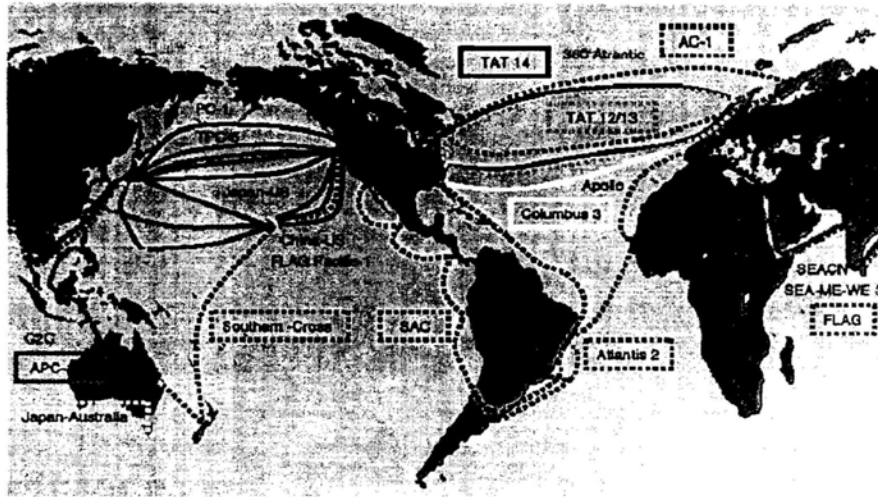


Fig 1.1 Global undersea optical fiber networks. TAT: Trans-Atlantic Telecommunications; TPC: Trans-Pacific Cable; FLAG: Fiber Link Around Globe (courtesy of lecture notes from IEG 4030, CUHK)

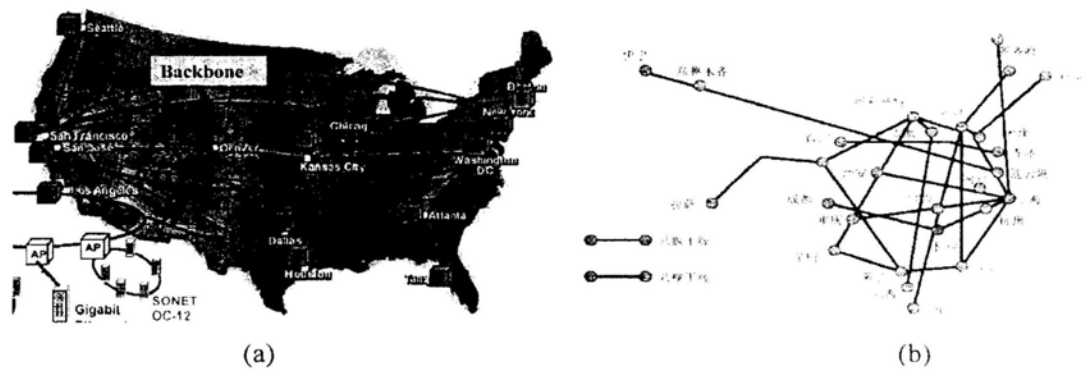


Fig 1.2 Backbone network infrastructures of (a) United States and (b) Mainland China (courtesy of lecture notes from IEG 4030, CUHK)

### 1.1.1 Broadband Optical Fiber Access Network

While over the last 10-15 years the telecommunications backbone network has experienced substantial growth, little has changed in the access network until recently. The tremendous growth of Internet traffic has accentuated the aggravating lag of access network capacity. The “last mile” still remains the bottleneck between high-capacity local area networks (LANs) and the backbone network [4, 5].

Telephone companies responded to this demand by deploying digital subscriber line (DSL) technology. While this is significantly faster than an analog modem, it is well shy of being considered broadband from current perspective. In addition, the physical area one central office can cover with DSL is limited to distances less than 5.5 km.

Cable television companies responded to this demand by integrating data services over their coaxial cable networks, establishing a new network structure called hybrid fiber coax (HFC). It had fiber running between a video head-end and hub to a curbside optical node, with the final drop to the subscriber being coaxial cable, repeaters, and tap couplers. The drawback of this architecture is that each shared optical node has only tens of Mb/s effective data throughput, which is typically divided between 500-2000 homes, resulting in frustrating slow speed during peak Internet traffic hours.

To alleviate bandwidth bottlenecks, optical fibers, and thus optical nodes, are penetrating deeper into the last mile to shorten the lengths of copper and coaxial networks. Compared with the conventional techniques based on copper or radio, the optical fiber shows great advantages: it has lower transmission loss and high bandwidth. Besides those merits, its immunity to the electromagnetic interference (which constitutes a real limiting problem with copper in dense urban areas), its small size and light weight (which leads to the ease for the installation of dense cables) and so on are also equally appreciated. Finally, it is expected that optical fiber will eventually be deployed throughout the access network, realizing fiber to the building (FTTB) and fiber to the home (FTTH) and providing a flexible, future-proof and full service network platform with potentially unlimited capacity.

The most popular broadband optical fiber access solution is the passive optical network (PON). In PON, The active components are only located in optical line terminal (OLT) and optical network unit (ONU). A PON uses a single trunk fiber that extends from an OLT to a passive remote node (RN), which then fans out to multiple optical drop fibers connected to subscriber nodes. No component in the network requires electrical power, hence the term “passive”.

#### *a. TDM-PON*

Nowadays, time-division-multiplexing PON (TDM-PON) has been widely adopted in industry. In TDM-PON, time-sharing is the preferred method for optical channel sharing now in an access network because it allows for a single upstream wavelength (e.g., 1310 nm) and a single transceiver in the OLT, resulting in a cost-effective solution. It can not be considered either shared medium or a point-to-point network; rather, it is a combination of both. In the downstream direction, packets are broadcasted by the OLT and extracted by their destination ONU based on the media access control (MAC) address. In the upstream direction, data frames from any ONU

will only reach the OLT, not other ONUs, which is similar to that of point-to-point architecture. PON frames from different ONUs transmitted simultaneously still may collide. Thus, in the upstream direction the ONUs need to share the trunk fiber channel capacity and resources.

With the PON technologies gaining popularity, two types of point-to-multi-point standards are both in active deployment. One is proposed by ITU-T, which includes ATM-PON (APON), Broadband PON (BPON) and eventually Gigabit PON (GPON) [6]. For the GPON, it provides 1.25 Gb/s or 2.5 Gb/s downstream data rate and the upstream bandwidth are scalable from 155 Mbit/s to 2.5 Gbit/s. GPON promises to provide multiple services: ATM for voice, Ethernet for data, and proprietary encapsulation for voice. The other is proposed by IEEE, which is called Ethernet-PON (EPON) [7]. It provides 1 Gbit/s symmetrical bandwidth (1 Gbit/s bandwidth for data and 250 Mbit/s bandwidth for encoding), and employs a single Layer 2 network that uses Internet protocol (IP) to carry data, voice and video. EPON has been rapidly adopted in Japan, and is also gaining momentum with carriers in China, Korea and so on. Consequently, EPON seems more promising in the development of PON.

#### *b. WDM-PON*

The main advantage of TDM-PON lies in the cost-effectiveness, because only one transmitter is needed at the OLT side and all of the ONUs can be made the same, which is favorable to the mass production. However, the time-shared characteristic makes the TDM-PON difficult to increase the data rate. With the maturity of WDM technologies, and the cost reduction in the WDM components, WDM-PON [8, 9] is expected as the ultimate solution for the broadband access. In the WDM-PON, the OLT transmits multiple wavelengths downstream and each wavelength is routed commonly by WDM multiplexer to serve a particular ONU. Upstream access is enabled by wavelength division multiple access (WDMA). The advantage of WDM-PON lies in its much higher capacity. Also, with dedicated bandwidth, each ONU can be guaranteed a certain quality of service, which is more difficult to do with shared bandwidth. The disadvantage of WDM-PON lies in its cost. It will require either a tunable receiver or a receiver array at the OLT to receive multiple channels. An even more serious problem for network operators would be wavelength-specific ONU inventory. Instead of having just one type of ONU, there would be multiple types of ONUs, based on their specific laser wavelength.

Based on WDM-PON, coarse WDM-PON (CWDM-PON) [10] is developed. The CWDM-PON is a category of WDM-PON -- it uses 20 nm spaced optical channels from 1270 nm to 1610 nm, totally 18 wavelength channels. The merit of CWDM-PON is that they take advantage of the low cost, un-cooled DFB lasers and less stringent wavelength multiplexing and de-multiplexing components, thus greatly reducing the cost. The main limitation lies in the finite number of

CWDM wavelengths, thus limiting the CWDM network size. What's more, there is no suitable wideband optical amplifier for the entire CWDM wavelength spans, thus limiting its reach range.

The passive wavelength routing characteristic provides another degree of freedom for the system design of the WDM-PON. However, there are several issues that should be addressed in the WDM-PON, such as survivability, surveillance, "colorless ONU" and so on, to enrich the functions of the future WDM-based broadband access network and simplify the operation, administration and management (OA&M) of the network. Therefore, the second chapter of this thesis will primarily focus on the issues utilizing the flexibility provided by the wavelength routing to realize these functions. In addition, a system demonstration of the WDM-based optical broadband access network with automatic optical protection function will be presented, showing the potential of WDM technologies in the broadband optical access networks.

### **1.1.2 All-Optical Nonlinear Signal Processing**

Optical fiber has proved its ability in transmitting high-speed high-capacity information over long distances. However, for an advanced flexible optical network, optical routing, switching and other network functions are also important. The nonlinear optical phenomena occurring in optical fibers result in noise and waveform distortion that are factors in signal degradation during transmission. It is therefore desirable to regenerate these deteriorated signals before they can not be recovered. Usually, these signal processing functions are performed in the electrical domain. The drawback of this method is that the optical-electrical-optical (OEO) conversion is necessary on these processing points, greatly increasing the complexity of the networks. Moreover, the electrical method is not transparent to data-rate and format, which makes the network upgrade difficult. As a result, it is preferable to achieve these functions in the optical domain.

Much effort has been put on this area based on the nonlinearity of fiber and semiconductor optical amplifier (SOA). The main nonlinear effects of fiber that can be used in all-optical nonlinear signal processing consist of self-phase-modulation (SPM), cross-phase-modulation (XPM), four-wave-mixing (FWM) and so on, which arise from the third-order nonlinear refractive index change of the silica fiber. The advantage of the nonlinear signal processing scheme based on fiber nonlinearity lies in its ultra-fast response to the signal change (on the scale of femtosecond); however, the relatively low nonlinear coefficient of the conventional fiber makes it necessary to use fiber several hundred meters long or even longer, which may make this technique sensitive to environmental disturbances. As a comparison, SOA is a compact device, so it will not suffer from this kind of instability. However, the slow recovery time of SOA results in the so called "patterning effect", limiting its applications in the data rate of 10 Gb/s or below.

The further advancement in this area relies on the newly-emerging photonic devices, such as high-nonlinearity fiber, photonic crystal fiber (PCF) [11] and so on. Among them, PCF is a very promising device since it offers much flexibility in fiber design. Consequently, a lot of parameters of the fiber can be tailor-made according to the system requirements. Realizing the importance of this device, part of the Chapter 3 will discuss some new applications of PCF in the all-optical nonlinear signal processing subsystems.

Besides the newly-emerging photonic devices, architecture is another consideration in the subsystem design. Especially, nonlinear optical loop mirror (NOLM) [12] is an interesting structure to combine the nonlinear effects of optical components with the interference of light via introducing some kinds of imbalance into the loop. NOLM has found various applications in optical fiber communications networks, such as optical signal regeneration, switching, demultiplexing and so on. In the second half of Chapter 3, research works on some new structures and applications of NOLMs will be presented.

## 1.2 Major Contributions of This Thesis

This thesis will cover two topics in the area of optical fiber communications. One is on the study of WDM-based broadband optical fiber access networks, with the emphasis on the novel network architecture design to improve the network reliability and functionality as well as the reduction of system complexity. One such system demonstration to show the potential of WDM technologies in the broadband optical access networks is described. The other is related to the all-optical nonlinear signal processing with the aim at improving the performance of current optical signal processing subsystems via newly-emerging devices or newly-designed configurations.

### *A. WDM-based broadband optical fiber access networks*

Two optical network architectures are considered: tree topology and ring topology. For the tree topology, a centrally controlled protection scheme has been proposed and experimentally characterized in the array waveguide grating (AWG)-based WDM-PON, which greatly simplifies the ONU structure and is beneficial to the system management. The optical layer survivability of the “Broadcast and Select” WDM-PON has also been studied due to its merits in easy upgrading and simple operation. For the ring topology, a simple and effective CWDM metro/access network architecture with commercially available unidirectional optical add-drop multiplexer (OADM) for automatic optical protection in a Hub/Access Node single-fiber ring has been proposed and demonstrated. This physical-ring/logical star architecture greatly simplifies the design compared with the previous works requiring bidirectional OADM.

Another research effort focuses on the in-service fault surveillance scheme in the current TDM-PON. In this method, the monitoring signals are generated all optically using the low-cost Fabry-Perot (FP) laser with an external reflection cavity. By analyzing the composite radio-frequency (RF) spectrum of the common supervisory channel at the central office (CO), the distribution fiber cut can be monitored continuously with negligible influence on the signal channels.

In addition, a system demonstration of the optical broadband access network is proposed using the CWDM metro/access single-fiber ring network architecture proposed earlier. It consists of one Hub and three Access Nodes (AN) and six CWDM wavelengths are used. The WDM technologies not only can provide huge bandwidth to subscribers such that they can enjoy various high-speed broadband multimedia services, but also simplify the service provisioning due to the passive wavelength routing characteristics performed in the optical layer. What's more, this network is equipped with the automatic optical protection and restoration function. In the future upgrading, this network can be made more flexible in service provisioning and be readily extended for applications in multi-wavelength 10GbE networks due to the data rate transparent property of this network.

#### *B. All-optical nonlinear signal processing*

In the first work, a new polarization-independent optical time-division-multiplexing (OTDM) demultiplexing scheme by incorporating a polarization-diversity loop into a conventional NOLM is proposed and experimentally demonstrated. 40-Gb/s to 10-Gb/s demultiplexing is successfully achieved with 0.6-dB polarization dependence. This scheme offers stable operation using the conventional components without sacrificing the operation speed or structural simplicity.

The second work is the design and demonstration of a novel optical frequency-shift-keying (OFSK) transmitter based on a phase-modulator-embedded NOLM, which features data-rate transparent, continuous tuning of the wavelength spacing and stable operation. The transmitter performance has been experimentally demonstrated, showing its flexibility in transmitter design and potential in high-speed optical fiber communication systems.

In the third experiment, a dispersion-imbalanced loop mirror (DILM) is constructed from a relatively short-length of dispersion-flattened high-nonlinearity PCF and used as a nonlinear intensity discriminator. The DILM not only rejects the low-intensity crosstalk components at the "0" level but also clamps the amplitude fluctuation at the "1" level. Thus it can be used for optical signal regeneration. Specifically, this work experimentally demonstrates its application in the nonlinear suppression of the incoherent interferometric crosstalk, which is one of the major impairments in a transparent optical network resulting in severe degradation of the signal. The

special characteristics of the PCF ensure a broadband signal quality improvement and make the DILM more compact and stable.

At last, utilizing the small birefringence of nonlinear PCF, we have achieved the polarization-insensitive operation of a FWM-based wavelength converter in a simple straight-line configuration with less than 0.9-dB polarization sensitivity. A wide wavelength tuning range of 32 nm is realized due to the dispersion-flattened property of this PCF. The results show that such wavelength converters are promising for wide-band wavelength conversion applications in future all-optical networks.

## **1.3 Outline**

The organization of the remaining chapters of this thesis will be as the following:

Chapter 2: Architecture designs in broadband optical fiber access networks and a system demonstration of the WDM-based optical fiber broadband access network to show the power of WDM technologies in broadband access;

Chapter 3: All-optical nonlinear signal processing technologies, which include the novel NOLM structural designs as well as its applications in optical fiber communications, and the applications of PCF in nonlinear optical signal processing subsystems to demonstrate its potential in future optical networks;

Chapter 4: Summary and conclusion

# Chapter 2 Broadband Optical Fiber Access Network Architecture Design

## 2.1 Introduction on Broadband Optical Fiber Access Network

### 2.1.1 Three Current Optical Access Technologies

#### *A. Active point to point links or active star*

A logical way to deploy optical fiber in the local access network is using a point-to-point (P2P) topology, with dedicated fiber running from the local exchange to each end-user subscriber. However, it could be cost prohibitive, because it requires significant outside plant fiber deployment and very high cost of providing and maintaining electrical power in the local loop and  $2N$  transceivers (we assume that there are  $N$  subscribers).

To reduce fiber deployment need, a star architecture is proposed. In this architecture the feeder fibers carry signal from the OLT to RN. RN terminates and electrically demultiplexes the signal and then distributes the signals to subscribers over fiber. It saves fiber but still needs power and more transceivers ( $2N+2$ ). Generally speaking, it is still very expensive.

#### *B. Passive Optical Network (PON)*

In PON, the active components are only located in OLT and ONU. A PON uses a single trunk fiber that extends from a central office to a passive optical splitter, which then fans out to multiple optical drop fibers connected to subscriber nodes. No component in the network requires electrical power, hence the term passive. The advantages of using PONs in optical access networks are:

1. It allow for long reach between central offices and customer premises, operating at distances over 20 km;

2. It minimizes fiber deployment in both the local exchange office and the local loop;
3. It provides higher bandwidth due to deeper fiber penetration, offering gigabit per second solutions;
4. It eliminates the necessity to install active multiplexers at splitting locations;
5. It is optically transparent end to end and is easily upgraded. The fiber laid in the network can be used for a long time, and the whole system can be upgraded by replacing the equipments of OLT and ONU.

### *C. Optical wireless technology*

It is an attractive candidate to provide connections where the buildings are close to the fiber-optic infrastructure but not directly connected with the fiber. However, it is vulnerable to the environment factors, including bad weather, atmospheric visibility and so on. It is a niche complementary solution to the fiber-based access network for special circumstances and needs.

### *D. Summary*

The PON is best suited for the optical access choice since its architecture is simple, and the whole network is easy to operate and service. When combined with the optical wireless technology, it may address the immediate issue of fiber availability by providing instant bandwidth to the end user.

In the following two subsections, we will give a brief introduction on two important PON architectures: TDM-PON and WDM-PON respectively.

## **2.1.2 TDM-PON**

Fig. 2.1 illustrates a typical TDM-PON architecture [13]. The RN is made of passive optics, such as the planar lightwave circuit (PLC) technology based  $1 \times 16$  or  $1 \times 32$  splitter/coupler. In the downstream direction, packets are broadcasted by the OLT transmitter and extracted by their destination ONU based on the MAC address. In the upstream direction, data frames from any ONU will only reach the OLT. PON frames from different ONUs transmitted simultaneously still may collide, so a suitable time-division-multiple-access (TDMA) scheme to allocate the shared bandwidth between the ONUs in the upstream direction is a key issue in the TDM-PON. Here we give a brief description about TDMA: all ONUs are synchronized to a common time reference, and each ONU is allocated a time slot. An ONU should buffer frames received from a subscriber until its time slot arrives. When its time slot arrives, the ONU would “burst” all stored frames at full channel speed. The possible time slot allocation schemes could range from a static allocation to a dynamically adapting scheme. There are more allocation schemes possible, including schemes utilizing traffic priority and quality of service (QoS), service level agreements (SLAs),

and oversubscription ratios. The OLT remains the only device that can arbitrate time-division access to the shared channel. The common wavelength assignment is also shown in Fig 2.1: for the upstream transmission,  $1.3\ \mu\text{m}$  is used because in this wavelength the F-P laser can be utilized at each ONU to lower the network cost.  $1.49\ \mu\text{m}$  is used for the downstream transmission.  $1.55\ \mu\text{m}$  is reserved as an overlay for the community antenna television (CATV) due the available optical amplifier in this wavelength range.

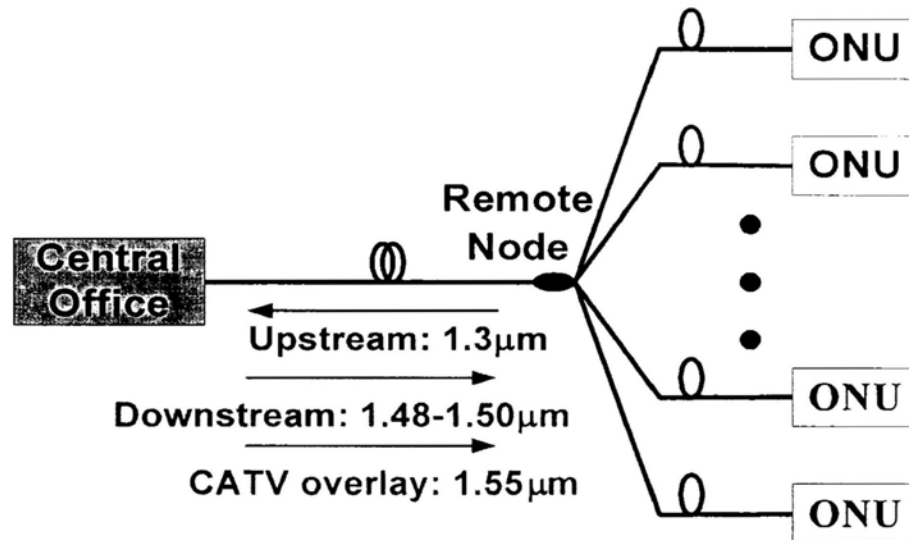


Fig 2.1 Architecture of TDM-PON and the corresponding wavelength assignment

Although the TDM-PON is one of the most popular techniques due to its cost-effectiveness, there still exist some problems (here we only consider those related to hardware implementation):

1. Power deviation: it is also called near-far problem. Due to unequal distances between OLT and ONUs, optical signal attenuation in the PON is not the same for each ONU. The power level received at the OLT will be different for each ONU. So the OLT receiver must be able to quickly adjust its zero-one threshold at the beginning of each received time slot, which is named as the burst-mode receiver [14]. The requirements for the burst-mode receivers are: high sensitivity, large dynamic range, fast response time, simplicity and robustness. Besides, there are some compromises that have to be made to achieve the optimal performance. For instance, it should be able to set the decision threshold in several preamble bytes. However, it can not be too sensitive to the amplitude changes caused by the noise. The holding time constant of the circuit should be large enough to ensure that the threshold will not drop too much during the consecutive zero patterns. However, too large holding time constant will cause a corresponding large gap time between packets, thus increasing the network capacity penalty. Consequently, the design of high-speed burst-mode receiver is still a challenging task.
2. Timing deviation: The timing of the upstream signals is complicated by a path delay that differs from ONU to ONU. In addition, the time-dependent variations in path length can also

be very different from ONU to ONU. The timing of transmissions from each ONU must be adjusted for the packets to arrive at the OLT separated by the guard time.

3. **Optical noise:** The sum of the spontaneous light from several tens of lasers held at threshold is comparable to the signal level from the one transmitting laser, leading to a significant increase in the bit rate in PONs. This effect is severe during the reception of packets from distant ONUs. So, it is not enough just to disallow ONUs to send any data. Even in the absence of data, lasers generate spontaneous emission noise. Thus, an ONU must shut down its laser between time slots and the laser should be able to stabilize quickly after being turned on.

### 2.1.3 WDM-PON

With the maturity of WDM technologies, and the cost reduction in the WDM components, WDM-PON is expected as the ultimate solution for the broadband access. In the WDM-PON, the OLT transmits multiple wavelengths downstream and each wavelength is routed commonly by WDM multiplexer to serve a particular ONU. Upstream access is enabled by wavelength-division-multiple-access (WDMA). There are mainly three possible topologies for WDM-PON: tree, ring and branch, as shown in Fig 2.2 (a), (b) and (c) respectively.

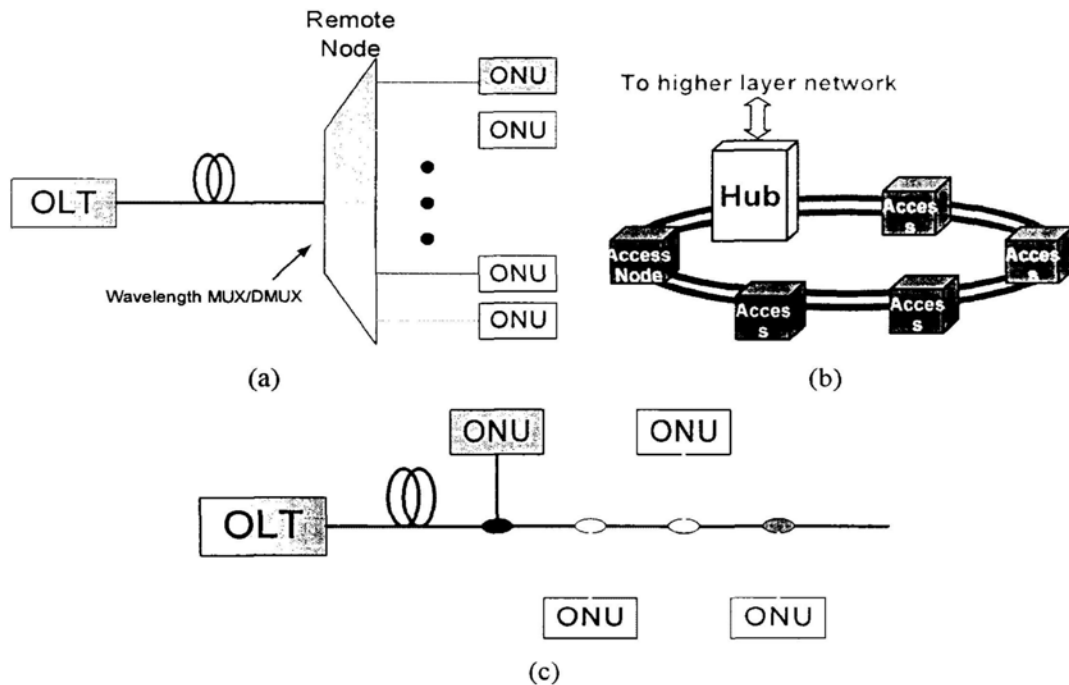


Fig 2.2 Three possible topologies for WDM-PON: (a) tree; (b) ring; (c) branch

The advantage of WDM-PON lies in its higher capacity. Also, with dedicated bandwidth, each ONU can be guaranteed a certain QoS, which is more difficult to do with shared bandwidth. What's more, since there is no power deviation and time deviation in WDM-PON, the burst mode receiver is not necessary any more, thus simplifying the electronics used in the network. The disadvantage of WDM-PON mainly arises from its cost. It will require either a tunable receiver or a receiver array at the OLT to receive multiple channels. An even more serious problem for network operators would be wavelength-specific ONU inventory. Instead of having just one type of ONU, there would be multiple types of ONUs, based on their laser wavelength.

To alleviate the high cost in WDM-PON, spectral slicing of broadband light sources, such as low-cost LED and amplified spontaneous emission (ASE) of EDFA [15-17] was proposed. However, the incoherent properties of these light sources greatly limit the transmission capacity and distance in WDM-PON. Consequently, as a compromise between the transmission capacity and low cost, CWDM is emerging as a robust and economical solution. It differs from DWDM in that the optical channel spacing between the light sources that are multiplexed into a single fiber is much wider, which is 20 nanometers according to the ITU standard [18]. Fig 2.3 illustrates the ITU CWDM wavelength grid: in addition to the C-band, there are the lesser-know wavelengths bands, called the Original (1310 nm window), Extend, Short & Long or more simply, the O, E, S & L bands [18]. These bands can potentially be used to provide 10x more bandwidth than the C-band or 10x wider wavelength spacing for the same bandwidth. The latter option was a logical solution to metro/access WDM technology and cost problem [19, 20]. This is because due to this wider spacing, as the temperature changes in the module, these wavelengths will not overlap, so the temperature control is not required. Thus, un-cooled DFB lasers and less stringent wavelength MUX/DMUX components can be used to lower the cost and simplify the operation of the network. From Fig 2.3, the current CWDM grid comprises 18 wavelengths specified with nominal wavelengths ranging from 1270 nm to 1610 nm inclusive. A typical attenuation curve for the installed base of ITU-T G.652 fiber is also shown. The mapping of CWDM wavelengths onto the fiber attenuation curve has been done for greater clarity and to highlight the high loss incurred by some wavelength (e. g. in the E-band) for this type of fiber. The main limitation of CWDM technology lies in the finite number of wavelengths and there is no suitable wideband optical amplifier to cover the entire spectral range, thus restricting the reach of the network.

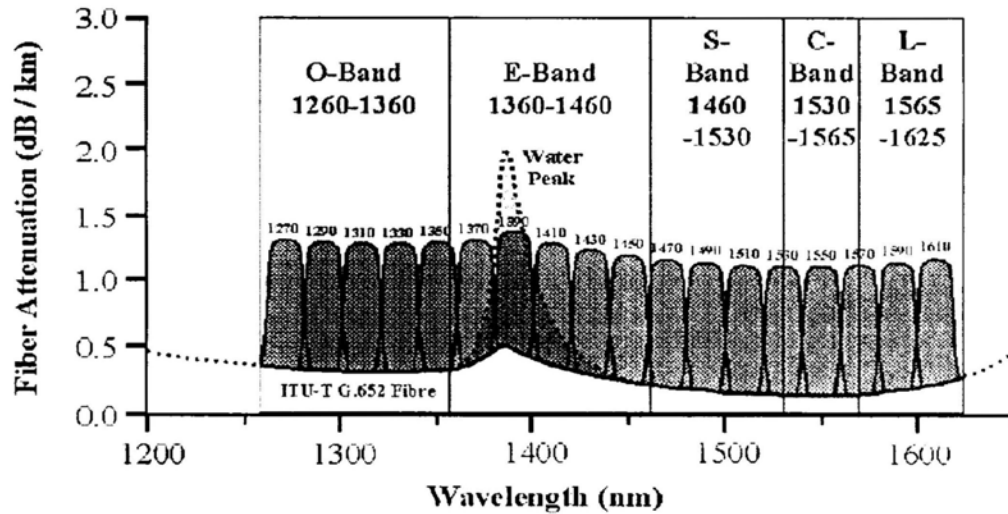


Fig 2.3 CWDM wavelength grid specified by ITU-T G.694.2

Another important issue in WDM-PON is how to realize the wavelength-independent ONU (“colorless” ONU) in order to lower fabrication cost in mass production and lower the OA&M cost. The main method to realize “colorless” ONU is to use the centralized light sources (CLS) at the OLT, as shown Fig 2.4. In this method, an array of light carriers are generated at the OLT side and sent to the ONU side. At the ONU side, the carriers are modulated with the upstream signals and then routed back to the receivers at the OLT side. Since there is no wavelength specific component in the ONU, thus realizing the “colorless” ONU. A typical implementation of this method is described in [21]. The modulator can be replaced by FP lasers via injection locking [22] to reduce the high cost of typical optical modulator. There are also some revisions on this method. One approach is to reserve a portion of the downstream signal in terms of continuous wave blocks on which upstream data can be modulated at ONU via either an optical modulator [23] or a SOA [24]. Another scheme is to reuse the downstream wavelength received at the ONU as upstream data carrier. In this scheme, usually the downstream data format will be the one with constant intensity envelope to facilitate the upstream intensity modulation, such as optical differential phase shift keying (DPSK) [25] and optical frequency shift keying (OFSK) [26]. To reduce the cost on the array of light carriers, a broadband ASE source [27] or supercontinuum [28] can be used as a substitute.

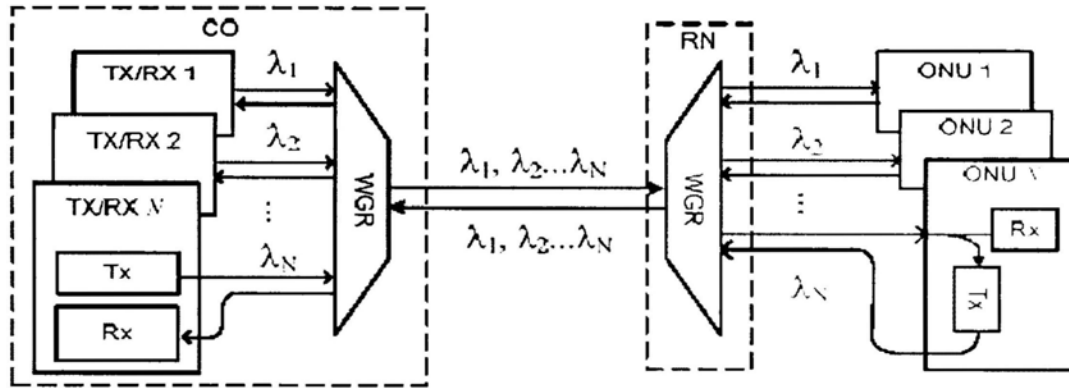


Fig 2.4 Network architecture of WDM-PON with centralized light source

## 2.1.4 Broadband Optical Access Network Deployment in Industry

The major broadband access solution now in industry is PON. Nowadays, PON has been one of the hottest topics in the industry of optoelectronics for telecom applications. Some market research shows that the worldwide OLT and ONU equipment revenue hit \$525 million in 2004, and is projected to grow to \$2.2 billion by 2008.

Currently, Asia is the major action point for PON, accounting for above 90% of worldwide PON subscribers. The subscriber number topped more than 2 million now, and it is expected to grow to almost 22 million in 2008 as the broadband boom continues. As a comparison, North America accounts for only 6% of total PON subscribers now, but will grow to 23% by 2008 [29].

Here, we will introduce three representative examples and their strategies in PON deployment: Verizon, SBC (now new at&t) in North America and NTT in Japan.

### A. Verizon

The Verizon's FTTx deployment project is called "Fios", and its purpose is to better position itself to compete head-on with cable companies by offering triple-play services [30]. It started in early 2003 to deploy fiber specifically for fiber to the premise (FTTP) application. Now, Verizon is moving ahead with ambitious plans to build and deploy fiber networks to millions of homes and businesses. In the year of 2004, the company passed (not necessarily serve) 1 million homes with FTTH. Now, they have passed an additional 2 million homes with its service, which offers



(FTTN) platform that utilizes VDSL in the last mile. Both networks will support SDV employing IP as the end-to-end protocol, which is another main difference from the Verizon deployment with RF overlay. The SDV delivery mechanism is particularly effective at point-to-point content delivery, sending a specific program to specific residences in a VOD format. They believe that the video over IP will be the dominant video delivery mechanism in the future. SBC intends to provide all of the subscribers in its Lightspeed project a video service option by the completion of the project in 2008. SBC began deployment with BPON. However, they view the GPON as the best direction for continued full service networks supporting IP video. It means that eventually SBC will migrate to the GPON network. Fig 2.6 shows the details of the current SBC FTTH broadband access network: the fiber is directly rolled out into the customer homes.

The architecture of SBC FTTH access network is shown in Fig 2.7. Broadband services are provided to FTTH RN from/to the OLT by Gigabit Ethernet (GbE) fiber; these are then cross-connected to existing twisted-pair copper in the Serving Access Interface (SAI), and are transported to/from the customer using Ethernet-based VDSL.

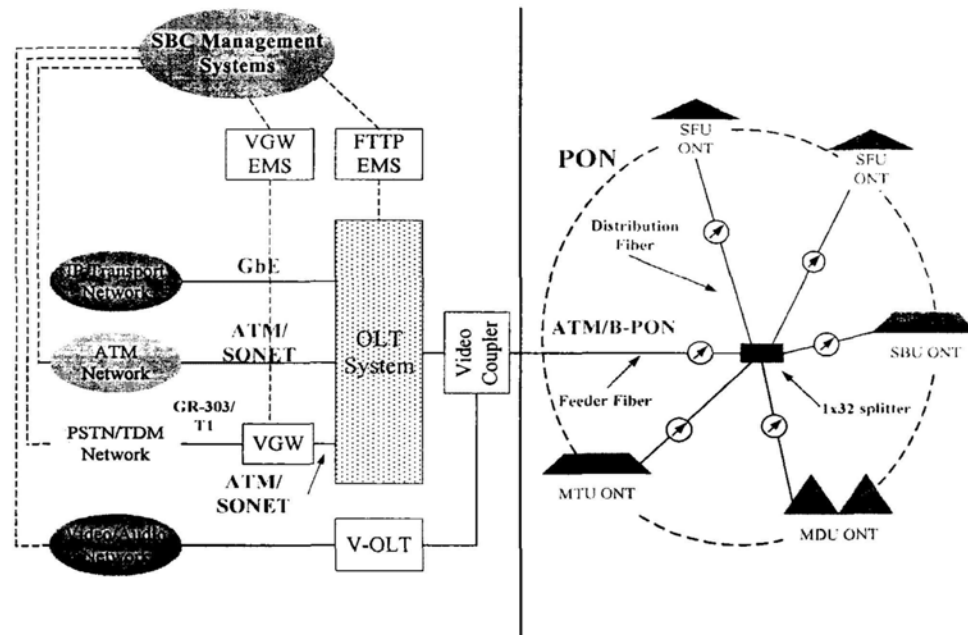


Fig 2.6 SBC FTTH broadband access network (in Greenfield areas) [31]

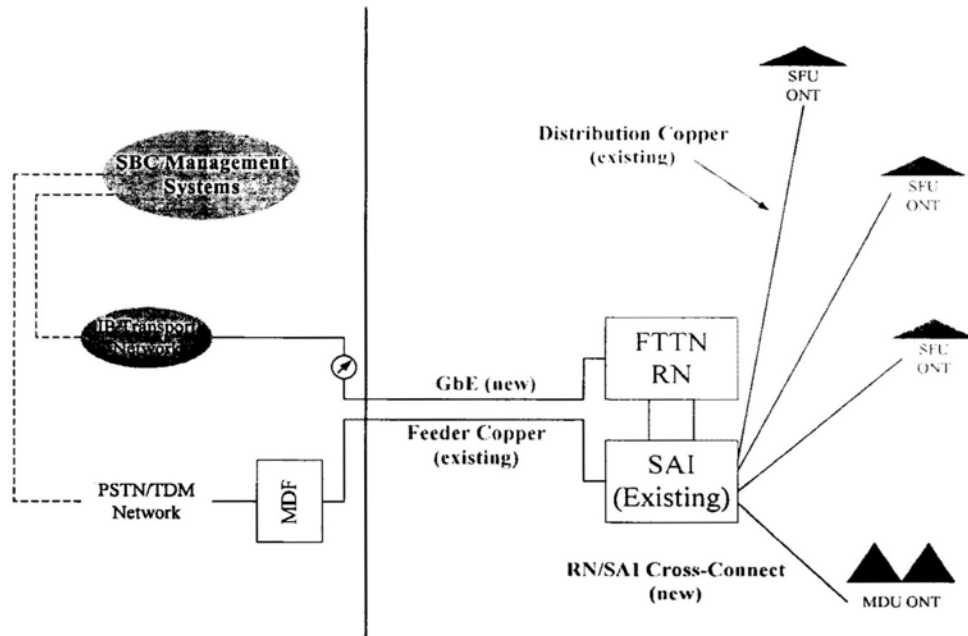


Fig 2.7 SBC FTTN broadband access network (in Brownfield/overbuild areas) [31]

C. NTT

Japan is leading in the FTTx deployment in the world [32]. As shown in Fig 2.8, from the end of 2001, the FTTH deployments in Japan experience an exponential increase. As a comparison, other access services, such as HFC and asymmetric digital subscriber line (ADSL) have been saturated.

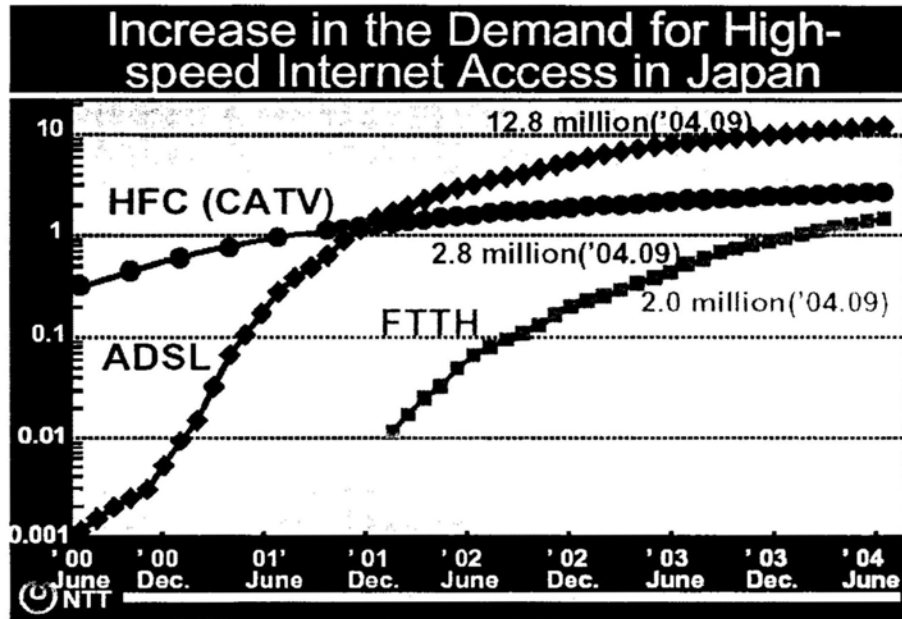


Fig 2.8 Broadband access demand in Japan [32]

By September 2004, there are over 2 million subscribers served by FTTH services. Now, 80,000 to 90,000 new homes will be added into this broadband service every month. There are several national FTTH providers available, such as NTT East, NTT West, KDDI, Yahoo! BB, USEN (Cable Music Broadcaster) and so on. Among them, NTT East and NTT West totally have more than 1.2 million subscribers, making up over 60% of FTTH users in Japan.

Fig 2.9 shows the configurations of NTT's several FTTx network architectures, named as B-FLET. It includes four types of structures. The first one is for the business customers, which utilizes a dedicated fiber to connect the CO and ONU. It can provide symmetrical bidirectional traffic of 100 Mbit/s with 1.55  $\mu\text{m}$  downstream and 1.3  $\mu\text{m}$  upstream. In the ONU, the media converter (MC) will convert the optical signals to electrical signals followed by conventional Ethernet LAN. The second one is family type. It uses the BPON standard with 622 Mbit/s downstream at 1.55  $\mu\text{m}$  and 155 Mbit/s upstream at 1.3  $\mu\text{m}$ . Two-stage splitters are applied to make the BPON serve up to 32 ONUs, thus realizing the FTTH. The third one is called hyper-family type. This type is similar to family type. The main difference is that GPON standard is used here so it can provide symmetrical 1 Gbit/s bandwidth. The last one is called condominium type, which is quite similar to the business type to achieve the FTTBasement.

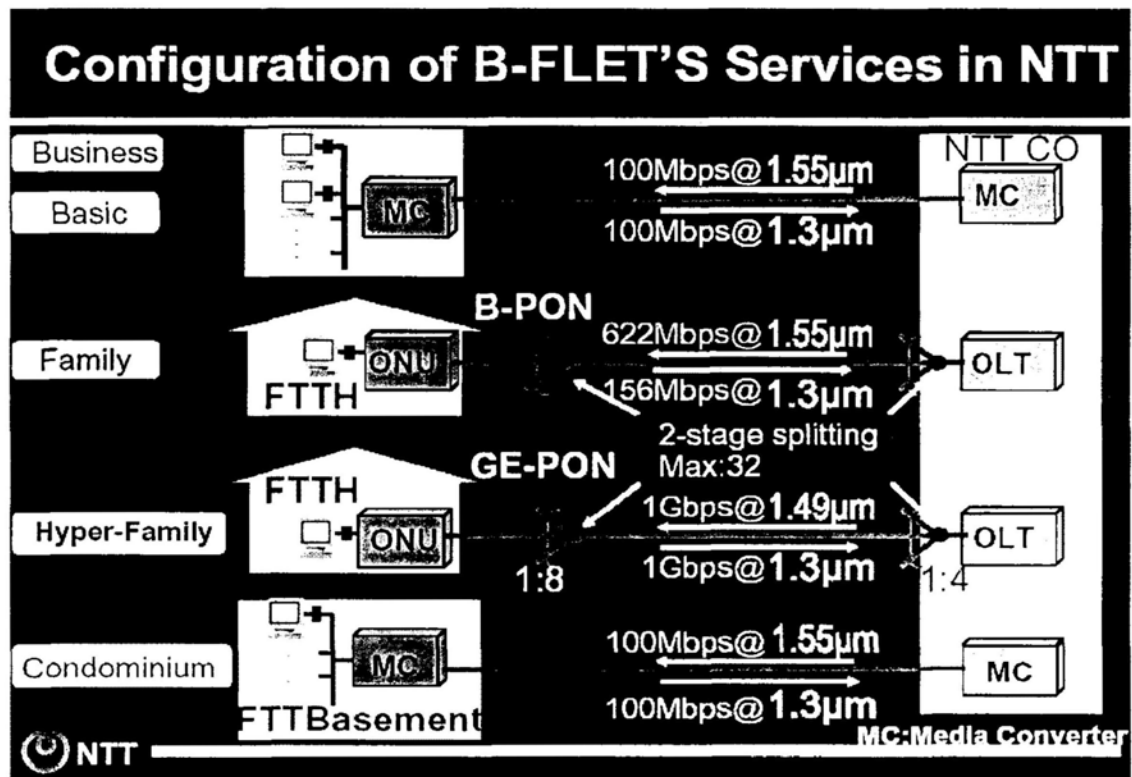


Fig 2.9 NTT FTTx network architectures [32]

NTT's target is to move 30 million customers to FTTH by 2010. To achieve this objective, they believe that the key point is how to create more and more attractive services, to upgrade their network service from single play to triple play (IP telephony, high-speed Internet and IP video service, all in IP).

*D. Summary*

The delivery of high bandwidth triple play (data, voice and video) service is now driving the development of current broadband access networks, thus stimulating the worldwide tide of FTTx deployments and plans. North America and Japan are leading in this tide. Other areas, including Great China, are also quite active and try to catch up with this trend. Eventually, our world will become an all-fiber, all-IP wired network supplemented by the wireless technology to increase the mobility.

## **2.2 Automatic Optical Protection Schemes in WDM-Based Broadband Access Network**

In WDM-based broadband access networks, the OLT and ONU are virtually point-to-point connected through the dedicated wavelength. However, when the fiber link failure occurs between the OLT and one of the ONUs, the affected ONU will become unreachable from the OLT, leading to loss in data. Therefore, fault management is one of the crucial aspects in network management to enhance the network reliability.

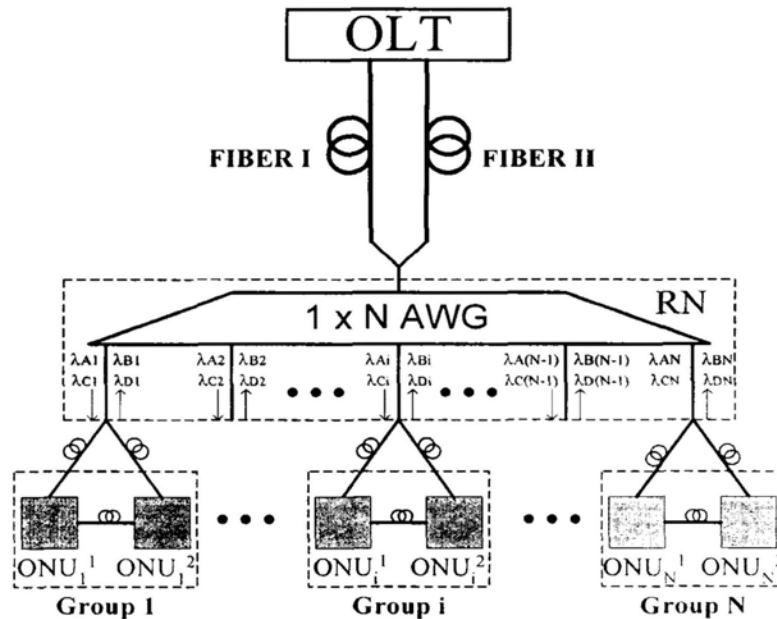
In this section, we propose several protection schemes under two access network topologies: tree topology and ring topology. For the tree topology, a centrally controlled protection scheme was proposed and experimentally characterized in AWG-based WDM-PON in subsection 2.2.1; the optical layer survivability of the "Broadcast and Select" WDM-PON has also been studied with the results shown in subsection 2.2.2. For the ring topology, in subsection 2.2.3, a single-fiber self-healing CWDM metro/access ring network with unidirectional OADM is proposed and demonstrated where broadband service can be distributed.

### **2.2.1 Centrally Controlled Protection Scheme in AWG-Based WDM-PON**

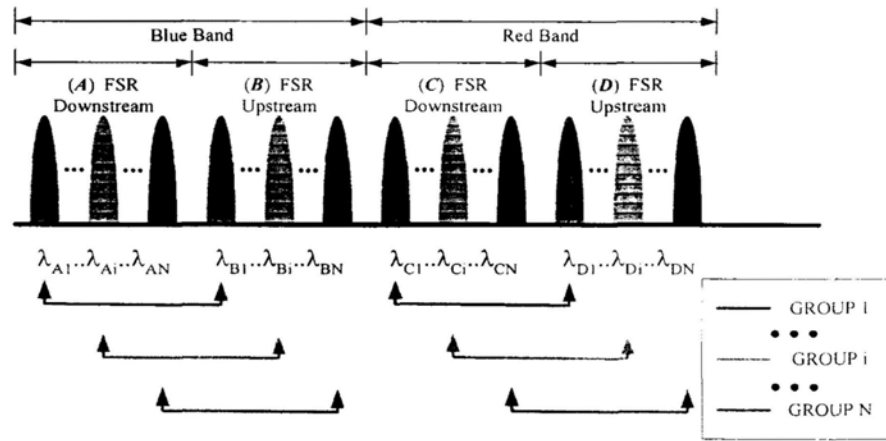
### 2.2.1.1 Introduction

In WDM-PON, the common method to realize the protection and restoration function is illustrated in ITU-T recommendations [5], where the duplicated network resources, such as fiber links or ONUs are implemented to provide network redundancy, and automatic protection switching is used to reroute the affected data traffic into those alternative protection path. This method is somewhat complicated, especially when the number of ONUs is large.

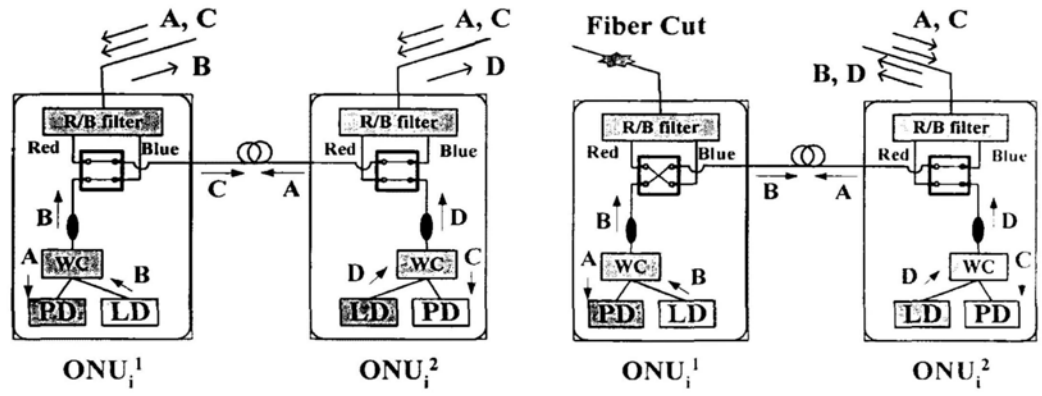
In [33], a novel principle, namely group protection technique was proposed to enhance the survivability in an AWG-based WDM-PON. By assigning two adjacent ONUs into one group and connecting them via an interconnecting fiber, the traffic can be rerouted through the adjacent ONU in case of any fiber cut between the RN and an ONU. Usually, the distance between two adjacent ONUs will be much shorter than the distribution fiber length, especially when the number of ONUs is large. Thus, this scheme will be superior over the common practice [5] in terms of the network resource saving and deployment cost reduction. To realize this principle, each distribution fiber link should be able to carry the information from the adjacent ONU in the same group. This goal was achieved through the periodical properties of AWG in wavelength routing. It means that the two ONUs in the same group will utilize the wavelength channels taking up the same position of each free spectral range (FSR). As a result, these serving channels will pass through the same AWG output port and these two ONUs can be separately connected to this port via  $1 \times 2$  3dB coupler. Fig 2.10 shows the schematic network architecture based on this principle, the corresponding wavelength assignment and the ONU group details in normal state and protection state.



(a)



(b)



(c)

Fig 2.10 (a) Schematic network architecture using the group protection principle based on the periodical properties of AWG; (b) corresponding wavelength assignment; (c) ONU group details in normal state (left) and protection state (right) [33]

Besides the periodical property, the cyclic property of AWG can also be combined with the periodical characteristic to realize this purpose [34]. Here, the cyclic property of AWG indicates that in a  $N \times N$  AWG, if a certain wavelength  $\lambda$  can be routed from input port  $a$  to output port  $b$ , then this wavelength  $\lambda$  can also be routed from input port  $\text{mod}(a+m, N)$  to output port  $\text{mod}(b+m, N)$ , where  $a$ ,  $b$  and  $m$  are integers that are smaller than  $N$ . Fig 2.11 shows the schematic network architecture based on this principle and the corresponding wavelength assignment. The ONU group design is the same as Fig 2.10 (c), so it is not shown here.

However, in both of the two above schemes, the switching elements (i.e. optical switches) are located at the ONU side. Here, we name them as the distributed protection schemes. Thus, the number of switches required is the same as the number of ONUs, greatly increasing the required network resources. In the following, a novel network architecture based on a centrally controlled protection scheme is proposed where only one set of protection equipment is located at the OLT

end instead of distributed at each ONU, thus named as “centrally controlled”. Such architecture not only simplifies the ONU design, but also significantly reduces the amount of required network resource.

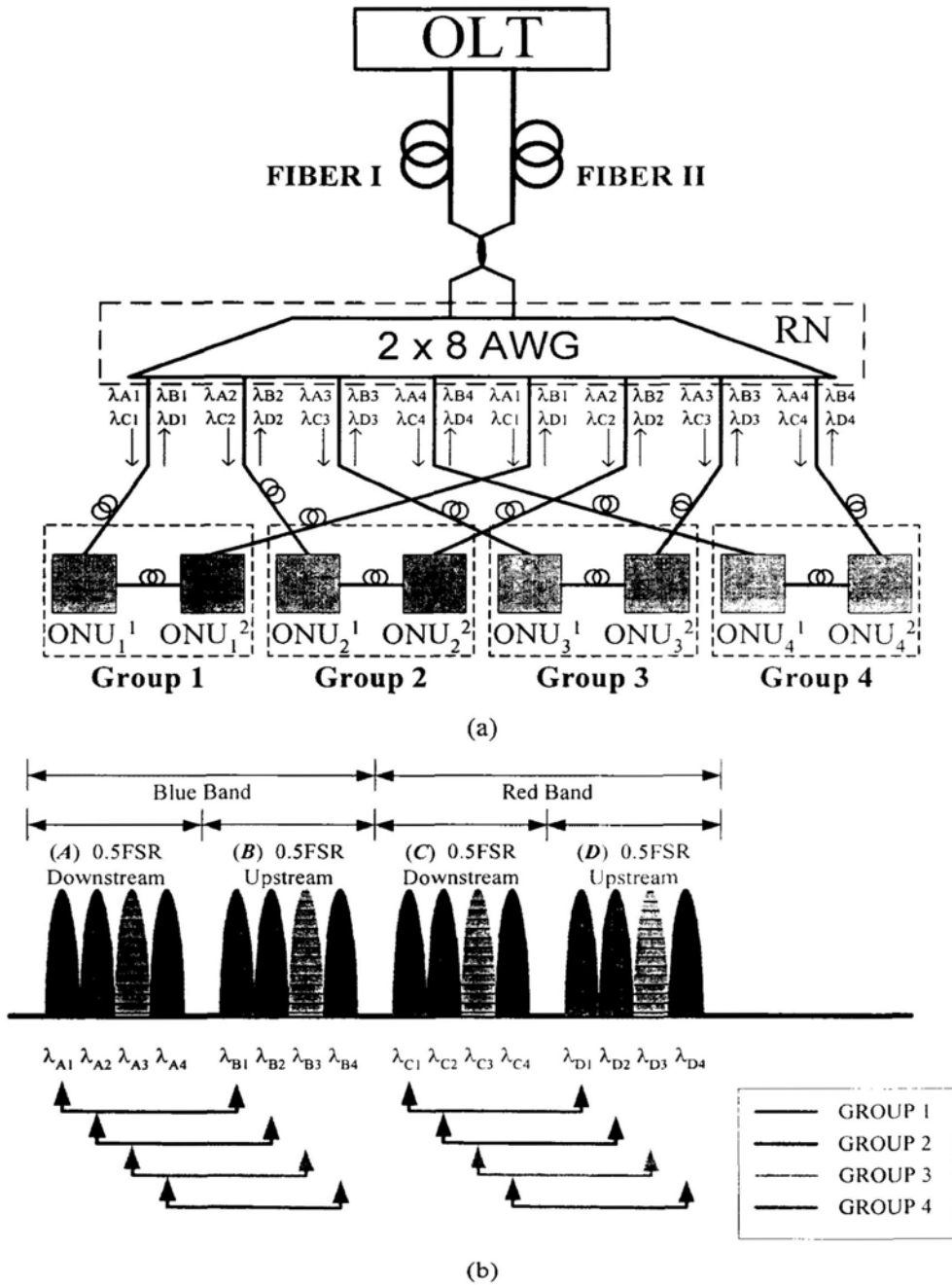


Fig 2.11 (a) Schematic network architecture using the group protection principle based on the cyclic properties of AWG; (b) corresponding wavelength assignment [34]

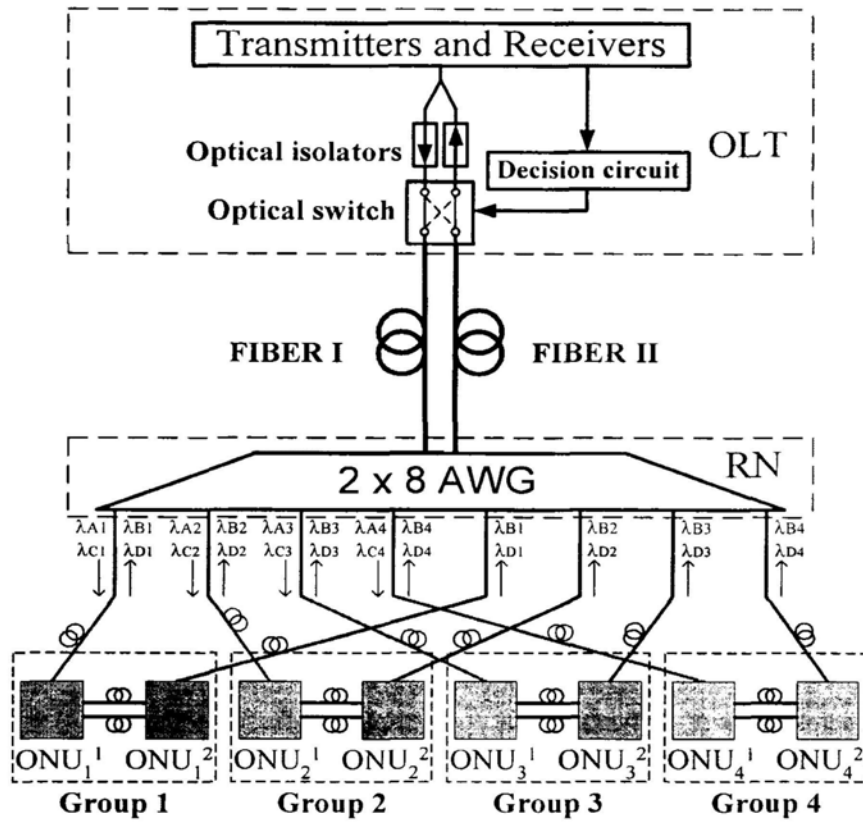
### 2.2.1.2 Principle of Operation

The network architecture with  $N$  (in multiple orders of two) ONUs is shown in Fig 2.12 (a). Without loss of generality, eight ONUs ( $N=8$ ) are considered here as an example to facilitate the illustration. At the OLT end, two optical isolators with opposite directions and a 2x2 switch are inserted before the two feeder fibers. In normal operation, the switch is set to the bar state to make sure that feeder fibers I and II are used for the downstream and the upstream traffic, respectively. A decision circuit is also incorporated in the OLT to detect the fiber link failure and to activate the wavelength re-routing mechanism for protection. At the RN end, feeder fibers I and II are connected to the two input ports of the 2x8 AWG, respectively, and the spectral transmission peaks of the two ports are spaced by half of the FSR of the AWG (i.e. port  $m$  and port  $m+N/2$ , where  $N$  is the entire input port number of AWG). At the ONU end, two adjacent ONUs are assigned to a group and each of them is connected to a specified AWG output port through a distribution fiber, as shown in Fig 2.12 (a). Here, we assume that the two fibers from the RN to  $ONU_i^1$  and  $ONU_i^2$  are diversely run. The fiber connection pattern is attributed to a proposed wavelength assignment plan, as illustrated in Fig 2.12 (b). Wavebands A and B in the blue band are allocated for the downstream and the upstream wavelength channels of  $ONU_i^1$  respectively, while wavebands C and D in the red band are allocated for those of  $ONU_i^2$  respectively. Each waveband covers half of the AWG FSR. Thus, totally 2 FSRs are used. Due to the spectral periodical and cyclic property of AWG, the wavelength  $\lambda_{Ai}$ ,  $\lambda_{Bi}$ ,  $\lambda_{Ci}$  and  $\lambda_{Di}$  will pass through both of the distribution fibers serving the ONU group  $i$ . The structure of each ONU group is depicted in Fig 2.12 (c). In each ONU, an R/B filter is connected to its respective distribution fiber. At  $ONU_i^1$ , a fiber coupler is used to combine its blue band outputs with that from  $ONU_i^2$ , which is via a piece of interconnecting fiber between the two ONUs ( $ONU_i^1$  and  $ONU_i^2$ ). A wavelength coupler (WC) is also employed to separate the upstream and the downstream wavelength channels. The design of  $ONU_i^2$  is similar to  $ONU_i^1$  except that the red band outputs of two ONUs in the same group are combined.

In normal operation mode, the switch at OLT is set to the bar state. Thus, fibers I and II are used to carry the downstream and the upstream traffic, respectively. Due to the periodical and cyclic properties of AWG and our proposed wavelength assignment plan, all of the downstream traffic will reach the leftmost four distribution fibers, which are connected to  $ONU_i^1$  ( $i=1,2,3,4$ ). Then, the R/B filter in  $ONU_i^1$  will route the received wavelength channels to the receivers in both ONUs in the same group. For the upstream wavelengths, they will be power-split by the coupler and transmitted in two different paths to the OLT. However, due to the existence of the isolator located at the OLT, only the upstream wavelengths passing through the leftmost four distribution fibers will be transported to the OLT while the other paths will be blocked. From the above

operation mechanism, it is obvious that only half of the distribution fibers and their corresponding interconnecting fibers are used while the other half is considered as backup, in normal operation mode. Therefore, we can name the former ones as the 'working fibers' while the latter ones as the 'protection fibers'.

In case of any working fiber failure, the decision circuit in the OLT will detect the loss of some upstream signals. An electrical control signal will then be generated to trigger the switch from the bar state to the cross state. Thus, fiber I becomes the upstream path while fiber II becomes downstream path. Consequently, all of the bidirectional data wavelengths are switched from the working fibers to the corresponding protection fibers, as shown in Fig 2.12 (c). The interconnecting fiber cuts can also be protected since they are equal to the corresponding distribution fiber break. In this way, a fast traffic restoration can be achieved.



(a)

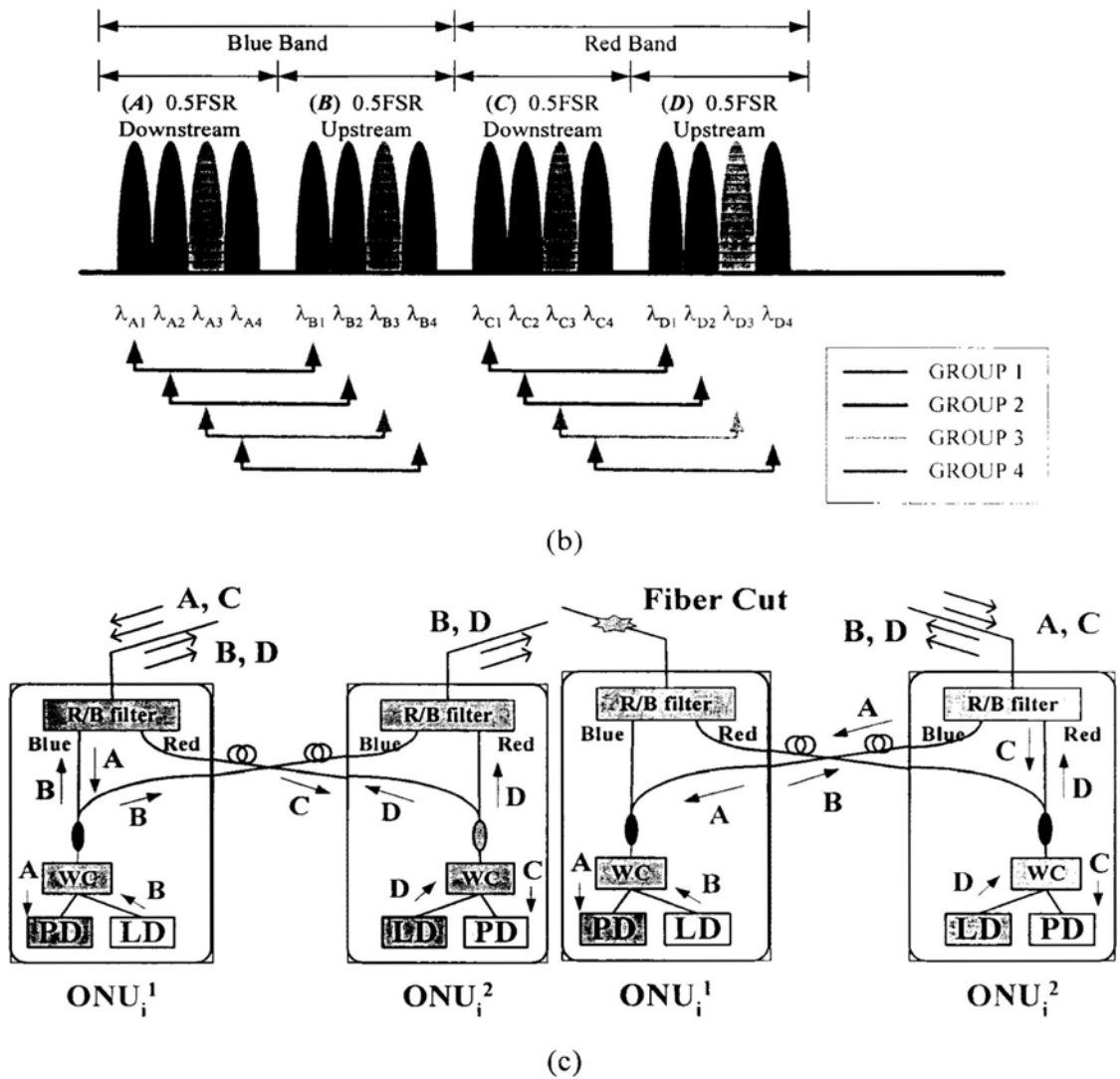


Fig 2.12 (a) Schematic network architecture using centrally controlled protection scheme; (b) corresponding wavelength assignment; (c) ONU group details in normal state (left) and protection state (right)

### 2.2.1.3 Experimental Demonstration

Fig 2.13 shows the experimental setup. A pair of ONUs, ONU1 and ONU2, were implemented. The LDs 1-4 were used as the transmitters at the OLT and at the two ONUs. Only LD1 and LD2 were directly modulated with 2.5-Gb/s  $2^{23}$ -1 pseudo-random binary sequence (PRBS) data to study the downstream and the upstream transmission performance under the normal and the protection modes while the LD3 and LD4 were left unmodulated. Previous experiment demonstration [9] has proved that the possible crosstalk power penalty was negligible even when 32 wavelengths (16 for upstream and 16 for downstream) were on and modulated, due to the fact

that the WDM-PON had a relatively small network span and the transmission power was carefully controlled. The 16 channel-AWGs used in the experiment had a 100-GHz channel spacing and an FSR of 12.8 nm. The Red/Blue filters had a bandwidth of about 18 nm in each passband. On the OLT side, EDFAs were inserted in front of the AWG in order to compensate the components' insertion losses and to achieve the required transmitted power. The isolators' functions were also included in the EDFAs. On the ONU side, the 50/50 couplers were used in place of the WC, for simplicity. The length of the standard single mode fiber link fiber between the OLT and the RN was 20 km, while that between the RN and the ONU was 2 km. The interconnecting fiber between the two ONUs was 2 km long.

The bit-error-rate (BER) performance of ONU1 for both the upstream and the downstream traffic were measured with the results depicted in Fig 2.14. The fiber link between the RN and the ONU1 was then intentionally disconnected to simulate the fiber cut scenario. In all cases the measured receiver sensitivities at 2.5 Gb/s varied from -24.5 dBm to -26 dBm. The additional 1.5 dB power penalty was mainly due to the fiber chromatic dispersion. We have also measured the switching time in case of the simulated fiber cut between the ONU1 and the RN. The optical power of the upstream signals from the ONU1 was monitored at the OLT end and the result was shown in the inset of Fig 2.14. The switching time was measured to be about 9 ms, which corresponds to the traffic restoration time.

Without the optical amplification, the power budgets between LD transmitter and the receiver is about 25 dB, if the LD output power is fixed at 1dBm. The insertion losses of R/B filter, switch, isolator and AWG are about 0.5 dB, 1dB, 1dB and 5 dB, respectively. The coupler in the OLT and each ONU will introduce 3-dB power loss. We assume the total fiber length (including both feeder fiber and distribution fiber) is 20 km, as we used in the experiment. At the 1550-nm wavelength range, the transmission loss will be around 4-5 dB. Thus, the entire induced loss will be about 21-22 dB. Consequently, there are still 3 or 4-dB power margins in our proposed network. The EDFAs we used in the experiment is to facilitate the experimental operation, such as the BER measurements. In practical applications, they can be removed.

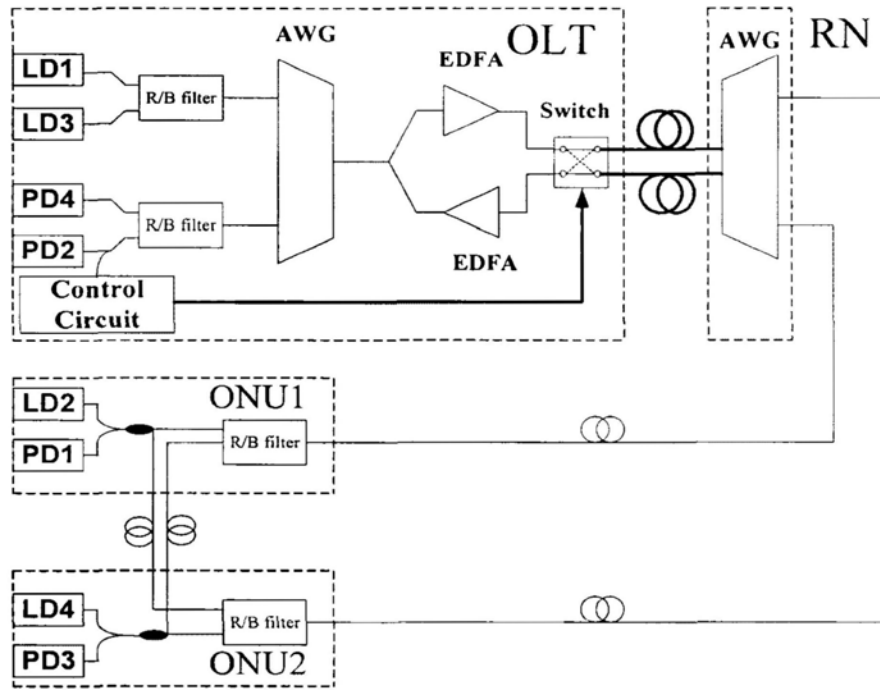


Fig 2.13 Experimental setup of the centrally controlled protection scheme

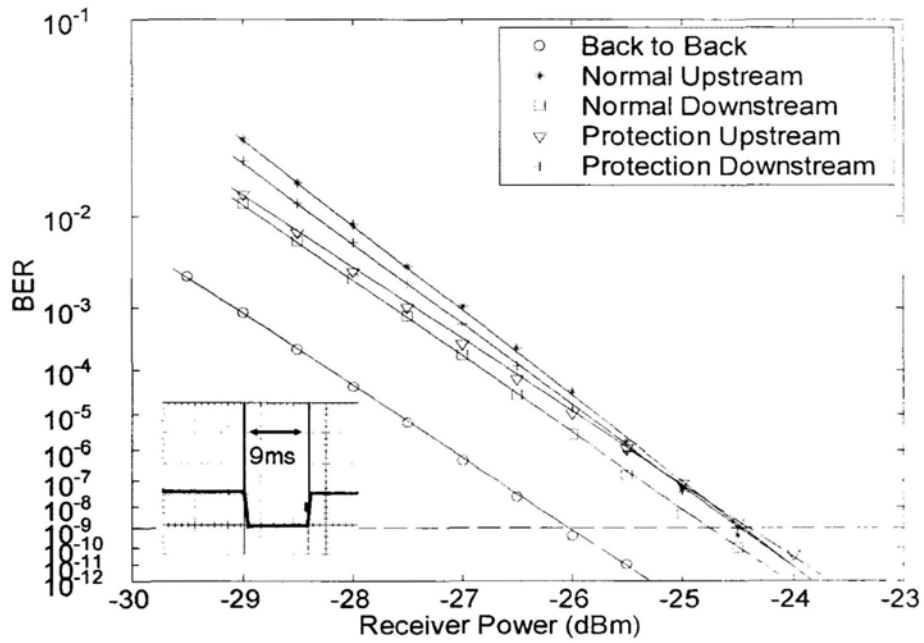


Fig 2.14 BER measurements under normal mode and protection mode. Inset shows the switching time during traffic restoration

### 2.2.1.4 An Improved Network Architecture Design

In the above network architecture, two feeder fibers are used. However, any of the feeder fiber failure will cause the loss of connectivity to all of the ONUs. Here, we propose an improved method to solve this problem without adding more feeder fiber as backup. The network architecture is shown in Fig 2.15. The difference between Fig 2.15 and Fig 2.12 is that one more 2×2 optical switch (optical switch 1) is inserted between the two isolators. The control signal for this switch is generated as follows: a small part of the upstream optical power from fiber I and fiber II are tapped out and converted to electrical signals by photodetectors. Then, the two electrical signals will be used as the inputs of an electrical AND logic gate, whose output will be the switch 1 control signal. Originally, both of the optical switches are in the bar state, so the signal transmission paths will be the same as the above structure.

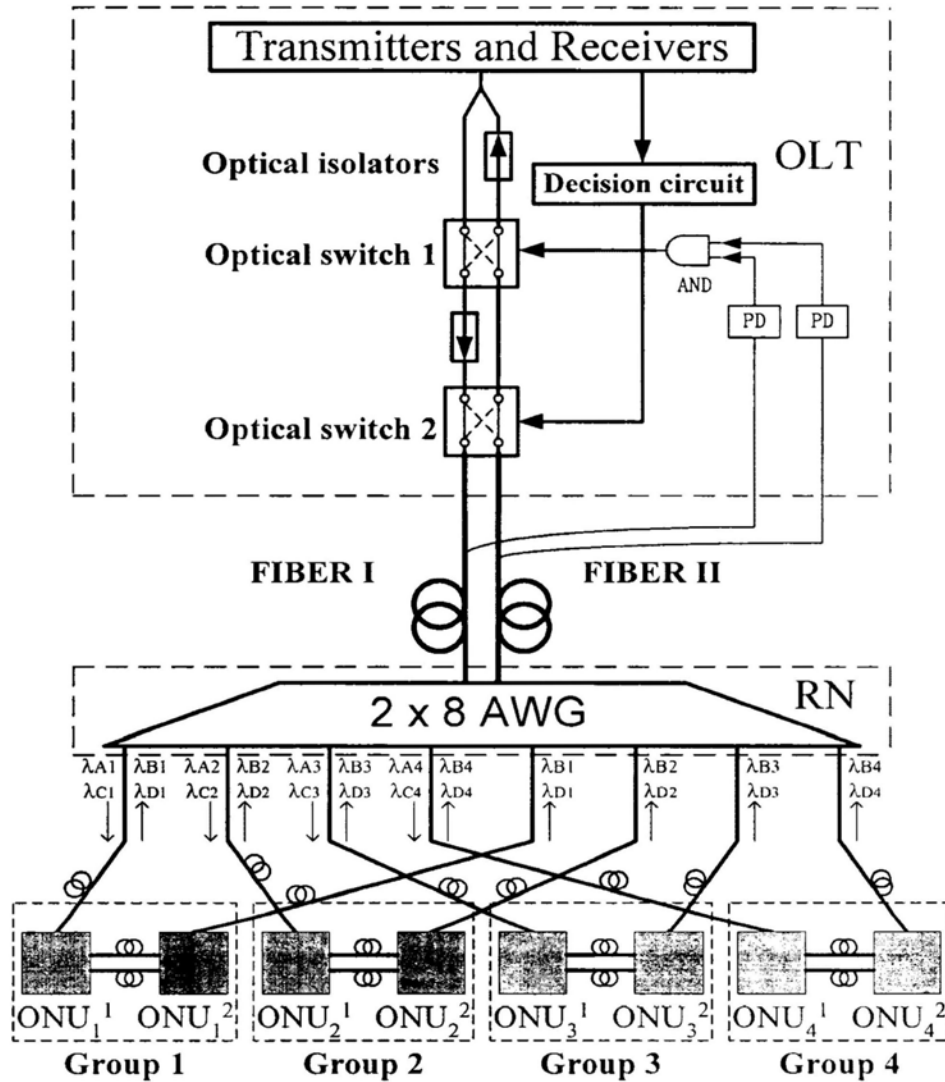


Fig 2.15 An improved network architecture based on centrally controlled protection scheme

The fiber cuts can be classified into three cases:

*CASE I (Distribution fiber cut)*

This case will lead to some power decrease in the feeder fiber, but not power loss, so it will not result in the state change of the optical switch 1. Thus, this case is the same as the situation in the basic implementation and has been discussed.

*CASE II (Fiber I cut)*

A total upstream power loss in fiber I will make the optical switch 1 to change from bar state to cross state. However, since fiber II still works, the receivers in the OLT will not find this failure, so optical switch 2 will maintain its states. Thus, all of the traffic, both downstream and upstream, will pass through fiber II. In this case, the concept of “working (distribution) fiber” and “protection (distribution) fiber” disappears, because all of the distribution fibers are used to carry signals.

*CASE III (Fiber II cut)*

A total upstream power loss in fiber II will make the optical switch 1 to change from bar state to cross state. What’s more, the receivers in the OLT will also detect this failure, because all of the upstream signals will be lost (a special case of some upstream signals loss) and the control circuit will trigger the optical switch 2 from bar state to cross state. Thus, all of the bidirectional traffic will pass through fiber I and achieve the fast traffic restoration.

Here, we need to take note of a specific problem. In this scheme, the two optical switches are serially connected to the feeder fibers, so the state change of one switch might affect the other’s state. For example, in CASE II, the state change of optical switch 1 will cause a temporary disconnection between the OLT and the feeder fibers. Thus, the receiver in the OLT will detect the upstream signal power loss and the control circuit will trigger the optical switch 2 to change its state, leading to an operation error. A solution to this problem is to set a clock to synchronize the control signals: only at the rising edge of the clock, these control circuits will check the system state and send out the control signals. The clock period should be a little longer than the switching time. Thus, the whole system will return to the stable state before the second clock arrives. But the clock period can not be too long, because it might cause a long delay between the fiber failure and the detection of this failure, leading to a long restoration time. For instance, the clock period can be set to 12 ms (assume that the switching time is about 9ms). Thus, the total restoration time will not exceed 21 ms.

### 2.2.1.5 Discussion

In this proposed scheme, the number of protection switches required is significantly reduced from  $N$  sets [33, 34] to only one or two. Thus, the structure of the ONU is much simplified; albeit it requires a pair of fibers connecting two ONUs in the same group. Nevertheless, the OLT can always keep track of the network status information, and thus facilitates the network management. However, there are still some limitations in this approach. One limitation of this proposed scheme is that it cannot support simultaneous fiber cuts in a working fiber as well as a protection fiber, of which the probability of occurrence is approximately  $N^2p^2/4+O(p^2)$ , where  $p$  is the probability of any working or protection fiber cut (here, we assume that their fiber cut probability is the same since the architecture is symmetric) and  $N$  is the number of ONUs in the network. Another limitation is the failure restoration for any one distribution fiber will lead to a transient interruption to all of the ONUs. Besides, each ONU may also receive the signals from its adjacent ONU in the same group, thus the security advantage of the WDM-PON may be undermined.

### 2.2.1.6 Summary

In this section, we have proposed a novel centrally controlled protection architecture for bidirectional WDM-PON networks. Fast automatic protection and traffic restoration against fiber failure and the transmission characteristics of a 2.5-Gb/s signal over the WDM-PON have been experimentally demonstrated and characterized. The proposed network architecture simplifies the ONU design and thus reduces network cost with negligible protection performance degradation.

## 2.2.2 Survivable “Broadcast and Select” WDM-PON

### 2.2.2.1 Introduction

The network architecture of broadcast-and-select WDM-PON [35] is compatible with that of the current TDM-PON. So it provides us a feasible way to gracefully upgrade current TDM-PON to future high-capacity WDM-PON with the minimum cost on network upgrade via utilizing the legacy infrastructures that have been deployed for the current TDM-PON. Besides, it offers better network flexibility in both broadcast and dedicated services provisioning as compared with the conventional WDM-PON [9]. In order to enhance the network reliability, automatic traffic restoration against any fiber failure is highly desirable. With the broadcast services from the OLT,

each ONU receives the same downstream signal. By grouping and inter-connecting two adjacent ONUs together [33, 34], protection against possible cut in the distribution fibers could be achieved. Considering the distance between two adjacent ONUs is usually much shorter than the length of distribution fiber when the number of ONUs is relatively large, the group protection method [33, 34] is potentially low cost when compared with the conventional method of duplicating fiber links to provide redundancy, as recommended by ITU-T [5]. In this section, we propose and experimentally demonstrate this broadcast-and-select WDM-PON network architecture with fast automatic optical protections, using the low cost CWDM components, while both broadcast and dedicated broadband traffic could be supported.

### 2.2.2.2 Principle of Operation

The proposed access network architecture is shown in Fig 2.16 with  $N$  ONUs (here,  $N=8$  for simplicity). At the OLT side, it consists of a CWDM multiplexer,  $N$  pairs of CWDM transceivers with each of them serving a designated ONU for dedicated bi-directional service and one additional optical transmitter for broadcast service. Under the current CWDM standard [18], totally eighteen wavelengths have been defined. Except for the wavelength of 1390 nm which is located at the water absorption peak of the standard single mode fiber (SSMF), there are seventeen wavelengths available. For the broadcast channel, it will experience relatively higher transmission loss in our proposed architecture (as will be described later) compared with those dedicated channels, so it would be designated to operate at 1550 nm where it has the lowest transmission loss in the fiber and could also be boosted up by commercially available EDFA. The other sixteen wavelengths would be assigned for dedicated bi-directional (upstream and downstream) services arbitrarily, thus supporting eight ONUs. At the RN, a  $2 \times N$  optical splitter is used to broadcast the signals to each ONU. From the OLT to the RN, there is one backup fiber link to protect the working feeder fiber from any possible fiber cut.

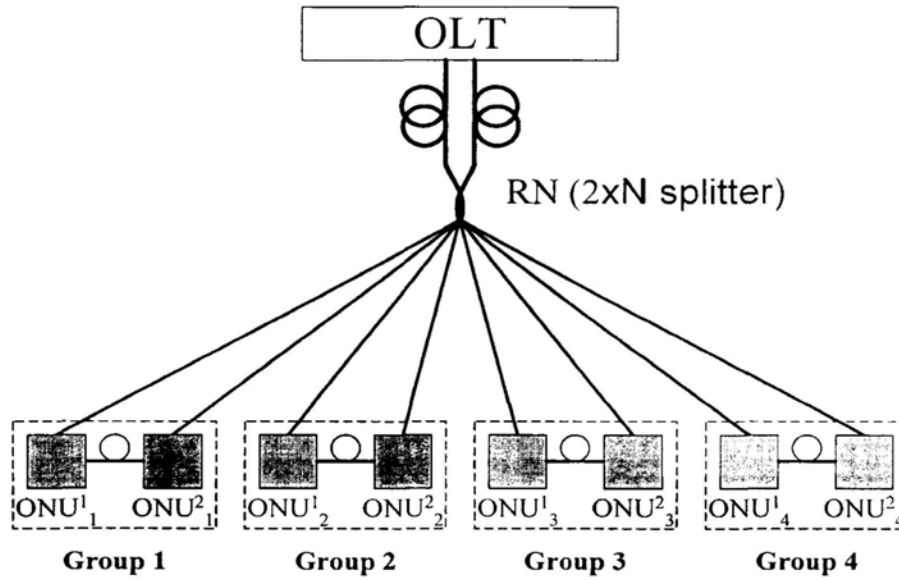


Fig 2.16 Proposed broadcast and select WDM-PON network architecture with eight ONUs

At the subscriber side, two adjacent ONUs (labeled as  $ONU^1_i$  and  $ONU^2_i$ ) are assigned to one group (i) and they are inter-connected by a pair of fiber links, as shown in Fig 2.17 (a). At  $ONU^1_i$ , a Broadcast/Dedicated band filter (B/D filter) is used to separate the traffic into two different paths, one for the dedicated service and the other for the broadcast service, before they are combined together by another band filter. Such B/D filter can be realized by using three-port thin film filter (TFF) of 1550-nm center wavelength, which is a commercially available component in which a designated wavelength can be dropped from port 1 to port 3 or added from port 3 to port 1. For other wavelengths, they can pass through from port 1 to port 2 without any restraint. For the path carrying the dedicated service, two three-port TFFs with different center wavelengths are cascaded to form a uni-directional OADM: one CWDM wavelength ( $\lambda_{1d}$ ) is dropped as the downstream traffic for  $ONU^1_i$  and the other CWDM wavelength ( $\lambda_{2d}$ ) is added as its upstream traffic. The two wavelengths could be chosen arbitrarily except for the broadcast wavelength ( $\lambda_B$ ). For other wavelengths, they could simply pass through  $ONU^1_i$  without any restraint in both directions. Through the protection fibers inter-connecting the two adjacent ONUs in the same group, these wavelengths can provide the protected traffic for  $ONU^2_i$ . For the path carrying the broadcast service ( $\lambda_B$ ), a 50/50 fiber coupler is used to drop half of the power of the broadcast signals for reception at  $ONU^1_i$ , while the rest would be passed to  $ONU^2_i$  via the fiber inter-connecting the  $ONU^1_i$  and  $ONU^2_i$ . A 1x2 switch is also incorporated in  $ONU^1_i$ . The structure of  $ONU^2_i$  is similar to  $ONU^1_i$  except that its dedicated wavelengths ( $\lambda_{2d}$  and  $\lambda_{2u}$ ) are different. From the above illustration, we can see that the broadcast channel will experience larger loss due to the addition of the fiber coupler for dropping signals.

Fig 2.17 (b) illustrates the protection mechanism of the proposed network architecture, when a fiber failure occurs at the distribution fiber link connecting to  $ONU^1_i$ , for example. In this case, the control circuit at  $ONU^1_i$  detects the power loss of the downstream signal and then automatically triggers its optical switch to change its state. Hence,  $ONU^1_i$  can still communicate with the OLT via the inter-connecting fiber and the distribution fiber connecting to  $ONU^2_i$ , without interrupting other in-service data streams. Consequently, the affected traffic due to the fiber failure is promptly restored and thus assuring the survivability of the proposed network.

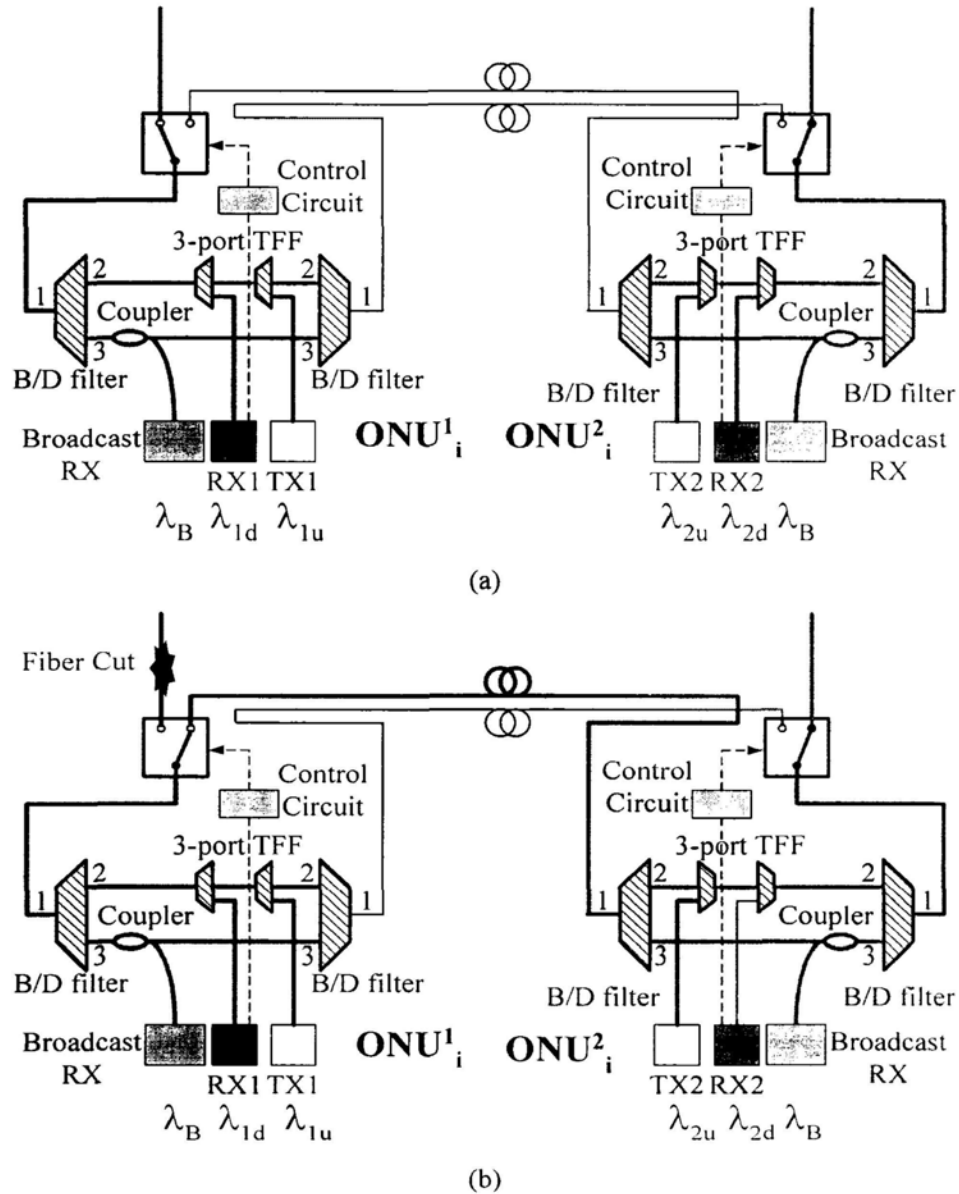


Fig 2.17 ONU design: (a) normal mode; (b) protection mode: bold lines show the active fibers for data communication. B/D filter: Broadcast/Dedicated band filter

### 2.2.2.3 Experimental Demonstration

The experimental setup was similar to Fig 2.16 except that only the distribution fiber failure protection was demonstrated. A 1×16 splitter constructed from two stages of 1×4 fiber splitters with a total insertion loss of 12.5 dB was used at the RN to simulate a PON serving 16 ONUs. The transmission fiber between the OLT and the ONU was 20-km SSMF. Only one group of ONUs, as shown in Fig 2.17, was implemented. Five commercial CWDM Gigabit Ethernet (GbE) small form pluggable (SFP) transceivers were used in the demonstration. Among them, the broadcast wavelength was chosen to be 1550 nm, while ONU<sup>1</sup><sub>i</sub> was assigned with 1530 nm and 1610 nm for the downstream and upstream signals, respectively. Similarly, ONU<sup>2</sup><sub>i</sub> was assigned with 1490 nm (downstream) and 1570 nm (upstream). The interconnecting fiber length was 1 km. To simulate the fiber cut scenario, the distribution fiber of ONU<sup>1</sup><sub>i</sub> was intentionally disconnected. With our proposed automatic protection scheme described above, the affected ONU could automatically restore its traffic. With this setup, we measured the BER performance using 1.25-Gb/s PRBS data for various traffics (dedicated upstream and downstream, as well as broadcast) of ONU<sup>1</sup><sub>i</sub> in both normal and protection modes, and the measurement results were depicted in Fig 2.18 and Fig 2.19. Here, the 1.25-Gb/s data was used to simulate the GbE signal. The output powers of these transceivers were varied from 0 dBm to 2 dBm. In all cases, the measured receiver sensitivities were around -28 dBm and the induced power penalties were negligible (<0.5 dB), which might be attributed to the chromatic dispersion of the fiber. There were 8-10 dB system margins for the dedicated traffic depending on the output power of the CWDM GbE transceivers. The system margins for the broadcast traffic were 6.3 dB (normal mode) and 2.7 dB (protection mode), respectively. This is because the broadcast traffic passed through the additional fiber couplers to drop the signals, thus inducing a larger power loss. The switching time (3 ms) was also measured, as shown in the inset of Fig 2.19.

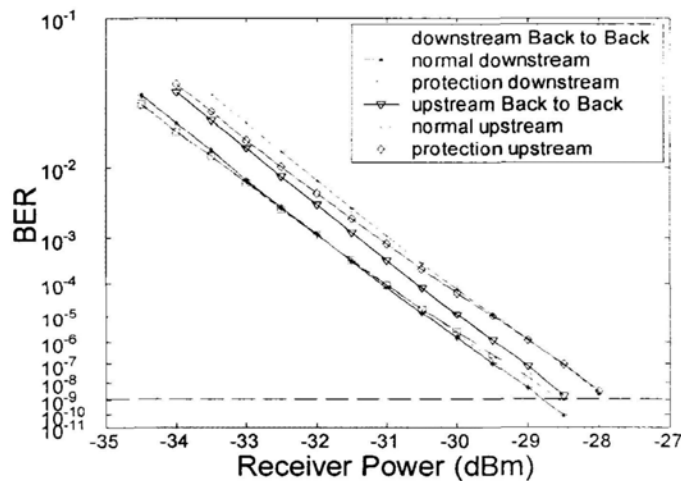


Fig 2.18 BER measurements of the dedicated traffics under normal and protection modes

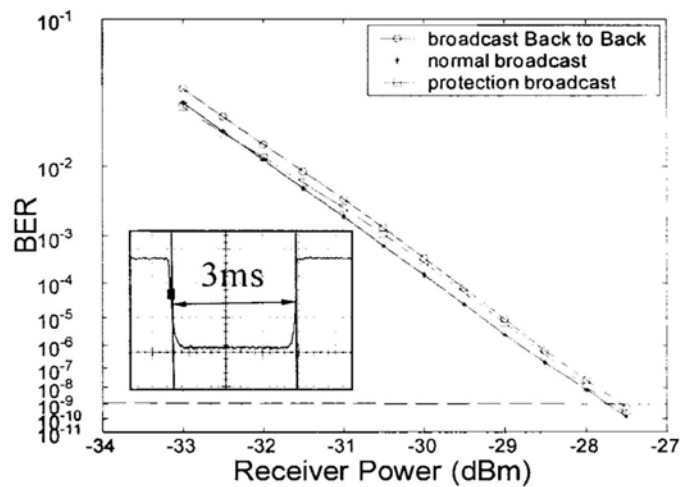


Fig 2.19 BER measurements of the broadcast traffics under normal and protection modes; inset shows the protection characteristics by monitoring the received power of the downstream signals

#### 2.2.2.4 Discussions

One important issue in this access network architecture is the relatively large loss induced at the RN by the fiber coupler/splitter. Usually, such a network will support 16 or 32 ONUs with the maximal transmission length of 20 km. In the case of 16 ONUs as we have demonstrated in the experiment, there were 8-10 dB system margins for the dedicated traffic. If we consider the entire CWDM wavelength range (except the wavelength residing near the water peak), the system margin can still be kept above 2 dB. For a network with 32 ONUs, there is additional loss of  $\geq 3$  dB induced by the  $1 \times 32$  splitter compared with the  $1 \times 16$  splitter, thus avalanche photo-diode (APD) receivers may be needed to guarantee enough system power margin.

Another limitation on the access network size is the number of wavelength channels. When only the CWDM standard wavelengths are used, our scheme can only support 8 ONUs. To support 16 ONUs, a hybrid CWDM/DWDM scheme is necessary. For instance, 16 DWDM wavelengths around the 1550nm range can be assigned for the dedicated downstream traffics, while 16 other CWDM wavelengths can be used for dedicated upstream traffics. In this case, the broadcast wavelength might be required to be shifted from 1550 nm to other wavelength window, such as 1310 nm where the fiber loss is higher. In the future, when the DWDM components become an economical option for access network applications, this structure can support 32 ONUs. For example, 64 DWDM wavelengths in the C+L bands are used for dedicated services and 1310 nm

is assigned for broadcast service. They can be easily separated with the 1.3  $\mu\text{m}$ /1.5  $\mu\text{m}$  band filters.

At last, the security advantage provided by the conventional WDM-PON might be undermined in our scheme due to the sharing of signals in all of the distribution fiber. Thus, the security issue has to be addressed using the mature encryption techniques in the electronic domain, as in the current PON.

### **2.2.2.5 Summary**

A broadcast and select WDM-PON is proposed and demonstrated where both the broadcast and the dedicated broadband services can be provided. By assigning two adjacent ONUs into one group and connecting them with an additional pair of fiber, fast automatic optical protection against distribution fiber failure can be realized. The transmission characteristics using 1.25-Gb/s CWDM GbE transceivers and system restoration against fiber failure have been experimentally demonstrated and characterized. This scheme also provides more flexibility and the possibility for smooth and graceful upgrade from the current TDM-PON to WDM-POM as the broadband service demand increases in the future.

## **2.2.3 Single-Fiber Self-Healing CWDM Metro/Access Ring Network with Unidirectional OADM**

### **2.2.3.1 Introduction**

Recently, hub/access-node ring architecture has emerged as a promising approach for WDM metro-access ring networks. The traffic from the access nodes (AN) is transmitted/received to/from a hub, and the hub is responsible for controlling and exchanging the traffic between the ANs and the higher layer network. Multiple optical transceivers, each of a distinct wavelength, are resided at the hub; while each of them serves the point to point communication between the hub and the designated AN. Hence, this effectively forms a physical-ring/logical-star architecture. Conventionally, a dual-ring has been employed for protection against fiber failure [36, 37]. Nevertheless, single-fiber bi-directional self-healing ring [38, 39] has recently been emerging, for reducing the required amount of fiber by half. However, they were mostly based on the specially

designed bi-directional add/drop multiplexer (BADM) [38, 39], which made the network design complicated. In this section, we propose and experimentally demonstrate a simple and effective CWDM hub/access-node single-fiber ring network architecture with automatic protection against any fiber failure. It utilizes the commercially available low-cost thin-film unidirectional OADM, instead of BADM, at each AN. As a result, the network design is greatly simplified and thus becomes more cost-effective.

### 2.2.3.2 Principle of Operation

In [38, 39], the multiple wavelength channels are divided into two groups: one for the working channels and the other for protection channels (or carrying the low priority traffic without protection). They are counter-propagating in clockwise (CW) and counter-clockwise (CCW) directions, respectively towards the destined AN, in which a specially designed BADM is used. If the working channel fails due to fiber cut, the traffic will be switched to the protection channel automatically, thus assuring the survivability of the system. However, the ring network can also be viewed from another perspective, which provides two different paths for the same connection between the hub and any AN. Thus, one path can be assigned as the working path and the other as the protection path. Under normal operation, these two different paths carry the same traffic for the connection and the destined AN retrieves the traffic from the working path. However, in case of fiber failure in the working path, the AN can switch to the protection path to retrieve the same traffic. With this optical path diversity, fast traffic restoration can be achieved.

Fig 2.20 (a) shows the proposed CWDM metro access network architecture with protection function. It consists of one hub and  $N$  ANs (here,  $N=4$  for simplicity) distributed around a single-fiber ring. At the hub, it includes  $N$  pairs of CWDM transmitters (Tx) and receivers (Rx), one CWDM multiplexer/demultiplexer (MUX/DMUX) and one  $1 \times 2$  50/50 fiber coupler. Each pair of Tx and Rx corresponds to one AN, responsible for the downstream and the upstream traffic respectively. For each Tx or Rx, a distinct wavelength is assigned. For instance, Tx<sub>2d</sub> at the hub with the wavelength  $\lambda_{2d}$  is designated for transmitting the downstream communication with AN<sub>2</sub>: while Rx<sub>2u</sub> with the wavelength  $\lambda_{2u}$  is for receiving the upstream traffic from AN<sub>2</sub>. The hub is connected to the ring via the  $1 \times 2$  50/50 fiber coupler. The ANs are labeled in ascending order along the CW direction on the ring network.

Fig 2.20 (b) illustrates the structure of AN<sub>2</sub>, for example. It consists of one  $2 \times 2$  optical switch, one unidirectional CWDM OADM and a pair of Rx and Tx, which are named as Rx<sub>2d</sub> and Tx<sub>2u</sub>, and are matched to the Tx<sub>2d</sub> and Rx<sub>2u</sub> at the hub, respectively. This OADM is responsible to add channel  $\lambda_{2u}$  and to drop channel  $\lambda_{2d}$  at AN<sub>2</sub>. The channel add-drop is performed via

commercially available low cost CWDM 3-port TFF. For a specific CWDM wavelength, it can be dropped from port 1 to port 3 or added from port 3 to port 1. For other wavelengths, they can pass between port 1 and port 2 without any restraint. Under normal operation, the 2×2 optical switch is set in bar state. Thus, AN2 can receive/send data from/to the hub through the CCW/CW direction. For other wavelength channels that are not destined to AN2, they can just pass through AN2 from either direction.

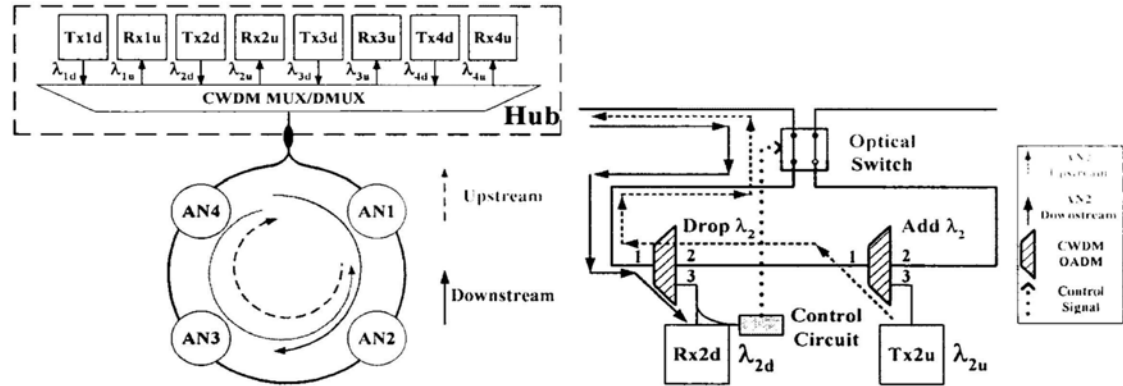


Fig 2.20 (a) Proposed single-fiber self-healing ring network architecture; (b) Structure of AN2 in the normal state: solid and dash arrows show the routing paths of the downstream and upstream traffic of AN2 respectively; both of the traffic for AN2 will pass through the left hand fiber, so AN2 can receive/send data from/to the hub through the CCW/CW direction

Fig 2.21 illustrates the protection mechanism of the proposed network architecture. in which a fiber failure occurs between AN2 and AN3, for example. In this case, the control circuit at AN2 as well as all subsequent ANs in the CCW direction (e.g. AN1) detects the loss of the downstream signal from the CCW direction. This automatically triggers its optical switch to change from bar state to cross state. Hence, AN2 as well as all affected ANs (say AN1) can still communicate with the hub via the CW direction of the ring without interrupting other in-service data streams. AN3 and AN4 remain un-affected. Consequently, the affected traffics due to the fiber failure are promptly restored and thus this assures the survivability of the proposed network.

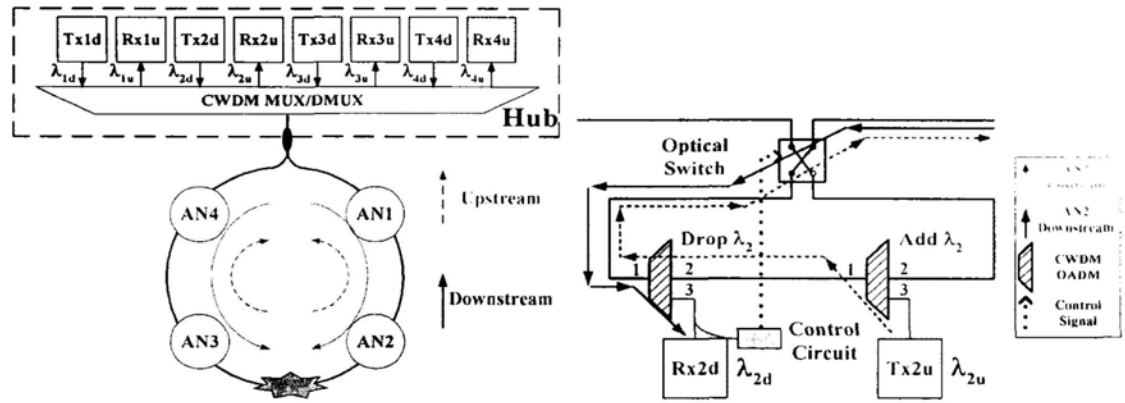


Fig 2.21 (a) Network structure in case of fiber cut between AN2 and AN3; (b) Structure of AN2 in the protection state: solid and dash arrows show the routing paths of the downstream and upstream traffic of AN2 respectively; both of the traffic for AN2 will pass through the right hand fiber, so AN2 can still communicate with the hub via the other direction of the ring without interrupting other in-service data streams

### 2.2.3.3 Experimental Demonstration

The experimental setup was shown in Fig 2.22, similar to Fig 2.20 except that it only includes one Hub and three ANs: AN1, AN2 and AN3, in ascending order along the CW direction on the ring network. The lengths of single mode fiber (SMF) spans between the Hub and AN1, AN1 and AN2, AN2 and AN3, AN3 and the Hub are 8.8km, 6.6km, 1.0km and 8.8km respectively. Six commercial CWDM GbE SFP transceivers were used for the demonstration. In principle, the wavelengths can be assigned freely. In our experiment, we adopted the following allocation plan. AN1 was assigned with 1590 nm and 1510 nm for the downstream and the upstream, respectively. Similarly, AN2 was assigned with 1610 nm (downstream) and 1530 nm (upstream); while AN3 was assigned with 1570 nm (downstream) and 1490 nm (upstream). The optical switches used at the ANs were commercially available opto-mechanical switches, and their switching times (including the response time of the control circuit) were measured to be 5 ms (at AN1), 3 ms (at AN2) and 8 ms (at AN3), respectively. The discrepancy in the switching time was due to the variance in the product performance. However, the switching times for all of the switches were below 10 ms. To simulate the fiber cut scenario, the fiber link between AN2 and AN3 was intentionally disconnected. With our proposed automatic protection scheme described above, the affected AN1 and AN2 could automatically restore their traffic.

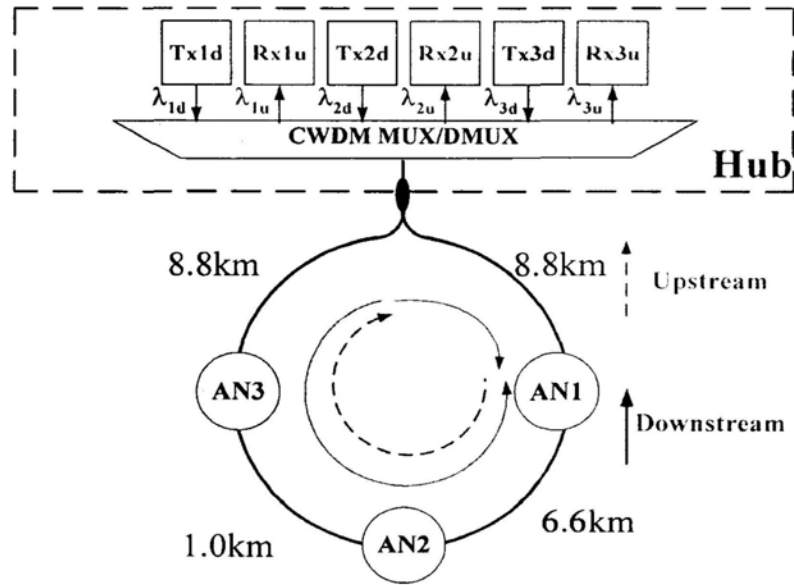


Fig 2.22 Experimental setup of the proposed single-fiber self-healing CWDM metro/access ring network

With this setup, we measured the BER performance using 1.25-Gb/s  $2^{23}$ -1 PRBS data for both upstream and downstream traffic of AN1 and AN2 in normal and protection modes, and the measurement results were depicted in Fig 2.23. Here, the 1.25-Gb/s data was used to represent the data rate of GbE signal. In all cases, the measured receiver sensitivities varied from -28.0 dBm to -26.5 dBm and the induced power penalties were negligible ( $<0.5$  dB), which were attributed to the chromatic dispersion of the fiber. The discrepancy in the BER slopes of the upstream and the downstream data may be attributed to the different performance of the respective receivers. By monitoring the received power of the downstream signal at AN1 and AN2, we have also measured the restoration times in case of the simulated fiber cut, and the results are shown in Fig 2.24. The measured restoration times were about 5 ms (at AN1) and 5.2 ms (at AN2), respectively. The restoration time curve of AN2 is more complicated than that of AN1, implying the restoration procedure of AN2: At first, the AN2 will detect the signal power drop and change its switching state (switching time: 3 ms) to obtain the traffic from another direction, as indicated in Fig 2.24 (b). At the same time, AN1 will also change its own switching state to react to the fiber cut, causing a temporary traffic interrupt. Since the switching time of AN1 is larger than that of AN2, AN2 will be influenced by this interrupt, showing another signal power drop on the curve, until the switch state of AN1 becomes stable. For a larger ring network which involves more ANs, the transients might become more complicated and cause the oscillations of the switching states. To solve this problem, a wait period could be added to the control circuit at each AN such that its switching can be completed at the time instant when all relevant switching transients from other affected ANs have ceased. This wait period at each AN could be determined by subtracting its intrinsic switching time from the maximum switching time

among all ANs. The signal propagation time between the ANs would be negligible as it is usually much shorter than 1 ms for metro-access applications. Consequently, traffic restoration of the whole system could be achieved with a total restoration time no more than the maximum switching time among all ANs.

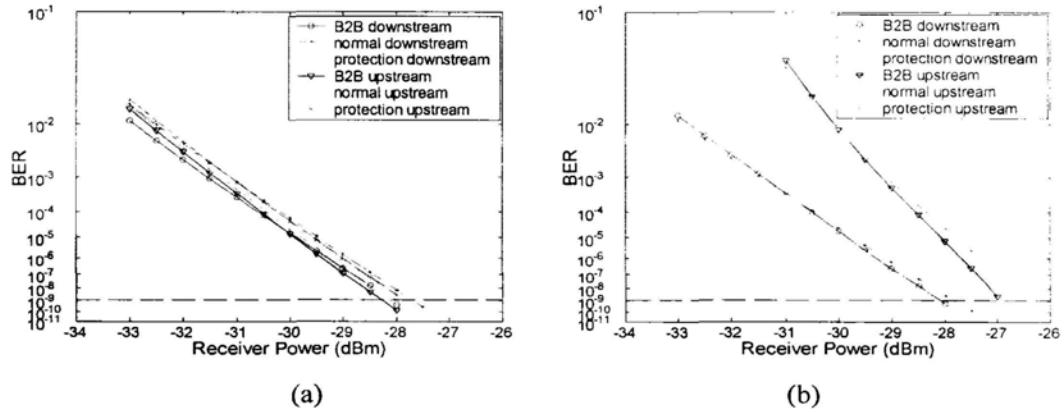


Fig 2.23 BER measurements under normal and protection modes: (a) AN1; (b) AN2

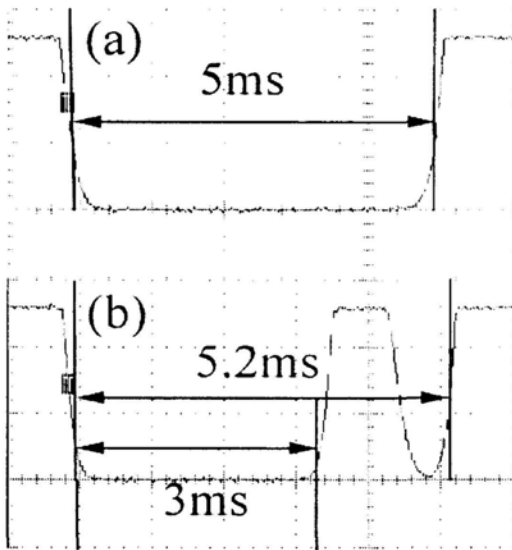


Fig 2.24 Measured protection characteristics by monitoring the received power of the downstream signals: (a) AN1; (b) AN2

### 2.2.3.4 Discussion

In such a single-fiber ring network with bi-directional transmission, Rayleigh backscattering induced crosstalk may degrade the system performance. The induced crosstalk can be divided

into inter-band crosstalk and intra-band crosstalk. When the counter-propagating signals are of different wavelengths, inter-band crosstalk exists. However, with our proposed scheme, this crosstalk can be readily filtered out by the in-line WDM devices. When the wavelengths of the counter-propagating signals are the same, it will cause intra-band crosstalk, but this situation will not occur in this scheme. For the upstream traffic, it will choose only one path from the AN to the hub; for the downstream traffic, the traffic from both directions will terminate on the same OADM (one is dropped and the other is blocked by this OADM). As a result, the Rayleigh backscattering has practically no effect on the performance of the system, as observed in our experiment. This is indeed an advantage of our proposed architecture.

Without the optical amplification, the power budgets of the GbE transceivers used in the experiment are above 26 dB. The insertion losses of the CWDM MUX/DMUX and the 1×2 fiber coupler are about 1 dB and 3.2 dB, respectively. When the signal passes through each AN, it will suffer from about 1 dB power loss due to the in-line TFF and the optical switch. We assume the total ring length is 20 km. Since the fiber loss over the entire CWDM wavelength range (except the wavelengths residing near the water peak) is no more than 0.5 dB/km, the transmission loss budget will be up to 10 dB. Thus, the proposed network can support 12 ANs. However, the total CWDM wavelength number is 18, which can only support up to 9 ANs. In order to support more ANs, the hybrid CWDM/DWDM architecture could be deployed in the future. A larger ring network can also be supported without sacrificing the number of ANs if we adopt powerful transceivers with higher power budget and/or suitable optical amplifiers in the system.

### **2.2.3.5 Summary**

We have proposed and demonstrated a simple and effective CWDM metro access network architecture using unidirectional OADMs for optical protection in a hub/access-node single-fiber ring. The transmission characteristics using 1.25-Gb/s CWDM transceivers and fast automatic protection against fiber failure have been experimentally demonstrated and characterized. This physical-ring / logical-star architecture provides greater simplicity over previous designs requiring bi-directional ADM. This CWDM metro access network architecture is data rate transparent and can be readily extended for application in multi-wavelength 10GbE single-fiber ring networks.

## 2.3 In-Service Fault Surveillance Scheme in the Current TDM-PON

### 2.3.1 Introduction

PON plays an active role in alleviating the last mile bottleneck for the next generation broadband optical access network. With the enormous communication capacity of the fiber link, any service outage due to fiber cut will lead to tremendous loss in business. Therefore, a simple but effective monitoring scheme is highly desirable for timely fault identification along the fiber link. Besides, the monitoring should be performed constantly while other channels are still in service to maximize the link utilization.

In a tree-structured PON, fiber failure detection using conventional optical time domain reflectometer (OTDR) is not suitable since the Rayleigh back-scattered light from different branches cannot be distinguished at the OTDR. In order to identify the failed fiber branch, several methods based on multi-wavelength OTDR [40, 41], and reflection of optical amplifier's residual ASE [42], have been proposed. However, these methods require rather expensive devices such as wavelength tunable pulse source or EDFA as the monitoring light source, resulting in high maintenance cost. In this section, we propose and demonstrate a novel supervisory scheme, which is based on RF spectral analysis proposed in [43], using cost-effective FP laser as the monitoring light source. In this scheme, the identifiers for all fiber branches are generated optically and share a common supervisory channel, nominally at the same wavelength. By analyzing the RF spectra of the common supervisory channel received at the central office, the multiple superimposed identifiers can be easily resolved and thus the status of all branches can be monitored continuously.

### 2.3.2 Principle of Operation

Fig 2.25 (a) shows the configuration of the monitoring light source. It consists of an FP-laser, an optical coupler and a mirror. A portion of the FP-laser power will be coupled into the lower port of the coupler and then reflected back to FP-laser by the mirror. In this way, an external fiber lasing cavity is formed. Consequently, the output of the monitoring light source will comprise a train of external cavity modes (in RF domain) with a unique mode spacing, corresponding to the unique external cavity length, as shown in Fig 2.25 (b). This unique characteristic serves as an

identification tag for the respective optical network unit (ONU) branch. For instance, if the cavity length of the monitoring light source at the end of the  $k$ -th fiber branch is  $L_k$ , the generated cavity mode spacing will be  $\Delta f_k = c/2nL_k$ , where  $c$  is the light velocity and  $n$  is the refractive index of fiber. The cavity length  $L_k$  can be adjusted easily by using different lengths of fiber in the cavity. Note that the FP-laser is operated in CW condition, not only simplifying the driving circuit design, but also providing the potential to reduce the cost of the FP-laser.

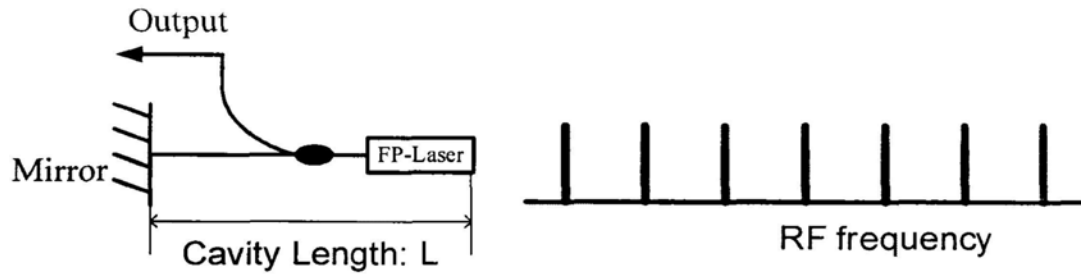


Fig 2.25 (a) Configuration of monitoring light source; (b) Generated RF frequency cavity modes

Fig 2.26 shows the proposed network architecture consisting of  $N$  branches. At each ONU, a proposed monitoring light source with a unique cavity mode spacing is attached and this serves to generate a unique identification tags for ONU branch labeling purpose. The working wavelength of the FP-laser should be chosen to be nominally the same for all branches and lies outside the transmission band for data wavelengths. The output of the monitoring light source will be coupled onto the fiber link and combined with the upstream data channel through WC. These monitoring signals with different identification tags generated from all ONUs will be superimposed together as they converge into the feeder fiber at the remote node and thus forms the common supervisory channel. At the central office, the received supervisory channel will be separated from the upstream data channel by another WC and fed into a monitoring receiver, where the monitoring signal will be detected and spectrally analyzed in RF domain. The individual identification tags  $F_k$  ( $k \in 1: N$ ) can be easily resolved by applying Fast Fourier Transform (FFT) to the obtained RF spectrum, each of which is represented by a distinctive peak in the output FFT waveform, as illustrated in Fig 2.27. For a normal fiber state, all of the  $N$  identification tags will be present. However, when one of the fiber branches, say the  $i$ -th branch fails, the corresponding identification tag,  $F_i$ , will be significantly reduced in amplitude in the obtained FFT waveform at the central office, indicating a fiber cut at that particular fiber branch.

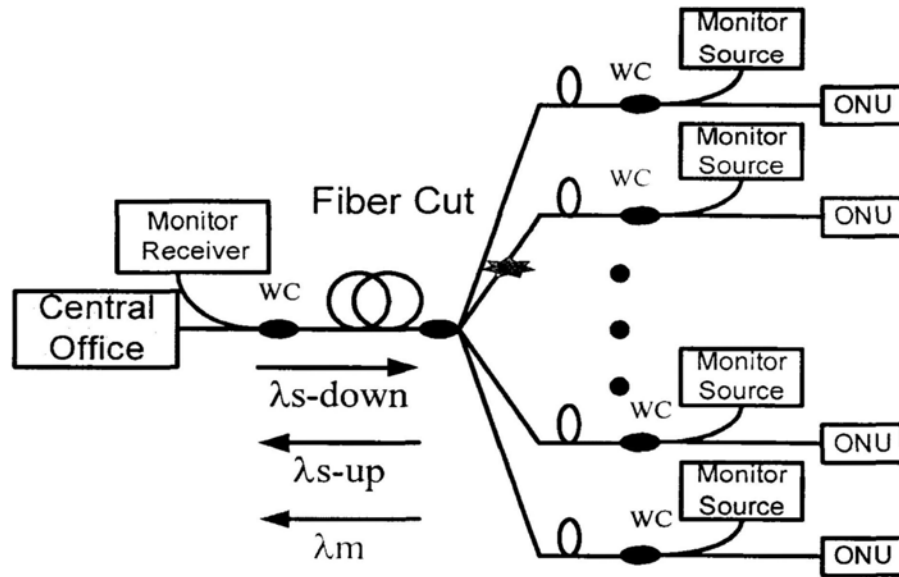


Fig 2.26 Network architecture of the proposed monitoring scheme;  $\lambda_{data-down}$ : downstream data channel;  $\lambda_{data-up}$ : upstream data channel;  $\lambda_m$ : monitoring channel

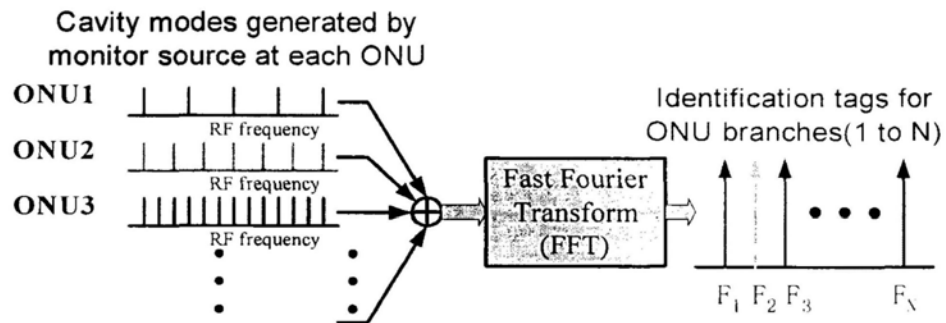


Fig 2.27 Operating principle of the proposed monitoring scheme

### 2.3.3 Experimental Demonstration

The experimental setup was similar to Fig 2.26. It had four branches with three monitoring light sources placed at branches  $B_{1,3}$  respectively. Branch  $B_4$  was left unmonitored. The wavelength assignment of the data channel and monitoring channel are as follows: the monitoring wavelength was chosen at 1310 nm; the data wavelengths for the upstream and the downstream traffic were at 1550 nm and at 1530 nm, respectively, which were realized with a set of CWDM transceivers. The two data channels were separated by a CWDM MUX/DMUX at the central office and the ONU end.

In each monitoring light source, the output power of the FP-laser was fixed at 0 dBm, followed by an 80/20 fiber coupler. The 20% port was used as the output of the monitoring light source, while the 80% port was used for the lasing cavity. The mirror was realized by the 4% reflectivity of the FC/PC connector end surface, for simplicity. The mode spacing of the three monitoring light sources were measured to be 28.1 MHz, 23.8 MHz and 21.2 MHz, respectively, which means that the corresponding cavity lengths were 3.55 m, 4.20 m and 4.72 m, respectively. These identification monitoring signals containing different cavity modes were superimposed to become the common supervisory channel (all monitoring signals have the same nominal wavelength), which is then transmitted via the 20-km feeder fiber link. At the receiving end, this supervisory channel containing all monitor signals was fed into an AC-coupled photo detector connected to an RF spectrum analyzer. The parameters of this RF spectrum analyzer were set to: 1000-MHz center frequency, 1000-MHz frequency span and 1-MHz resolution bandwidth. Fig 2.28 (a) showed the composite RF spectrum in case of no fault in all of the branches. By applying FFT to it, three distinct peaks,  $F_1$ ,  $F_2$  and  $F_3$  were obtained, as shown in Fig 2.29 (a). The DC component was filtered out numerically before the FFT computation to make the identification tags more clear. The sub-peaks on the right side of the picture were the second-order harmonic components of the peaks. These peaks should be avoided when we allocate the identification tags. To simulate the fault identification process, the fiber branch  $B_2$  was intentionally disconnected. The captured RF spectrum was shown in Fig 2.28 (b), and the resultant FFT output was depicted in Fig 2.29 (b). It was shown that the amplitude of the identification tag  $F_2$  disappeared altogether, which was a clear indication of fiber failure at branch  $B_2$ .

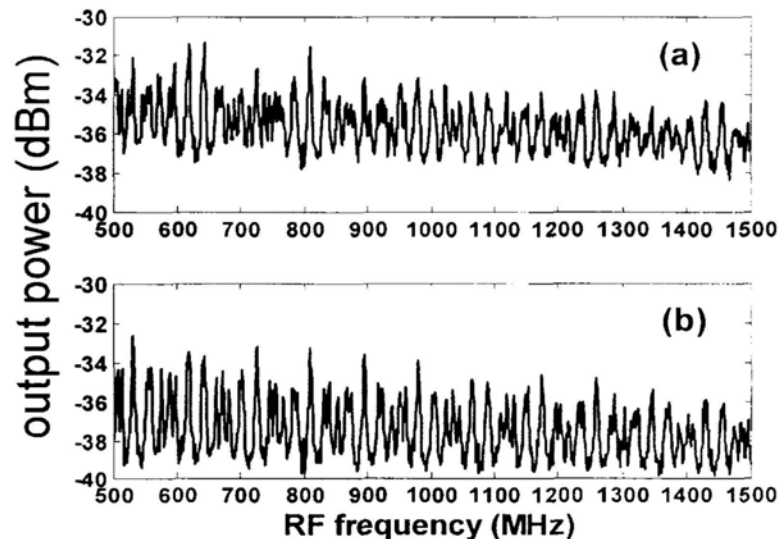


Fig 2.28 RF spectrum of the monitoring channel: (a) healthy state; (b) fiber branch B2 is broken

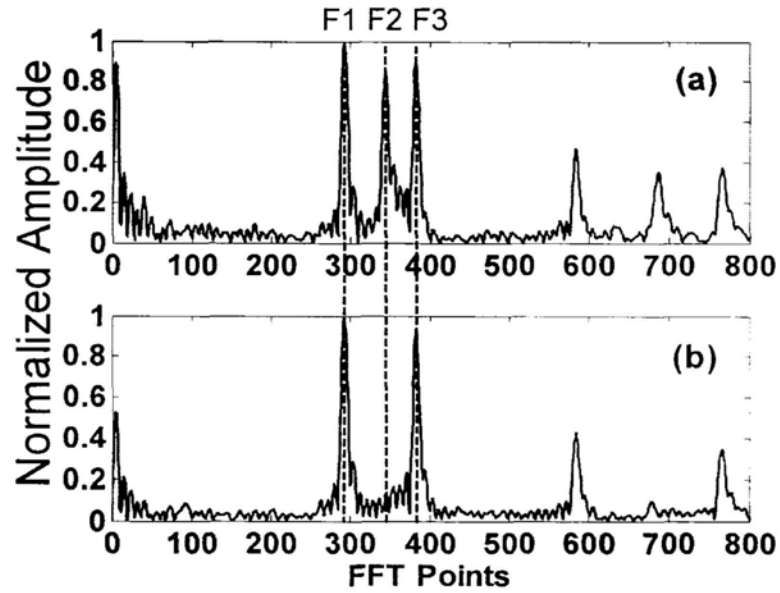


Fig 2.29 Corresponding FFT output: (a) healthy state; (b) fiber branch B2 is broken, where F2 is absent

The non-intrusive nature of this proposed scheme was also confirmed by the BER measurement. Here, we focused on the upstream data channel because it has the same transmission direction as the monitoring channel and is more likely to be affected by the upstream monitoring channel. We used a 1550-nm CWDM transceiver operated at 1.25-Gb/s  $2^{23}$ -1 PRBS NRZ to simulate the upstream transmission. The BER characteristics were measured under three cases: back-to-back; all of the monitoring light sources were turned on; and all of the monitoring light sources were turned off. The corresponding BER curves were shown in Fig 2.30. The results showed that negligible power penalty (0.2 dB at  $10^{-9}$  BER) was observed when the proposed monitoring scheme was applied to a normal transmission link.

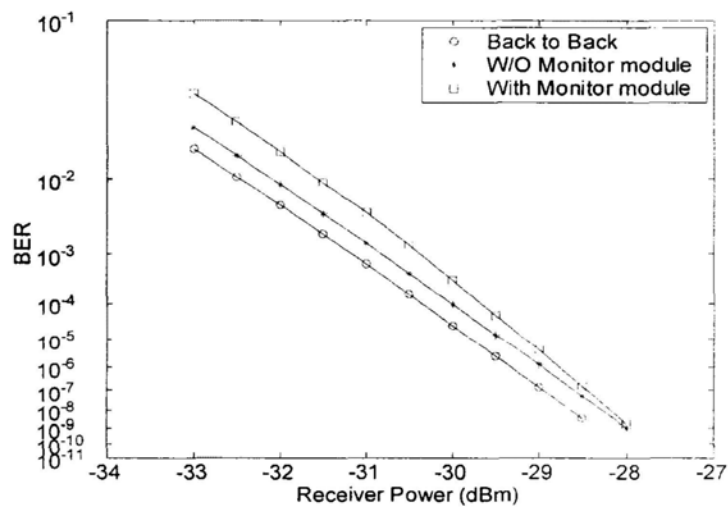


Fig 2.30 BER performance with and without proposed monitoring module

### 2.3.4 Discussion

In theory, each identification tag should be represented by a distinctive peak, in the form of a line, in the output FFT waveform. However, in practice the captured RF frequency span is limited, so such a line will evolve to a narrow band with a certain width, as shown in Fig 2.29. If we assume that the monitoring light source's external cavity length is  $L$ , the captured RF frequency span is  $M$ , and the sampling rate is high enough to fulfill the Nyquist sampling theorem, then the bandwidth of the identification tag's peak should be  $2\pi/M$  after FFT. On the other hand, as the RF signal frequency spacing is  $\Delta f=c/2nL$ , the identification tag should be at the position of  $2\pi/\Delta f=4\pi nL/c$ . In order to distinguish the two different identification tags, their interval should be larger than two times the bandwidth of the peak. Thus  $\Delta(4\pi nL/c) > 4\pi/M$ , and the difference in cavity length should satisfy  $\Delta L > c/nM$ . In our experiment,  $M=1$  GHz,  $n=1.5$ , and  $c=3\times 10^8$  m/s, so  $\Delta L > 0.2$  m. If the cavity lengths are varied from 5 m to 10 m, then this scheme can accommodate about 24 ONUs. On the other hand, as observed in the experiment, the second-order harmonic components of the identification tag peaks in the FFT spectra may interfere with other identification tag peaks and thus should be avoided. One of the simplest ways to achieve this goal is to make sure that the longest cavity length is not beyond two times of the shortest one. As mentioned in the previous paragraph, if the cavity lengths are varied from 5 m to 10 m, this condition can be fulfilled. Other cavity length range can also be used, for instance, 2 m to 4 m. However, it will limit the ONU number to 9. Considering that the ONU number in current PON is usually 16 or 32, the cavity length range can be set to 5 m to 10 m (for 16 ONUs) or 10 m to 20 m (for 32 ONUs), which can support all of the ONUs with enough margins.

In practical applications of the traditional triplex PONs, the wavelengths of 1.48  $\mu\text{m}$  and 1.55  $\mu\text{m}$  are allocated for downstream data and RF video services; while 1.3  $\mu\text{m}$  is for the upstream data service. To ensure that the upstream monitoring wavelength has enough isolation from the 1.3  $\mu\text{m}$  upstream data channel, the 1.2  $\mu\text{m}$  wavelength might be considered as a suitable candidate for the upstream monitoring wavelength.

### 2.3.5 Summary

A novel monitoring scheme for in-service fault identification in PON is proposed and experimentally demonstrated. Identification tags in the form of external cavity modes with unique mode spacing are generated optically using FP-lasers with external fiber cavity. By constantly examining the intensities of all the identifying tags in the FFT output waveform at the

monitoring receiver, the link quality of all fiber branches can be monitored without interrupting the existing data channels.

## **2.4 System Demonstration of the WDM-Based Optical Broadband Access Network**

### **2.4.1 Introduction**

In this section, we report a testbed demonstration of the optical broadband access network using the CWDM metro/access single-fiber ring network architecture with automatic optical protection and restoration function (the operation principle has been described in section 2.2.3). It consists of one Hub and three ANs and six CWDM wavelengths are used. The WDM technologies not only can provide huge bandwidth to subscribers such that they can enjoy various high speed broadband services, but also simplify the service provisioning due to the passive wavelength routing characteristics performed in the optical layer. Based on this testbed, three kinds of emerging broadband services, including high definition (HD) video streaming, 3-dimensional (3D) video streaming and real time video streaming (video conferencing) are operated on this system, where the testbed equipments and results are shown in the Appendix of this thesis with equipment and video photos. This is not only a demonstration of the power of next generation fiber-based broadband access network, but also a trial to show the potential "killer application" to accelerate the progress of the optical fiber communication industry and information technology.

### **2.4.2 Emerging Broadband Services**

#### *A. High-definition television (HDTV)*

HDTV means broadcast of television signals with a higher resolution than traditional formats can allow. The original impetus for developing HDTV comes from the wide-screen movies. Soon after wide-screen was introduced, movie producers discovered that individuals seated in the first few rows enjoyed a level of participation in the action not possible with conventional movies. Evidently, having the screen occupy a great field of view (especially peripherally) significantly increases the sense of "being there".

The majority of proposed HDTV systems are working toward approximately a 100% increase in the number of horizontal and vertical pixels when compared with standard-definition television (SDTV). This typically results in a factor of 2-3 improvement in the angle of the vertical and horizontal fields. Most of HDTV proposals also change the aspect ratio from 4:3 to 16:9 – thus making the image more "movie-like". Currently, the standard resolutions for HDTV include 1080p (1920×1080, non-interlaced), 1080i (1920×1080, interlaced), 720p (1280×720, interlaced) and so on.

The bandwidth required for uncompressed 1080p HDTV is about 1.5 Gb/s. Through the video-image compression technologies, the required bandwidth can be greatly reduced. For instance, using MPEG-2 as the compression codec, the bandwidth can be reduced to 10 Mb/s. However, this kind of lossy compression technology that is used in all digital HDTV storage/transmission systems will then cause the received picture to appear distorted when compared to the uncompressed source. Therefore, the tradeoff between the bandwidth and compression ratio is necessary. In the future, when the optics technologies make the storage/transmission bandwidth not a problem, the customers may enjoy the HDTV with better qualities.

#### *B. Three-dimensional television (3D TV)*

3D TV is expected to be the next revolution in the history of television, whose purpose is to display an object from arbitrary perspective, so its three-dimensional shape must be known. It has only recently become feasible to deal with the high processing and bandwidth requirements for real-time acquisition, transmission, and display of high-resolution 3D TV content.

In the 3D TV systems, image acquisition consists of an array of hardware-synchronized cameras that capture multiple views of the scene. The multiple video signals are encoded via the current compression standard and then transmitted with existing broadband protocols. At the receiver end, the multiple video signals are decoded, rendered and displayed on a 3D display. Here, 3D rendering means creating 2 views with horizontal parallax, one for each eye, which if perceived by a human will create a depth impression. The 3D TV system can plug into today's digital TV broadcast infrastructure and co-exist in perfect harmony with regular TV. Since current digital broadcast networks can carry hundreds of channels and presumably a thousand or more channels after the introduction of MPEG-4, it is plausible that a number of them can be dedicated to 3D TV. The introduction of 3D TV can proceed gradually, with one 3D channel at first and more to follow, depending on market demand.

#### *C. Video conferencing*

Video conferencing has been around for sometime, and is now gaining in popularity. It cannot replace person to person completely, but in many situations being able to see and hear remote co-workers, does improve communication and cut down on travel time and costs.

For a video conference audio and video signals must be transmitted in real time, i.e., a lot of information has to be sent every second, requiring a very high bandwidth (usually more than several hundred Mb/s). Therefore for digital video some form of compression is required. The type and degree of compression used varies from system to system. It is interesting to note that for most uses, we are more tolerant of poor video than poor audio, and so some systems concentrate on providing consistently good audio. The advancement on transmission technologies may greatly increase the video and audio qualities of video conferencing in the future.

The basic hardware components for video conferencing include: camera (for video capturing), microphone (for audio capturing), monitor (for video output), speakers (for audio output), video board (to capture the signal from the camera and convert it to digital form) and network card (for connecting to the network for transmission).

### **2.4.3 Testbed Description**

The testbed setup is shown in Fig 2.31. It only includes one Hub and three ANs: AN1, AN2 and AN3, in ascending order along the CW direction on the ring network. The lengths of SMF spans between the Hub and AN1, AN1 and AN2, AN2 and AN3, AN3 and the Hub are 8.8km, 6.6km, 1.0km and 8.8km respectively. Six commercial CWDM GbE SFP transceivers are used for the demonstration. AN1 is assigned with 1570 nm and 1490 nm for the downstream and the upstream, respectively. Similarly, AN2 is assigned with 1590 nm (downstream) and 1510 nm (upstream); while AN3 is assigned with 1610 nm (downstream) and 1530 nm (upstream). The Hub is equipped with two projectors for 3D video streaming and the Cisco switch used here is responsible for controlling and exchanging the traffic between the ANs and the higher layer network. The ANs are equipped with widescreen liquid-crystal display (LCD) and digital video (DV) to demonstrate the HD and real time streaming.

The schematic diagram of the Hub is shown in Fig 2.32. Three CWDM transceivers with the nominal center wavelengths of 1570 nm, 1590 nm and 1610 nm are located at the Hub. They are plugged into the SFP GbE optical ports of one Cisco 3750 switch (model number: WS-C3750-48TS-S, including 4 SFP ports and 48 10/100 Mbps ports). Two of the 10/100 Mbps ports are used. One is used to connect the higher layer network (i.e. Department LAN); the other is used to

connect the local equipments of the Hub. Here, the local equipment is one work station (Model number: Dell Precision 670n), which is linked to two parallel projectors (Model number: Dell MP 2300). This work station can be used for 3D display.

Fig 2.33 shows the schematic diagram of the AN. At each AN, one CWDM transceiver with the nominal center wavelength of 1490 nm (AN1) or 1510 nm (AN2) or 1530 nm (AN3) is used. It will be plugged into the SFP GbE optical port of one Cisco 3750 switch (model number: WS-C3750-24TS-S, including 2 SFP ports and 24 10/100 Mbps ports). One of the 10/100 Mbps port is used to connect the local equipments at each AN. Here, the local equipment is one PC (Model number: Dell Optiplex GX620DT) that is linked to one widescreen 24" LCD monitor. It can be used for HD display. The DV camera (Here, Sony HD video cameras are used. Model number: HDR-FX1E or HDR-HC1E) can also be connected to this PC via the 1394 card, which is used for real time video capturing.

Among the three emerging broadband services, HD video streaming requires 10 Mb/s bandwidth; 3D video streaming requires up to 20 Mb/s bandwidth (depending on the quality of the video) and real time streaming requires 30 Mb/s. As a contrast, one CWDM wavelength used here can provide 1 Gb/s capacity, much larger than the service required bandwidth, proving the power of WDM technologies in the future broadband service delivery.

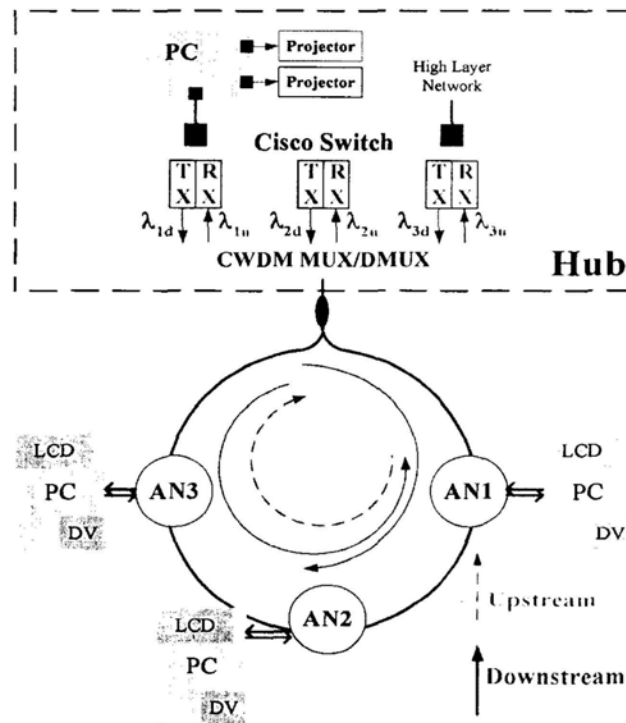


Fig 2.31 Testbed setup

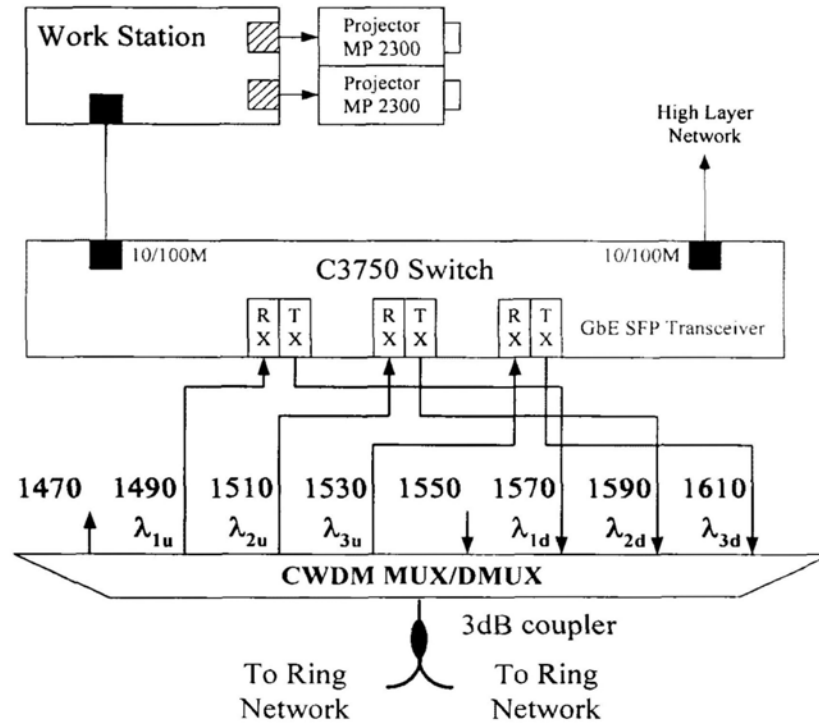


Fig 2.32 Schematic diagram of the Hub

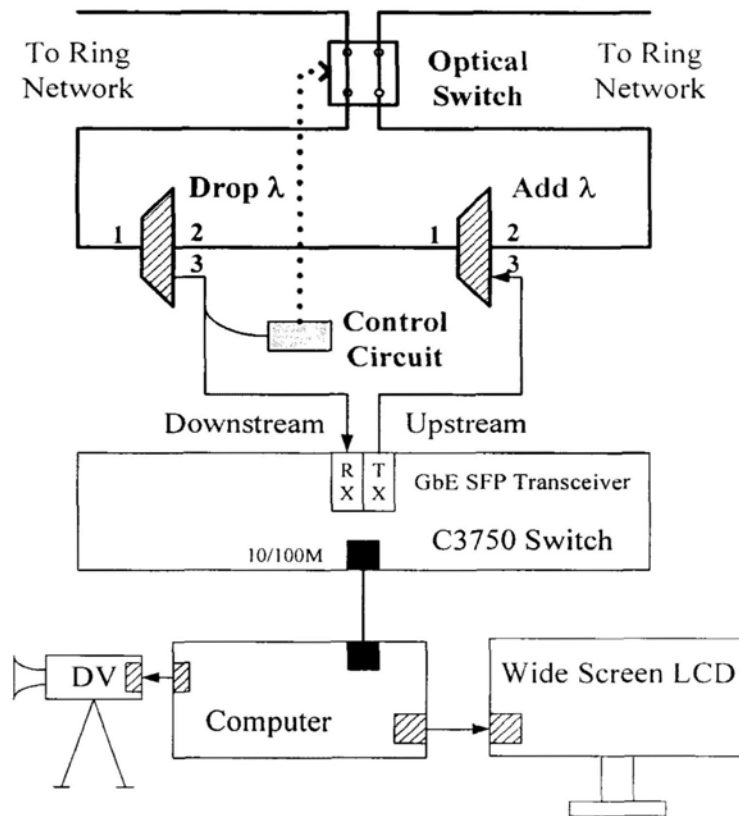


Fig 2.33 Schematic diagram of the Access Node (AN)

## **2.4.4 Summary and Future Work**

This section reports a testbed demonstration of the optical broadband access network using the CWDM metro/access single-fiber ring network architecture with automatic optical protection and restoration function. Based on this testbed, three kinds of emerging broadband services, including HD video streaming, 3D video streaming and real time video streaming are operated on this system. Among them, HD video streaming is a very promising application, which surely will step into our daily lives in the near future. Real time video streaming will find application in video conferencing and video phone, whose main initial customers will be the commercial companies. With the cost reduction of this technology, the average family customers may also be able to enjoy this service in the predictable future.

The future work includes the following three aspects:

1. Wireless broadband technologies can be incorporated at the edge of this testbed to show a more complete broadband access to end users with more flexibility and mobility.
2. This testbed can be extended for applications in multi-wavelength 10 GbE network when the corresponding 10 GbE transceivers are commercially available.
3. Upgrading this testbed to support more broadband services, such as HD real-time video streaming. It might be very useful in medical and educational applications and so on.

## **2.5 Summary**

In this chapter, we first briefly review the background on current broadband optical fiber access network technologies and their deployments in industry. Then, several novel network architecture designs are proposed and experimentally demonstrated to improve the network reliability and functionality as well as the reduction of system complexity. At last, one system testbed demonstration of the WDM-based optical broadband access network is presented to show the power of WDM technologies in future advanced broadband services delivery.

## Chapter 3 All-Optical Nonlinear Signal Processing Technologies

### 3.1 NOLM Structure Design and Its Application

#### 3.1.1 Introduction on NOLM

Nonlinear optical loop mirror (NOLM) structure was first proposed in reference [12] in 1988 and has found various applications in the field of all-optical nonlinear signal processing, such as optical signal regeneration, switching, demultiplexing and so on. The basic structure is shown in Fig 3.1, which primarily consists of one 2×2 coupler and a block of nonlinear medium (usually a span of nonlinear fiber) to form a loop. In practice, a polarization controller (PC) should also be incorporated into the loop to compensate the natural birefringence of the fiber in the loop, which is not shown here.

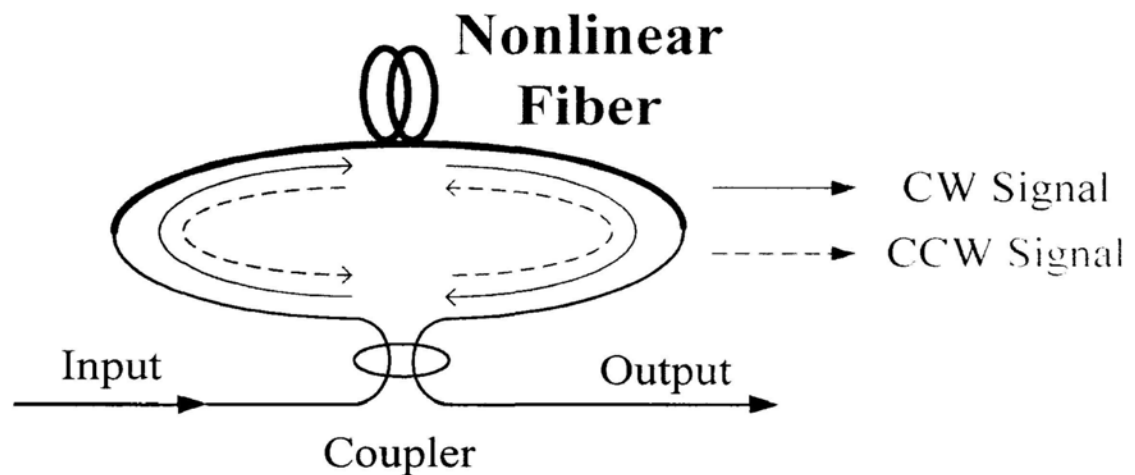


Fig 3.1 Basic NOLM structure

The operation principle is as the following:

First, let's consider the symmetrical case, which means that the coupling ratio of the coupler in the NOLM is 50% and there is no other asymmetrical components added into the loop. In this case, a single input is split into two counter-propagating lights at the coupler equally, which return in coincidence to recombine at the coupler. This is because they follow the same path in the opposite directions, so the optical path length is precisely the same for both propagating lights, which is an important feature of this device. Since the loop is symmetrical, the two lights experience the same phase shift in the loop. Thus, the two overlapping lights will interfere with each other in phase and all of the light will be reflected back to the input port, just like a mirror. This is where the name "loop mirror" comes from and this state is called the "mirror state".

Now, if we introduce some imbalance between two counter-propagating lights, the phase shift between them will not be the same. Thus, the interference of the two lights will cause some of the light to be switched out from the output port. In particular, if the phase shift is exactly  $\pi$ , all of the input light will appear at output port, which is called the "through state".

The phase shift in the loop can be induced via self-phase modulation (SPM) or cross-phase modulation (XPM) effect of the fiber nonlinearity. In the following, we discuss these two cases, respectively.

#### *A. SPM effect-based NOLM*

In this category, there are several ways to introduce the imbalance between two counter-propagating lights:

The first method is illustrated in [12]. The structure is the same as Fig 3.1, except that the coupling ratio of the coupler is not 50%. Therefore, the induced phase shift during propagation will no longer be identical for the two paths since the phase shift due to SPM effect is intensity dependent. This is a quite simple scheme, and the main shortcoming of this method is that it can not achieve a complete mirror state. In other words, there is always some light appearing at the output port.

The second way is to asymmetrically place a bi-directional optical amplifier in the loop (the coupling ratio of the coupler should be kept at 50%), as shown in Fig 3.2, which is called nonlinear amplifying loop mirror (NALM) [44]. Thus, the CW light will have much higher power intensity than the CCW light, resulting in different phase shifts induced during the propagation in the loop. The disadvantage of NALM is that this is an active device, increasing the

complexity in operation. A similar architecture replaces the optical amplifier with a loss component to make the design passive, but it will introduce much higher loss to the signals.

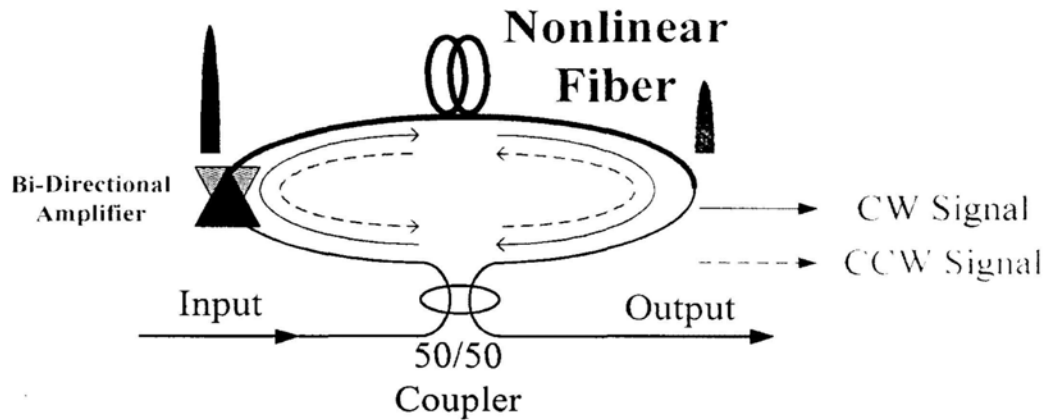


Fig 3.2 Structure of NALM and the operation principle

The third method relies on the asymmetric dispersion map in the loop, as shown in Fig 3.3, which is named as dispersion imbalanced loop mirror (DILM) [45]. In the CW propagating direction inside the loop mirror, the incident pulse disperses quickly and then remains broad in the nonlinear fiber, inducing little nonlinear phase shift; on the other hand, the CCW propagating pulse remains short for the entire nonlinear fiber span, where the fiber is almost dispersionless: thus the pulse acquires a large amount of nonlinear phase shift that is intensity dependent. A dispersion compensation module should be added at the output port to compensate the effect of the dispersive medium in the loop. One significant characteristic of DILM is that since dispersion acts only on pulses, continuous wave input light of arbitrary intensity will be reflected, whereas only the short pulses will be switched out. This characteristic is used to suppress the pedestal of the short pulses.

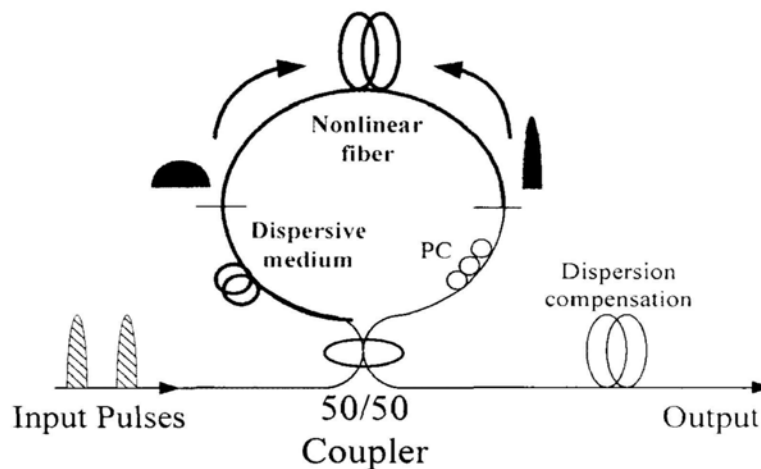


Fig 3.3 Structure of DILM and the operation principle

The applications of this kind of NOLM include: ultra-short pulse (soliton) self switching [46], signal regeneration [47, 48], pulse compression and pedestal suppression [49] and passive mode-locking of a short pulse fiber laser [50].

### B. XPM effect-based NOLM

This type of NOLM is proposed in [51]. In this mode, two wavelengths are involved where a source of one wavelength is used to switch a signal of another wavelength. The basic structure is shown in Fig 3.4. A weak single input (in the figure, the signal is illustrated as a continuous wave light. However, it can also be in other forms, such as pulse trains, data signals and so on) is split into two counter-propagating beams at the 50/50 coupler. The high-power control signal is coupled into the NOLM from one side of the loop via either a common coupler or a WDM coupler. Since the signal power is weak, the SPM effect induced phase shift can be neglected. In this case, the main phase shift is introduced by the control light via the XPM effect. Because the propagation direction of the control light is the same as the CW signal but opposite to the CCW signal, the CW signal will experience a significant phase shift while the CCW signal will not, resulting in the switching operation of the NOLM. This type of NOLM provides a way to control one light beam via another light beam, thus “all-optical”. One disadvantage of this NOLM lies in its polarization-dependent operation since the XPM itself requires polarization alignment between the two light beams.

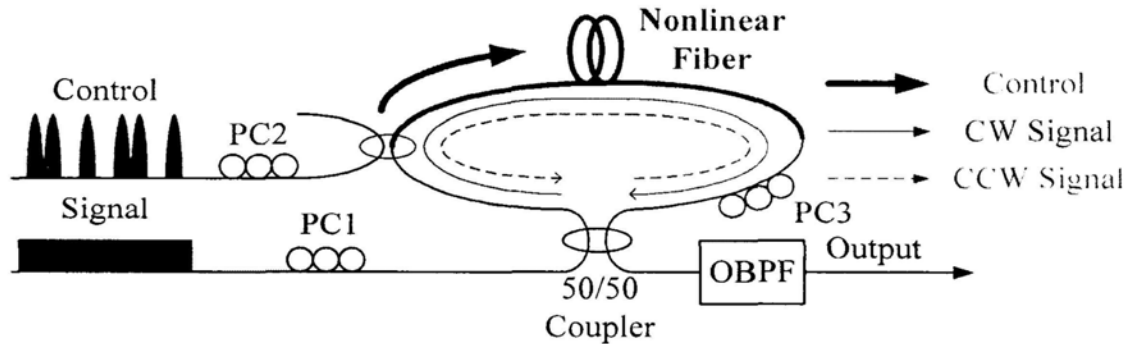


Fig 3.4 Principle of two-wavelength operation of NOLM

The applications of this kind of NOLM include: OTDM demultiplexing [52], wavelength conversion [53], return-to-zero (RZ) to non-return-to-zero (NRZ) format conversion [54] and all-optical logic gate [55, 56].

Apart from nonlinear fiber, some other nonlinear devices can also be put into the loop to act as the nonlinear medium, such as SOA. This kind of NOLM is first proposed in [57] and called terahertz optical asymmetric demultiplexer (TOAD). Compared with the fiber based NOLM, it is more compact, thus providing more stable operation. However, the slow recovery time of SOA

results in the so called “patterning effect”, limiting its applications in the data rate of 10 Gb/s or below.

In the next two subsections (3.1.2 and 3.1.3), we will focus on the fiber based NOLM structures, reporting two research works on the new structural design of NOLM and discussing their applications in all-optical signal processing systems.

## **3.1.2 Polarization-Independent NOLM Using Polarization-Diversity Loop**

### **3.1.2.1 Introduction**

NOLM features a stable switching operation with fast response time ( $<1$  ps). Thus, when it is used as an all-optical demultiplexer in high-speed OTDM systems, it can provide extremely narrow gating window for demultiplexing, which is beneficial to reduce the inter-channel crosstalk. However, the NOLM operation is in principle polarization dependent, which is a major obstacle to applying it in practical high speed systems, where the signal polarization is random.

Several methods have been proposed to realize polarization-independent demultiplexing operation [58-62]. In [58, 59], the NOLM was constructed from some special components, such as polarization-maintaining fiber (PMF) cross-spliced at the mid point or twisted fibers, which were difficult to realize, in practice. In [60], a birefringent crystal was put into the loop to act as a full-wave plate for data wavelength and a half-wave plate for the control pulse wavelength, which limited the NOLM operation to narrow-band operation. In [61], the signal pulse was split into two orthogonal polarization components and fed into a conventional NOLM from different ports of the 3-dB coupler with suitable time delay. The walk-off between the control and signal pulses allowed the two orthogonally polarized signal components to be switched independently by the same control pulses and recombined after their polarization states were aligned. This relied on the walk-off between the control and signal wavelengths, posing more limitation on the switching speed and the choice of the control and signal wavelengths. In [62], a pair of short PMF was put at the input and output ports of a conventional NOLM. The signal pulse width was required to be smaller than half of the bit duration to prevent overlapping between the fast axis component and slow axis component, leading to the limitation in switching speed.

In this section, we propose and experimentally demonstrate a new configuration to achieve a polarization-independent NOLM (PI-NOLM) based OTDM demultiplexer by incorporating a polarization diversity loop into a conventional NOLM. Although the polarization diversity loop technique is not a new concept, how to apply it into a NOLM has not been well addressed. Compared with previous schemes, it enables polarization-independent operation using conventional components without sacrificing operation speed, wavelength range or structural simplicity.

### 3.1.2.2 Principle of Operation

The operation principle of the proposed scheme is shown in Fig 3.5. The main difference from a conventional NOLM is that a polarization beam splitter (PBS) is incorporated into the fiber loop to form one polarization diversity loop, which includes a span of DSF as the nonlinear medium and one PC. The input signal pulse train is bi-directionally coupled into the NOLM via a 3-dB coupler and transmits in both CW and CCW directions, as illustrated with thin solid arrows and thin dashed arrows in Fig 3.5, respectively. The signal in each direction is further split into two orthogonal polarization components by the PBS (namely TE and TM in the figure) with a corresponding amplitude ratio given by the input state of the polarization. A control pulse train (as illustrated with thick solid arrows in Fig 3.5) is uni-directionally coupled into the NOLM via a coupler with its polarization at  $45^\circ$  (through PC2) to the port A of the PBS such that the control pulse train will be split into two orthogonally polarized components with equal amplitude in the polarization diversity loop to induce equal phase shift in both directions.

In the polarization diversity loop, the PC4 should be adjusted such that the recombined pulse trains will pass through the PBS instead of reflection (i.e. port A to port B or port B to port A). As both control pulses and CW signal pulses enter the polarization diversity loop from the same port of PBS, they will have the same polarization in this loop. Hence, the CW signal pulses will experience the maximum phase shift if it falls into the control pulse window. On the other hand, the CCW signal pulses will be injected into the polarization diversity loop from the other port of the PBS, thus its polarization in this loop is orthogonal to the control pulses. This means that the CCW signal will experience  $1/3$  of the maximum phase shift if it falls into the control pulse window or even zero phase shift if it does not fall into the window. The latter case is easy to achieve when the control pulse is much narrower than the bit duration. Consequently, the CW signal pulses will experience the maximum phase shift (regardless of the input signal polarization but only depending on the control pulse power); while the CCW signal pulses will experience a much smaller phase shift. When they interfere at the 3-dB coupler of the NOLM, the polarization-independent demultiplexing of the input signal is achieved. An optical delay line

should be incorporated into the NOLM to prevent the CCW signal pulses at those unwanted channels from being affected by the control pulses in the polarization diversity loop. This is not a stringent requirement, especially if the control pulse window is very narrow compared with the bit period, as in a lot of NOLMs.

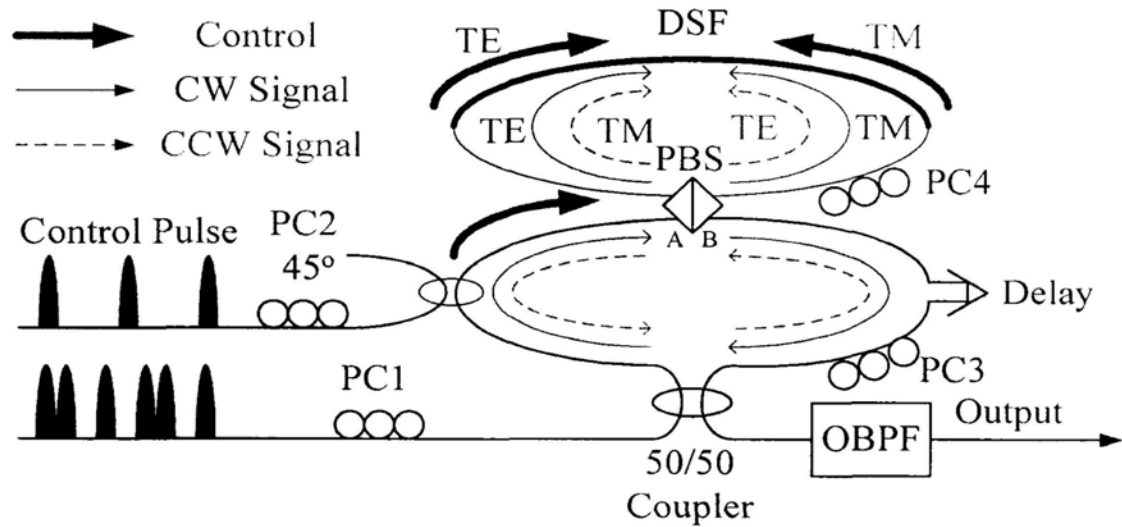


Fig 3.5 Proposed PI-NOLM and operation principle

### 3.1.2.3 Experimental Demonstration

The experimental setup was shown in Fig 3.6. The signal pulses (center wavelength: 1555 nm) were generated from a mode-locked semiconductor laser (MLSL) at 10.61 GHz with 1-ps pulse width, then externally modulated by a LiNbO<sub>3</sub> Mach-Zehnder modulator (MZM) with  $2^{31}-1$  PRBS data, and optically multiplexed up to 42.44 Gb/s. The PC1 is used to control the input signal polarization state. The control pulses (center wavelength: 1545 nm) were generated from a mode-locked fiber ring laser (MLFL) at 10.61 GHz (driven by the same radio frequency generator) with 3-ps pulse width. Its polarization could be adjusted via PC2 and the delay in this arm was used to adjust the relative position of the control and signal pulses. The NOLM consisted of a 3-dB coupler, a side port (3-dB coupler) for the input of control pulses, a PBS, 4-km DSF (zero dispersion wavelength: 1550 nm), and two PCs (PC3 and PC4) for adjusting the system. The delay line described in Fig 3.5 was replaced by using an optical patch cord of suitable length. An optical band-pass filter (OBPF) with 2-nm bandwidth was put at the NOLM output to block the control pulses and filter out the signals.

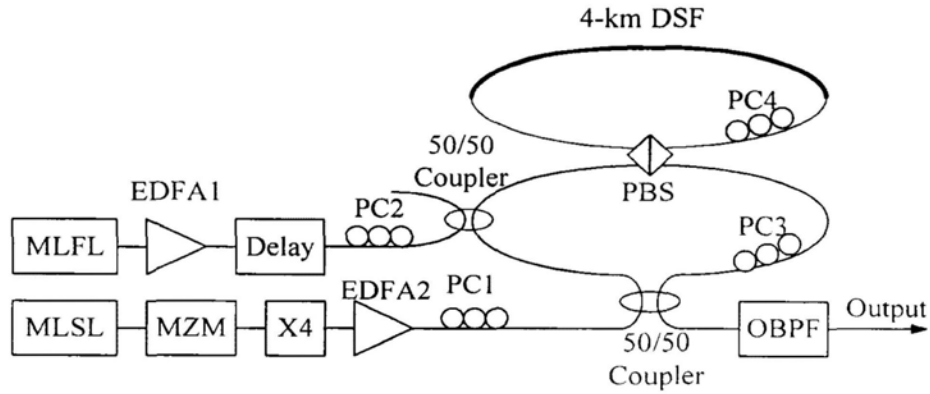
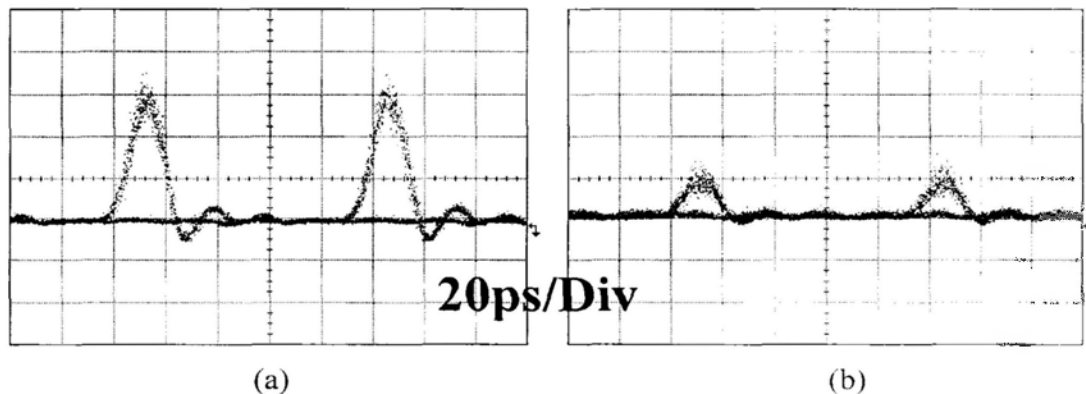


Fig 3.6 Experimental setup for polarization-independent OTDM demultiplexer

The adjustment of the system included three steps: Step 1-- only turn on the signal pulses and open the NOLM loop at the point between PBS and PC3. Then we adjust the PC4 to make sure the reflection is minimal. We can obtain the results by monitoring the power at the NOLM output to be minimal. Step 2-- close the NOLM loop and adjust PC3 to ensure the power at the NOLM output port is minimal. In this way, the NOLM is working in the mirror state. Step 3--turn on the control pulses and amplify them to 20 dBm through an EDFA. Then adjust the PC2 to realize the polarization independent operation. By tuning the delay on this arm, we could obtain different OTDM channels at the output.

For purpose of comparison, a conventional NOLM was also built with a similar setup (without the PBS and PC4). By tuning the input signal state, we obtained the best and the worst cases of the conventional NOLM switching operation, with the eye diagram (after pre-amplification before the oscilloscope) shown in Fig 3.7 (a) and (b). The polarization dependence was 6.3 dB by measuring the switched signal power. When our proposed scheme was used, the polarization dependence was reduced to 0.6 dB, with the eye diagram for the best case and worst case shown in Fig 3.7 (c) and (d).



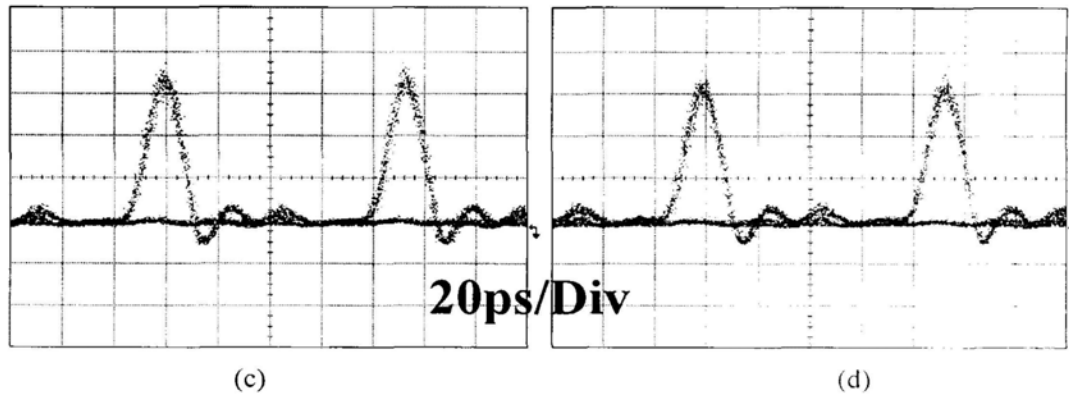


Fig 3.7 Eye diagrams of the switched 10.61-Gb/s signal pulses from 42.44-Gb/s OTDM signals: (a) and (b) show the best and worst cases of the conventional NOLM; (c) and (d) show the best and worst cases of PI-NOLM

We also measured the BER performance of the conventional NOLM and our proposed PI-NOLM and compared them with the baseline, as shown in Fig 3.8. Here, only one of the four OTDM channels was chosen as a representative. For the conventional NOLM, the best case exhibited 0.5-dB power penalty. However, for the worst case, it showed an error floor at  $\text{BER}=10^{-5}$  when the received power was -10 dBm, so it was not shown in the figure. For our proposed scheme, the best case had a 1.4-dB power penalty and the worst case had a 1.8-dB power penalty when compared with the baseline. The reasons for the penalty include: (1) the SPM effect may cause the broadened spectrum of the control pulses to overlap with the signal wavelength, leading to crosstalk. This phenomenon is more serious in our PI-NOLM because the polarization diversity requires double control power or even more; (2) the polarization isolation of the PBS is not perfect (extinction ratio: 24 dB) so a small part of signals power is reflected to form the noise.

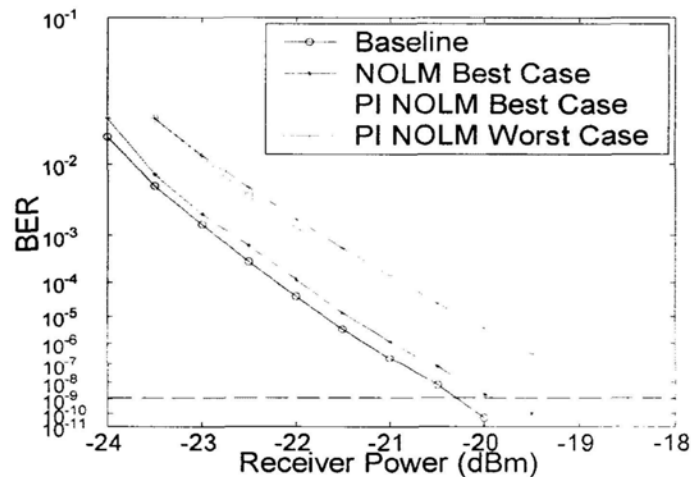


Fig 3.8 BER performance of the 10.61-Gb/s demultiplexed data from 42.44-Gb/s OTDM signals in various situations

We have also measured the other three channels' performance. However, here only the BER performance of the four channels in the worst case with our proposed scheme was shown in Fig 3.9 and compared with the baseline. From the results, we can see that all of the four channels had similar performance and the power penalties were less than 2 dB in all cases.

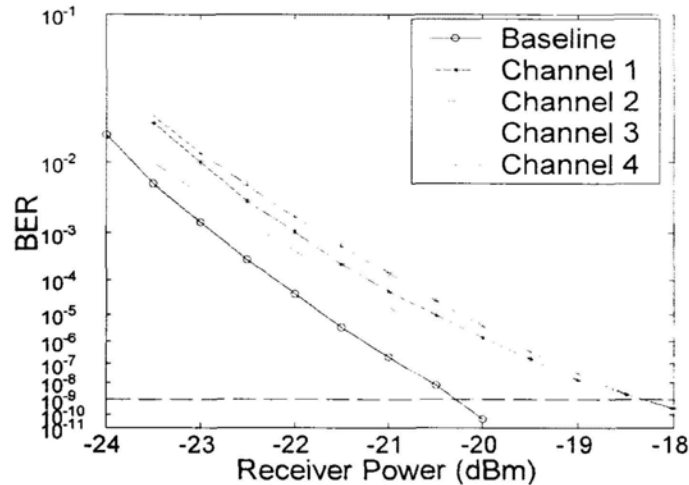


Fig 3.9 BER performance of the four 10.61-Gb/s demultiplexed channels from the 42.44-Gb/s OTDM signals in the worst case when the proposed PI-NOLM was used

### 3.1.2.4 Summary

We have proposed and demonstrated a new polarization-independent NOLM structure by incorporating a polarization-diversity loop into a conventional NOLM. This NOLM configuration is used to achieve polarization-insensitive 42.44-Gb/s to 10.61-Gb/s OTDM demultiplexing in the experiment. The polarization dependence is reduced from 6.3 dB to 0.6 dB and the power penalties are less than 2 dB in all cases, which proves the effectiveness of our proposed scheme. The proposed PI-NOLM offers stable operation using the conventional components without sacrificing the operation speed or structural simplicity. This scheme can be readily upgraded for 80-Gb/s OTDM demultiplexing applications.

### 3.1.3 OFSK Transmitter Based on Phase-Modulator-Embedded NOLM

### 3.1.3.1 Introduction

Optical frequency-shift-keying (OFSK) is a modulation format which employs two closely-spaced wavelengths (optical frequencies) where one carries the data stream while the other synchronously carries the complementary data stream. In the application of long haul transmission, the spacing of the two optical frequencies is half of the data rate and the phase transition between the two adjacent bits is continuous, thus forming the minimum-shift-keying (MSK), which has the advantage of larger dispersion tolerance due to its smaller bandwidth [63]. With its constant intensity nature in time domain, OFSK format has also found applications in some specific networking functions, such as optical label swapping [64], data re-modulation in access networks [65], etc., where the data rate transparency and the tunability of the wavelength spacing are necessary in the transmitter design.

Several designs of OFSK transmitter have been reported. In [64], it was realized by direct modulation of distributed feedback (DFB) laser, followed by an electro-absorption modulator (EAM). However, the bit rate was limited to 2.5 Gb/s. In [65], it was based on optical phase modulation followed by an optical delay interferometer (DI). However, the data rate and the wavelength spacing were constrained by the fixed DI's frequency response. Also, the data had to be differentially pre-coded. In [66], it was realized by polarization modulation via an optical phase modulator followed by a polarizer. However, the signal's polarization had to be carefully controlled, which made the operation difficult.

In this section, we propose a novel OFSK transmitter using a phase modulator–embedded loop mirror. It features data-rate transparency and continuous tuning of the wavelength spacing. The feasibility and performance of the transmitter are experimentally investigated. It may find applications in optical label swapping, data re-modulation in access networks, etc.

### 3.1.3.2 Principle of Operation

Fig 3.10 illustrates the operation principle of the proposed OFSK transmitter. It comprises a fiber loop with a 3-dB fiber coupler and an optical phase modulator is placed inside the fiber loop. Two continuous-wave light beams ( $\lambda_1$  and  $\lambda_2$ ) with a certain wavelength spacing are fed into a fiber loop, via two different ports of the 3-dB coupler; that is,  $\lambda_1$  is fed into one of the ports (say Port 1) of the fiber loop, while  $\lambda_2$  is fed into the other (say Port 2). Polarization controllers (PC1 and PC2) are used to align the input light beams' polarization with the main axis of the optical phase modulator so as to achieve the best phase modulation performance. The optical phase modulator used is a commercially available product made from LiNbO<sub>3</sub> crystal and the driving

radio frequency (RF) data signal is applied to the crystal via the traveling-wave electrodes. Therefore, the addition of the RF signal is directional, i.e. the light transmitted from port A to port B will be phase modulated by the applied signal, but the modulation is little for the light transmitted in reverse direction.

Before feeding in the data signal, we adjust the polarization controller PC3 in the fiber loop to make this fiber loop operate in “mirror” state. Then, the two CW wavelengths,  $\lambda_1$  and  $\lambda_2$  are fed into the fiber loop via Port 1 and Port 2, respectively. When the input data symbol is “0”, no voltage is applied to the optical phase modulator. As a result, there is no phase shift induced to both optical wavelengths, thus the wavelength  $\lambda_1$  will be reflected to the output port via the optical circulator. When the input data symbol is “1”, a voltage  $V_\pi$  is applied to the optical phase modulator. As described above, only the light propagating clockwise will experience the  $\pi$  phase shift. Thus, the fiber loop will change from the “mirror” state to “through” state, thus the wavelength  $\lambda_2$  will appear at the output port. Consequently, the output composite signal becomes an OFSK signal in which the data level on each optical carrier are complementary to each other and the composite signal exhibits constant optical intensity. The optical isolator at Port 2 is used to prevent the light reflection from affecting the lasing performance of LD2. In practice, the possible polarization fluctuation in the fiber loop may make the loop deviate from the desired state, thus hindering stable operation. This can be alleviated by using polarization-maintaining components in the fiber loop.

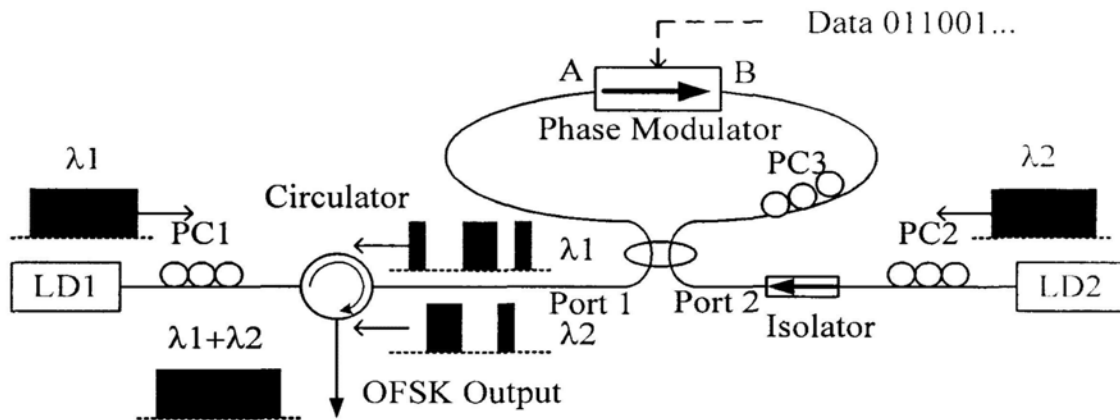


Fig 3.10 Proposed OFSK transmitter design and operation principle

### 3.1.3.3 Experimental Demonstration

Fig 3.11 shows the experimental setup where the OFSK transmitter part is similar to Fig 3.10. The two optical frequencies are  $\lambda_1=1546.00$  nm and  $\lambda_2=1546.60$  nm with 0.60-nm spacing, and the corresponding spectrum at the OFSK transmitter output is shown in the left inset of Fig 3.11. The modulating signal applied to the phase modulator was 10-Gb/s NRZ  $2^{31}-1$  PRBS data. Fig 3.12 shows the captured waveforms of the individual wavelengths ( $\lambda_1$  and  $\lambda_2$ ) as well as the output OFSK signal ( $\lambda_1 + \lambda_2$ ), where both individual wavelengths exhibited complementary waveforms; while the combined signal showed constant intensity envelope. The generated OFSK signal was then amplified by an EDFA to about 6 dBm and filtered by optical band pass filter (OBPF1) with 3-dB bandwidth of 1 nm to suppress the excessive ASE noise. The center of OBPF1 was set to be the middle wavelength (1546.30 nm) of the two input wavelengths. The amplified OFSK signal was then transmitted over 40-km SMF followed by an 8-km DCF for complete dispersion compensation. After transmission, it was observed that the constant-intensity envelope was preserved, as shown in the right inset of Fig 3.11. The received signal was filtered by OBPF2 with a 3-dB bandwidth of 0.2 nm for signal demodulation.

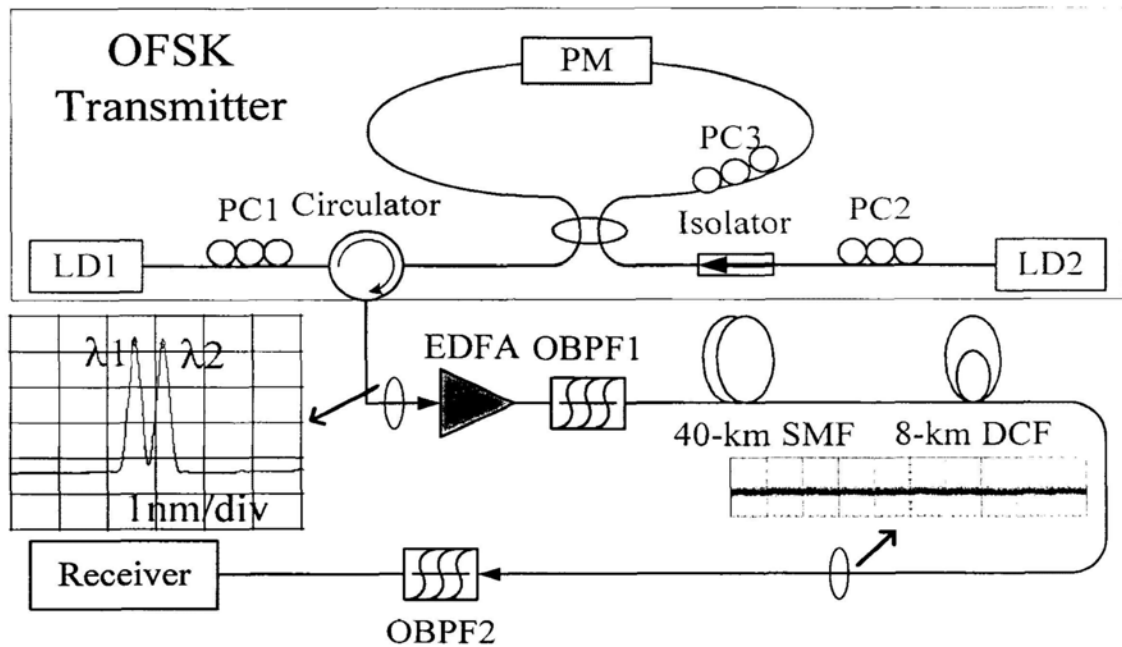


Fig 3.11 Experimental setup of the proposed OFSK transmitter: left inset shows the spectrum at the transmitter output; right inset shows the waveform of the OFSK signal after transmission

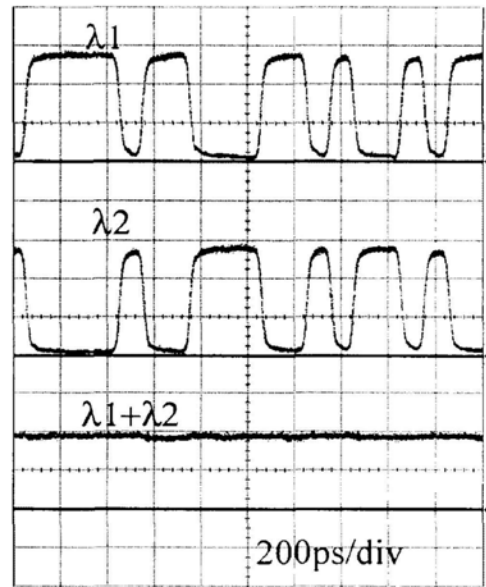


Fig 3.12 Measured waveforms of individual wavelengths and the composite OFSK signal

The system performance of the proposed OFSK transmitter was experimentally characterized and compared with that of a conventional amplitude-shift-keying (ASK) signal generated from a conventional intensity modulator and the results is shown in Fig 3.13. In the back-to-back case, OFSK signal shows about 0.2-dB power penalty compared with the ASK signal, which can be attributed to the non-ideal extinction ratio of the OFSK signal. After 40-km transmission with 6-dBm input power, the OFSK signal shows negligible degradation in BER performance while the ASK signal exhibits 0.2-dB power penalty. This might be attributed to the better tolerance of the OFSK signal against fiber nonlinearity impairments [67].

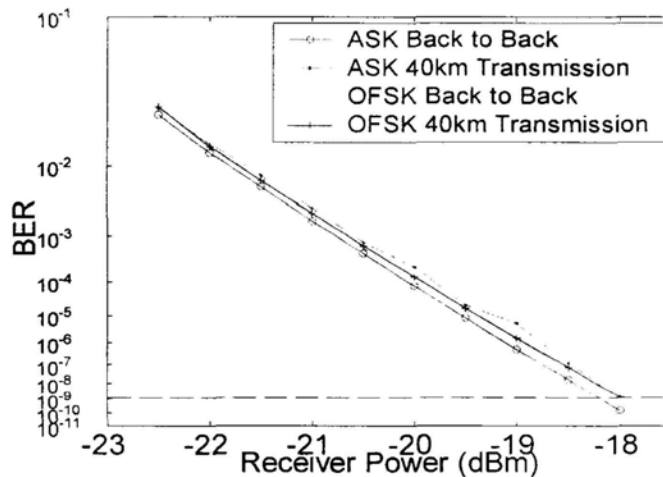


Fig 3.13 BER measurements of 10 Gb/s ASK and demodulated OFSK signal before and after transmission

To further investigate the performance of the OFSK transmitter, we tuned the wavelength spacing of the two optical carriers from 0.15 to 1 nm in 0.05-nm step (input power: 3 dBm) and measured the power penalties of the demodulated signals with reference to the case of 0.6-nm wavelength spacing. The measurement results are shown in Fig 3.14. For the wavelength spacing ranging from 0.3 to 1 nm, the power penalty is very small. However, when the wavelength spacing was tuned to be less than 0.3 nm, large power penalty was observed due to the spectral overlapping between the two wavelengths or insufficient spectral isolation of OBPF2. For wavelength spacing larger than 1 nm, signal distortion by excessive filtering at OBPF1 will introduce more power penalty. Moreover, larger wavelength spacing means lower spectrum efficiency. Therefore, the optimal wavelength spacing should be chosen between 0.3 to 0.6 nm.

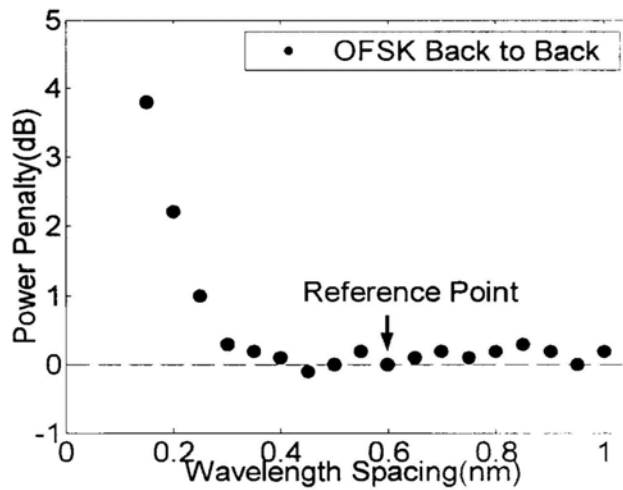


Fig 3.14 Power penalties for different wavelength spacing of the demodulated OFSK signal

Furthermore, the proposed OFSK transmitter was characterized at different operation data-rates from 1 Gb/s to 10 Gb/s with 1 Gb/s step at 3-dBm input power level. The measured receiver sensitivities were shown in Fig 3.15 and compared with a conventional ASK transmitter described above. It shows that the generated OFSK signals at different data-rates have comparable performances with the ASK transmitter, proving that the proposed OFSK transmitter is data-rate transparent. As the optical receiver used in the experiment was optimized for 10 Gb/s, the receiver sensitivity achieved at low data rates might not be optimum.

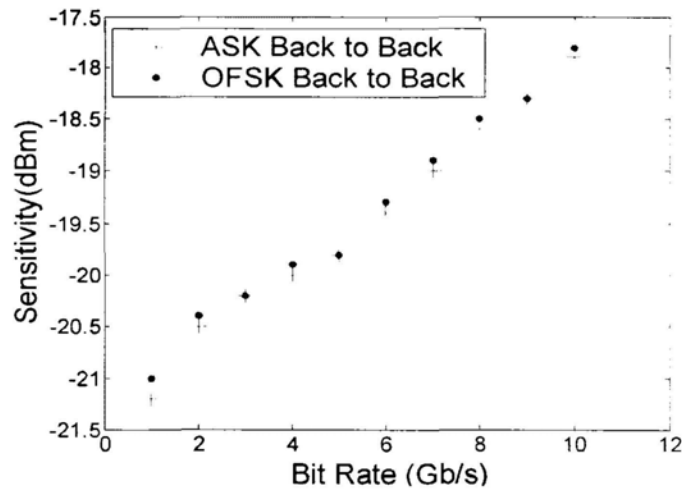


Fig 3.15 Receiver sensitivity comparisons of ASK and demodulated OFSK signal at various data-rates

### 3.1.3.4 Summary

We have proposed a novel OFSK transmitter based on a phase-modulator-embedded optical loop mirror, which offers data-rate transparency and continuous tuning of the wavelength spacing. The transmitter performance has been experimentally characterized, showing its flexibility in transmitter design and may find application in many fields, such as optical label swapping, data re-modulation in access networks, etc.

## 3.2 Nonlinear Optical Signal Processing Systems Based on PCF

### 3.2.1 Introduction on PCF Development

The photonic crystal fiber (PCF), known as holey fiber or microstructure fiber, is a new class of optical fiber that has emerged in recent years, and has found various applications in many fields of optics. In this section, we start from the photonic crystal to introduce the concept of photonic bandgap (PBG), and then give a brief introduction on the principle, application and fabrication of PCF.

### 3.2.1.1 Photonic Crystal Bandgap

The concept of photonic crystal was first introduced in [68]. Photonic crystals can be interpreted as regular microstructures exhibiting a large modulation of the refractive index and with periodicity in one-, two- or three- dimensions. Usually, the period should be on the scale of light wavelength. The basic principle of photonic crystal can be analogous to the conventional semiconductor. The conventional semiconductor also contains the periodical structures where the period is on the scale of the electronic wavelength (in this sense, the conventional semiconductor can be called electronic crystal). Thus, an energy bandgap will be formed on the energy diagram. Now if some impurity is doped into the semiconductor, an impurity energy level will appear in this energy bandgap. Similarly, a photonic bandgap will also come into being in the photonic crystal where the photons with certain energy (thus wavelength) can not exist or propagate in it. In the same way, if we introduce some defects in the photonic crystal, we may observe a sharp defect mode in the PBG, which means that the photons with the corresponding wavelength will be confined in the photonic crystals, forming a high-quality resonator. The examples of photonic crystal include: DFB-laser (one dimension); photonic crystal fiber (two dimensions) and three-dimensionally periodic dielectric structure in some semiconductor lasers (three dimensions).

### 3.2.1.2 Principles and Applications of PCF

PCF was first proposed in 1992 and the first working example – “endlessly single-mode” fiber – was realized in 1996 [69]. Since then a series of breakthroughs in PCF technology have been achieved, leading to a radical enhancement in the possibilities of optical fibers. Generally speaking, PCFs are a class of optical fibers that employ a microstructured arrangement of low-index material in a background material of higher refractive index. The background material is often undoped silica and the low index region is typically provided by air voids running along the length of the fiber. Thus, the lightwave is guided within the imperfection (“defects” or “inclusion”) of the 2D microstructure arrays.

PCF may be divided into two categories -- high index guiding fibers and low index guiding fibers. Similar to conventional fibers, high index guiding fibers guide light in a solid core by the modified total internal reflection (M-TIR) principle. The total internal reflection is caused by the lower effective index in the microstructured air-filled region. Low index guiding fibers guide light by the PBG effect. The light is confined to the low index core because the PBG effect makes the light propagate in the microstructured cladding region impossible. The strong wavelength dependency of the effective refractive index and the inherently large design flexibility of the PCFs allow for a whole new range of novel properties.

### A. High index guiding fibers

In this category of PCF, the lightwave is guided in a solid core by M-TIR. M-TIR is analogous to the total internal reflection known from standard optical fibers. It relies on a high index core region, typically pure silica, surrounded by a lower effective index provided by the microstructured region. The analysis of such fiber can be approximated by a step index fiber with the use of effective index in the cladding. Here, the cladding effective index can be loosely understood as the average index in the microstructure weighted by the intensity distribution of the light, as shown in the following equations:

$$n_{eff} = \frac{\int_{-\infty-\infty}^{\infty} \int_{-\infty-\infty}^{\infty} n(x, y) I(x, y) dx dy}{\int_{-\infty-\infty}^{\infty} \int_{-\infty-\infty}^{\infty} I(x, y) dx dy} \quad (3.1)$$

For different wavelength, the lightwave will show a different intensity distribution. Consequently, the refractive index of the microstructured cladding in PCFs exhibits a wavelength dependency that is very different from pure silica - an effect which allows PCFs to be designed with a complete new set of properties not possible with standard technology.

As an example, the strong wavelength dependence of the refractive index allows design of endlessly single-mode fibers [70], where only a single mode is supported regardless of optical wavelength. Fig 3.16 shows the scanning electron microscope (SEM) image of the end of this photonic crystal fiber, where a hole has been omitted in the central core.

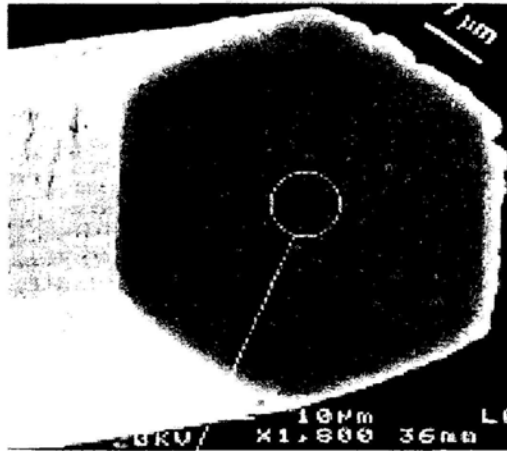


Fig 3.16 SEM image of the end of the endlessly single-mode PCF

The principle of this endlessly single-mode fiber can be understood as the following: In a standard step-index fiber with core radius  $\rho$  and core and cladding indices  $n_{co}$  and  $n_{cl}$ , the number of guided modes is determined by the  $V$  value:

$$V = (2\pi\rho/\lambda)\sqrt{n_{co}^2(\lambda) - n_{cl}^2(\lambda)} \quad (3.2)$$

For the fiber to be single mode, the  $V$  value must be less than 2.405. In this PCF, at shorter wavelengths the field becomes more concentrated in the silica regions and avoids the holes, thus raising the effective cladding index  $n_{cl}$  and decreasing  $V$ . Consequently, this dispersion counteracts the explicit dependence of  $V$  on wavelength  $\lambda$  and so extends the single-mode range.

Another practical application is the high nonlinearity PCF that boosts nonlinear effects by concentrating the light in a very small core. Fig 3.17 shows the SEM images of the end of several kinds of high nonlinearity PCF [71].

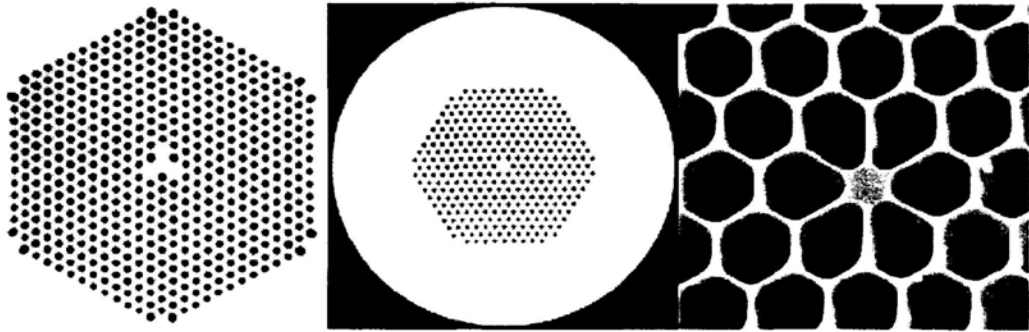


Fig 3.17 SEM images of the end of several kinds of high nonlinearity PCF

Furthermore it can be tailored to have an anomalous dispersion at much shorter wavelengths than conventional single mode fibers by adjusting the ratio of hole's diameter and hole's pitch [72].

The high nonlinearity PCF has found various applications in all-optical signal processing system based on the nonlinear effects in fiber, such as SPM [73], XPM [74] and FWM [75]. What's more, when anomalous dispersion is combined, this PCF can be used to generate the supercontinuum at visible and near infrared (IR) wavelengths from low energy picosecond pulses [76].

#### *B. Low index guiding fibers*

In this kind of PCF, the light is guided using the PBG instead of total internal reflection, so the core need not have a higher refractive index than the cladding [77]. Among them, a special case is the air-guiding fibers, where the field is confined to an air-filled core [78]. Like other PBG fibers, air-core fibers only guide light in a limited spectral region. For fibers guiding around 1550 nm, a typical bandwidth is  $\sim 200$  nm. Outside this region, the fiber core is anti-guiding. Fig 3.18 illustrates the SEM image of the end of air-guiding PCF.

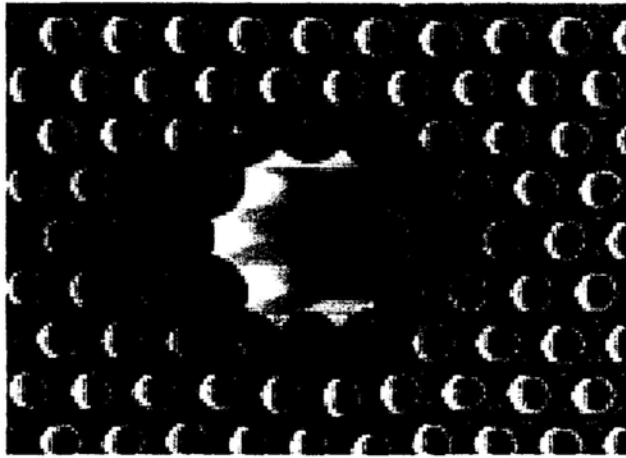


Fig 3.18 SEM images of the end of air-guiding PCF

Guiding light in a hollow core holds many promising applications such as high power delivery without the risk of optical damage, gas sensors or extreme low loss guidance in vacuum. Furthermore, this class of fiber has other spectacular properties not found in any other fiber type. They are almost insensitive to bending and extreme dispersion properties and the anomalous dispersion values in the thousands of ps/nm/km regime are easily obtained. Due to a negligible contribution from the core material (air), the total dispersion of PBG fiber is to a high degree dominated by waveguide dispersion.

### 3.2.1.3 Fabrication of PCF

Fabrication of PCF, like in conventional fiber fabrication, starts with a fiber preform. PCF preforms are formed by stacking a number of capillary silica tubes and rods to form the desired air/silica structure. This way of creating the preform allows a high level of design flexibility as both of the core size and shape as well as the index profile throughout the cladding region can be controlled. This is very useful for fabrication of e.g. polarization maintaining fibers with highly asymmetric core regions, where multiple of the capillary tubes are replaced with solid silica rods.

When the desired preform has been constructed, it is drawn to a fiber in a conventional high-temperature drawing tower and hair-thin photonic crystal fibers are readily produced in kilometer lengths. Through careful process control, the air holes retain their arrangement all through the drawing process and even fibers with very complex designs and high air filling fraction can be produced.

Finally, the fibers are coated to provide a protective standard jacket that allows robust handling of the fibers. The final fibers are comparable to standard fiber in both robustness and physical dimensions and can be both striped and cleaved using standard tools. One recent impressive progress in PCF fabrication is the report of low loss PCF where the loss has been reduced to the level of 0.3 dB/km [79].

### **3.2.1.4 Outlook**

Photonic crystal fiber (PCF) technology offers many new advantages beyond conventional fiber, while in some respects out-performing it. Many more advanced applications are currently being explored, for instance, hollow-core PCF for super-high power delivery, cold atom guiding, high sensitivity spectroscopy, nonlinear optics & sensing, enhanced control of group velocity dispersion for optical communications and ultrashort-pulse lasers and amplifiers, polarization-preserving fibers with extremely small beat-lengths, and high power PCF lasers, amplifiers and power delivery systems.

## **3.2.2 A Nonlinear Intensity Discriminator with a Wavelength-Tunable DILM Based on Dispersion-Flattened High-Nonlinearity PCF**

### **3.2.2.1 Introduction**

In a transparent optical network, one of the major impairments is the incoherent interferometric crosstalk [80], which arises from the beating between a main optical signal and an interfering optical signal at a closely spaced frequency. When the frequency difference falls within the detector bandwidth, a beat signal will be generated, resulting in a severe degradation of the signal. This degradation is much larger than those predicted from simple power-addition without field interference. For such crosstalk, it is preferable to suppress it in the optical domain instead of the electrical domain. One promising technique to suppress the crosstalk is to use a dispersion-imbalanced loop mirror (DILM) [45]. In Reference [81], DSF is used as the nonlinear element. However, the necessity of selecting the signal wavelength within the zero-dispersion wavelength region may limit the flexibility of the optical network. Dispersion-flattened fiber (DFF) is also used to increase the wavelength tuning flexibility [82]. However, the relative low nonlinear

coefficient of the fiber makes it necessary to use fiber several hundred meters long or even longer, which may make the DILM sensitive to environmental disturbances. Consequently, high-nonlinearity fiber, which leads to a shorter fiber length, would be preferable for making the DILM a more stable and compact device. In this section, we experimentally demonstrate the nonlinear suppression of incoherent interferometric crosstalk in a DILM based on only 64-m-long dispersion-flattened high-nonlinearity PCF with low normal dispersion. The advantage of using this kind of fiber lies in the following four aspects: First, since the PCF has a very small dispersion slope in the 1550 nm region, a wide operating wavelength range of more than 25 nm is obtained. Second, the high nonlinearity of the PCF greatly shortens the required loop length, making the DILM more compact and stable. Third, since the PCF has a normal dispersion over a wide wavelength range, the modulation instability induced amplitude noise [83] can be suppressed and a clear eye diagram can be observed. This is a real advantage over other conventional high nonlinearity fiber with very small dispersion slope, such as the fiber reported in [84], since they will exhibit an anomalous dispersion in some of the wavelength range that we concern. Last but not the least, the PCF we used is fully spliced to Standard SMF instead of free space coupling, as reported in many experimental works related with PCF, which makes it easier for our DILM to achieve a stable operation.

### 3.2.2.2 Experimental Demonstration

The experimental setup is shown in Fig 3.19. The upper part of Fig 3.19 is used to generate the input optical signal with adjustable incoherent interferometric crosstalk. First, the input optical signal is a  $2^{31}-1$  RZ PRBS signal at 10 Gb/s, which is obtained by external modulation of a wavelength tunable actively mode-locked fiber laser with a pulse width of 2.5 ps. Next, the optical signal is split into two parts via an 80/20 fiber coupler. The 20% arm incorporates a decorrelating 2 km DSF [81, 82], a tunable picosecond delay line, a polarization controller PC1 and a variable attenuator. Thus, the noise in a signal channel induced by homo-frequency incoherent crosstalk can be simulated and investigated. The power level of the crosstalk with respect to the signal channel can be varied by adjusting the variable optical attenuator. The polarization and time delay can be aligned to maximize the crosstalk effect in order to simulate the “worst case” scenario. After combining the signal channel and crosstalk channel together with a 50/50 fiber coupler, the signal is then amplified by an EDFA with a saturation power of +23 dBm and launched into the DILM.

The lower part shows the constructed DILM. The DILM consists of a 64-m-long dispersion-flattened high-nonlinearity PCF [85], a 100 m DCF and a polarization controller PC3. The PCF used here was supplied by Crystal Fiber A/S and has a threefold symmetric hybrid core region

with a core diameter of  $1.5 \mu\text{m}$  [85]. The overall dispersion of this PCF is flat over a wide wavelength range (less than  $-3 \text{ ps/km/nm}$  over  $1500\text{-}1600 \text{ nm}$ ) with a nonlinear coefficient of  $11.2 (\text{W}\cdot\text{km})^{-1}$ . The dispersion variation as a function of wavelength is within  $1 \text{ ps/km/nm}$  in the wavelength range from  $1465 \text{ nm}$  to  $1655 \text{ nm}$ . Also, the attenuation of the fiber is less than  $10 \text{ dB/km}$  in the  $1550 \text{ nm}$  range and both ends are spliced to SMF, yielding a total loss of  $2.6 \text{ dB}$ . Because this PCF shows some birefringence, a polarization controller, PC2, is used before DILM to adjust the input polarization and overcome this birefringence. If this birefringence can be eliminated in the fabrication process, the PC2 can be removed from the scheme. Thus, this scheme will become polarization insensitive and more attractive. The dispersion of the DCF is  $-165 \text{ ps/nm/km}$  at  $1550 \text{ nm}$ . When this kind of DCF is combined with a suitable length of SMF for dispersion compensation, the average dispersion is below  $\pm 1 \text{ ps/km/nm}$  over  $1520 \text{ nm}\text{-}1570 \text{ nm}$ . The natural birefringence of the fiber can be compensated by adjustment of PC3 in the loop. A  $1\text{-km}$  long SMF is attached to the DILM output for chirp compensation. Since the SMF is outside the loop, it will have a negligible effect on the stability of the loop.

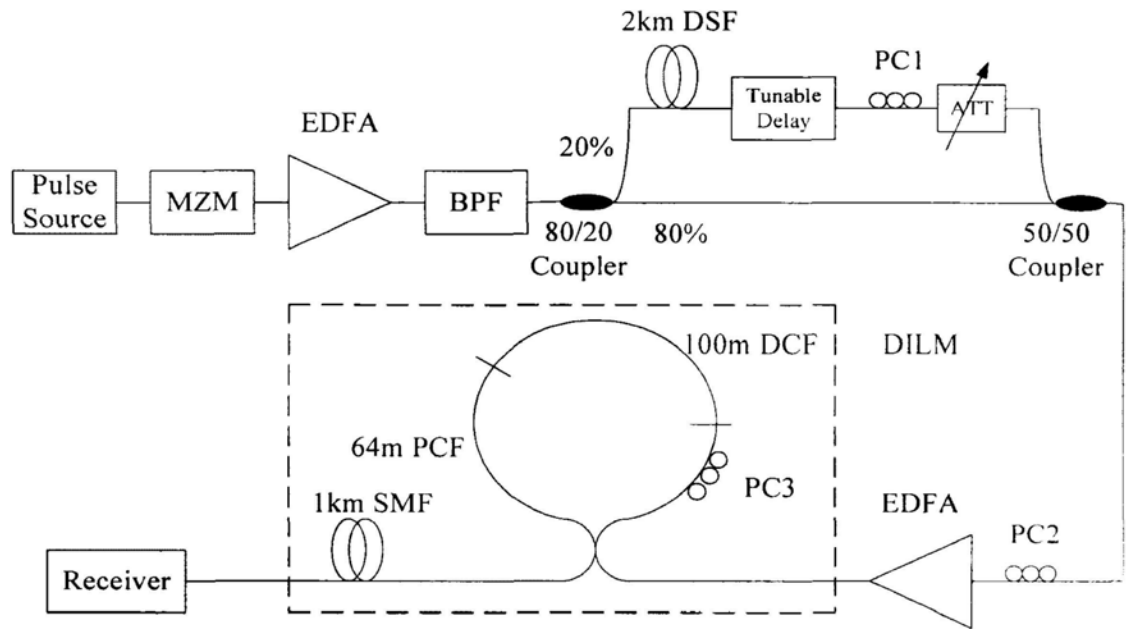
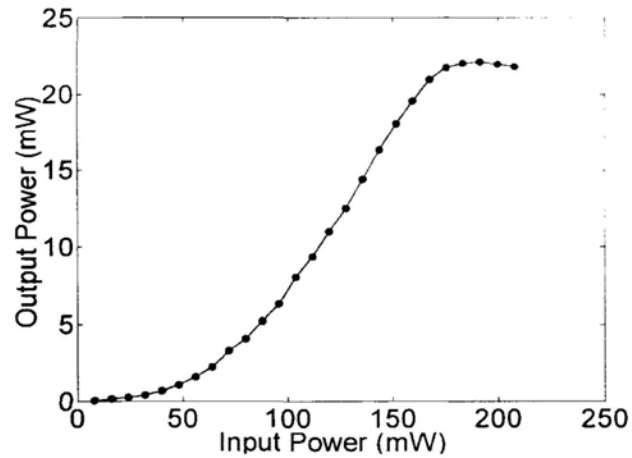


Fig 3.19 Experimental setup. MZM: Mach-Zender modulator; ATT: Attenuator.

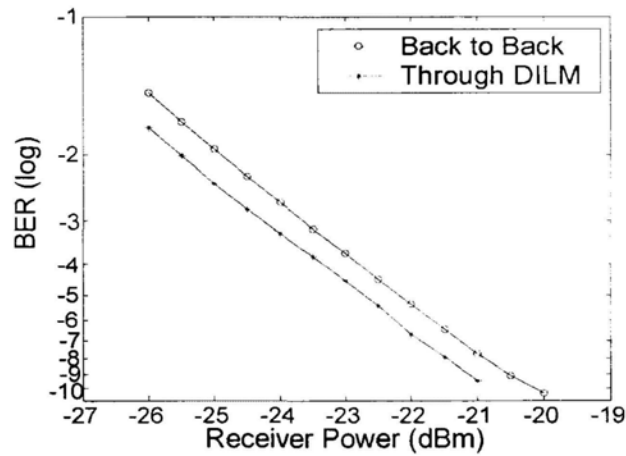
### 3.2.2.3 Experimental Results and Discussions

At first, we tune the signal wavelength to  $1550 \text{ nm}$  to study the transfer characteristics of the DILM. For pulse input without noise injection, the transmitted power as a function of input power is measured and shown in Fig 3.20 (a). The results show that the DILM can be used as a

nonlinear intensity discriminator for signal restoration: the nonlinear filtering not only rejects the low-intensity crosstalk components at “0” level but also clamps the amplitude fluctuation at “1” level [45]. Without noise loading, the measured BER through the DILM at +23 dBm of input power is shown in Fig 3.20 (b) as asterisks. When compared to the BER without DILM (circles), one can see that the insertion of DILM improves the signal quality about 0.3 dB in receiver sensitivity by enhancing the extinction ratio and shortening the pulsewidth [81, 82].



(a)



(b)

Fig 3.20 (a) Transfer characteristics of DILM and (b) BER measurements w/o DILM in case of no noise loading

Then, the crosstalk noise is added to study the DILM performance in suppressing the incoherent interferometric crosstalk. Fig 3.21 shows the measured eye diagrams with and without the DILM corresponding to a crosstalk level of -10 dB, which is really a severe crosstalk in the network. It is seen that the DILM produces clear eye diagram (b) from a severely degraded input signal (a).

The power penalty improvements (at  $\text{BER}=10^{-9}$ ) with the DILM are measured at various crosstalk levels with the results shown in Fig 3.22 (a). In case of no DILM, the power penalty is small at the crosstalk level of less than -20 dB. However, the power penalty shows an exponential increase as the crosstalk level is further increased, in agreement with the results in [80]. In case of -10 dB crosstalk level, the induced power penalty is even larger than 20 dB and cannot be measured in our experiment. When the DILM is added, it dramatically reduces the power penalty, resulting in a less than 2 dB power penalty for a relative crosstalk level from -30 dB to -10 dB.

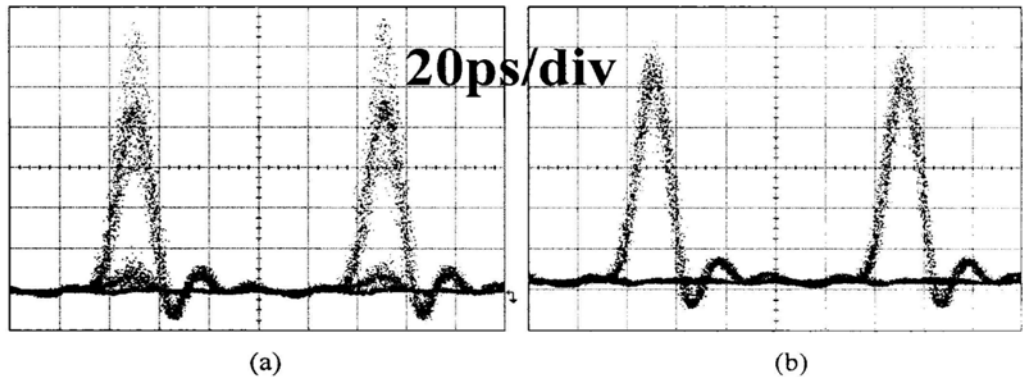


Fig 3.21 Eye diagram measured (a) before and (b) after the DILM in case of -10dB crosstalk level at 1550nm

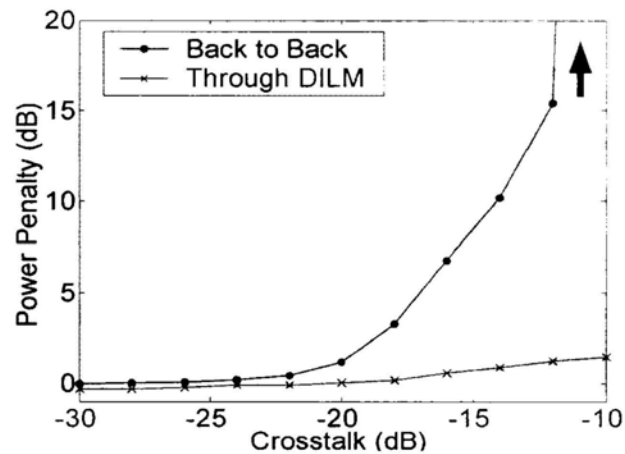
The significant penalty reduction and performance improvement is also dependent on the time delay between the signal and the crosstalk. Fig 3.22 (b) shows the power penalty reduction with DILM for various time delays from -10 ps to 10 ps. In all cases, the crosstalk level is fixed at -10 dB and the wavelength is chosen at 1550 nm. When there is no DILM, the power penalty is about 2 dB when the absolute value of the time delay is larger than 6 ps. When the signal and the crosstalk come closer to each other, the power penalty greatly increases until it could not be measured. The application of DILM can significantly reduce the power penalty to less than 2 dB for all cases.

In order to investigate the wide operating wavelength range of the DILM, we tune the actively mode-locked fiber laser for various wavelengths from 1545 nm to 1570 nm with 5 nm wavelength spacing. In all cases, the crosstalk level is fixed at -10 dB, and the results for the power penalty improvement with the DILM are shown in Fig 3.22 (c). The power penalty without the DILM is so large that it can not be measured in this situation. The result shows that the signal quality enhancement is achieved over a wide wavelength range of 25 nm. It is likely that our setup can operate over a wider wavelength range but the demonstration is limited by the tuning range of the actively mode-locked fiber laser.

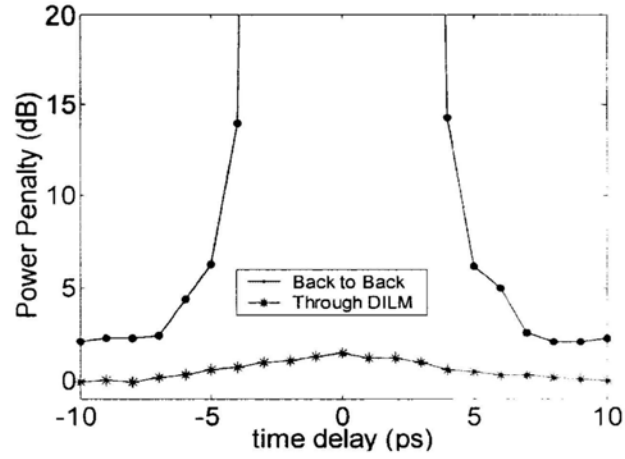
In the DILM, the SPM effect of the PCF is used to accumulate the phase change. A previous report shows that when SPM operates in the anomalous dispersion regime of the fiber, the output signal will become noisy due to the modulation-instability induced amplitude noise [83]. Fortunately, the PCF used in the experiment has a normal dispersion over a wide wavelength range, thus avoiding this problem. This shows another advantage for the application of this PCF in DILM.

In our experiment, the input pulse width is about 2.5 ps. To improve the spectral efficiency in the transmission, a wider signal pulse width will be preferred. When a larger duty ratio signal is used as the input of the DILM, in order to accumulate enough phase change in the PCF span, we can increase the input pulse power or adopt a span of new PCF with higher nonlinearity or longer length. On the other hand, a span of DCF with higher dispersion value or longer length might be needed to broaden the input pulse to a certain extent.

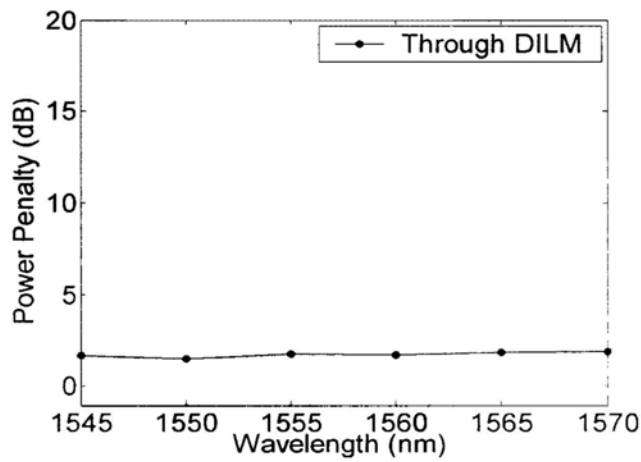
As an intensity discriminator, the DILM can also be used as a 2R (reamplifying and reshaping) regenerator for signal restoration in presence of white noise, e.g. ASE noise, as shown in [86]. However, the receiver sensitivity can not be improved if the DILM is directly put in front of the receiver. This is because the bit error is caused by the overlap between noise distributions associated with marks and spaces, but the DILM can not differentiate that overlap. Only when the DILM is put into the transmission line can it become effective. Although it can not improve the receiver sensitivity, the reshaping of signal can greatly reduce the signal deterioration in the subsequent transmission and thus extend the transmission reach, as analyzed in [87].



(a)



(b)



(c)

Fig 3.22 (a) Power penalty measurements at various crosstalk levels for 1550 nm without time delay; (b) Power penalty measurements at 1550 nm with -10 dB crosstalk for various time delays and (c) Power penalty measurements at -10 dB crosstalk for various wavelengths without time delay

### 3.2.2.4 Summary

Nonlinear suppression of the incoherent interferometric crosstalk has been demonstrated using a DILM constructed from a relatively short-length of dispersion-flattened high-nonlinearity PCF. As a nonlinear intensity discriminator, the DILM not only rejects the low-intensity crosstalk components at the “0” level but also clamps the amplitude fluctuation at the “1” level. With the DILM, the crosstalk-noise induced power penalty is greatly suppressed to less than 2 dB even when the relative crosstalk level is up to -10 dB. The special characteristics of the PCF ensure a

broadband (more than 25 nm range, which is mainly limited by the EDFA amplification range) signal quality improvement and make the DILM more compact and stable.

## 3.2.3 Polarization-Insensitive Wide Band Wavelength Converter Using PCF with Small Birefringence

### 3.2.3.1 Introduction

In a wavelength-routed optical network, wavelength conversion [88] plays an important role in reducing wavelength blocking and providing more flexibility in network management. In particular, all-optical wavelength conversion based on FWM in fiber is a promising technique due to its ultrafast response and transparency to both bit-rate and modulation format. However, FWM in fibers strongly depends on the relative state of polarization (SOP) of the signal to the pump (i.e. >20 dB), which is a major obstacle to applying it in real system where the incoming signal polarization is random. Several polarization-insensitive schemes have been reported, such as polarization-diversity loop [89], non-degenerate FWM using two orthogonal pumps with different wavelengths [90], etc. In this section, we realize the polarization-insensitive operation with a simple straight-line configuration using only a short span of dispersion-flattened high-nonlinearity PCF with small birefringence. The polarization dependence is reduced to less than 0.9 dB and a wide wavelength tuning range of 32 nm is achieved.

### 3.2.3.2 Principle of Operation

Fig 3.23 shows the operation principle of the polarization-insensitive scheme. The PCF we used in the experiment exhibits a small birefringence with 5-ps delay between the fast and slow axes, which is mainly induced during the fabrication stage and the process of coiling fiber on the spool. When the combined light enters into the PCF, both signal and pump will be split into two orthogonal polarization components with a corresponding amplitude ratio given by the input SOP.

According to reference [91], for a birefringent fiber where the principal axis is fixed along the whole fiber length and phase mismatching due to chromatic dispersion can be ignored, when the

coherent length  $L_{coh}$  (here, we define  $L_{coh} = \frac{\pi}{2|k_x - k_y|} = \frac{\lambda}{4 \Delta n}$ , where  $\lambda$  is the wavelength

and  $\Delta n$  is the refractive index difference between  $x$  and  $y$  polarizations) is much smaller than

the fiber length  $L$ , there is no correlation between the two axes in the four wave mixing generation, which can be expressed as the following equation:

$$\hat{E}_c(L) = Ke^{\alpha L} \chi^{(3)} [E_{px}(L)E_{px}(L)E_{sx}^*(L) + E_{py}(L)E_{py}(L)E_{sy}^*(L)] \quad (3.3)$$

where  $\hat{E}_c$  denotes the amplitude vector of the converted light,  $K$  is a constant,  $\alpha$  is the loss coefficient of the fiber,  $\chi^{(3)}$  is the tensor component of the third order nonlinear susceptibility of the fiber,  $E_{px}$  and  $E_{py}$  represent the pump light amplitude for  $x$  and  $y$  directions respectively,  $E_{sx}$  and  $E_{sy}$  represent the signal light amplitude for  $x$  and  $y$  directions respectively and  $*$  denotes the complex conjugate.

It happens that all of the above conditions can be fulfilled in the PCF we used. Thus, two independent FWM will occur in the PCF along both fast and slow axes of PCF simultaneously. By adjusting the input polarization of the pump to make it  $45^\circ$  to the principal axis of the fiber, the two orthogonally polarized components of the pump will have equal amplitude. Consequently, the converted signals on both axes will have the same conversion efficiencies (defined as the ratio of the converted signal power to the input signal power), so the sum of them will become constant regardless of the SOP of the input signal. In principle, a span of PMF should be added after the PCF to compensate the birefringence induced by the PCF on the converted signal. However, in 10 Gb/s experiments, the delay caused by this birefringence (5 ps) is only 1/20 of the bit period (100 ps) so it has negligible impact on the converted signal. Thus, the compensation procedure is omitted, further simplifying the whole configuration.

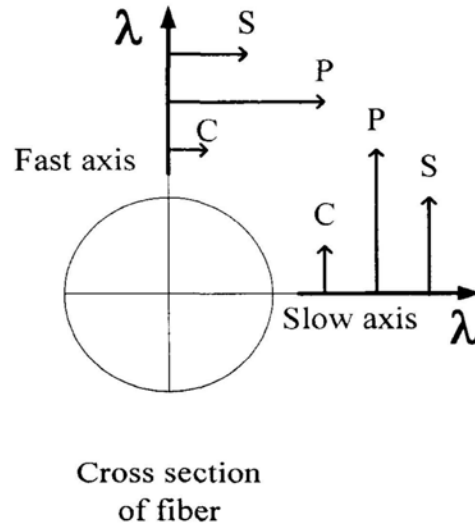


Fig 3.23 Schematic operation principle: the circle shows the cross section of PCF with birefringence; S, P and C represent the signal, pump and converted signal respectively

### 3.2.3.3 Experimental Demonstration

Fig 3.24 shows the experimental setup for 10 Gb/s operation. The input signal is  $2^{31}-1$  10 Gb/s NRZ PRBS generated by one DFB-LD followed by an external Mach-Zehnder intensity modulator. This input signal is combined with a wavelength-tunable CW pump laser using a 3-dB coupler. The combined signal is launched into a high power EDFA with the total output power of 800 mW. The power of the pump is about 3 dB higher than the power of the signal. The amplified light is then injected into a segment of 41-m PCF provided by Crystal Fiber [85]. It has a dispersion around  $-1$  ps/km/nm over 1500-1600 nm with a nonlinear coefficient of  $11.2$  (W·km) $^{-1}$ . The dispersion slope is less than  $1 \times 10^{-3}$  ps/km/nm $^2$ . The attenuation of the fiber is below 10 dB/km in the 1550-nm range. Both ends are spliced to SMF and the total loss of the 41-m PCF is 2.4 dB. Moreover, this fiber exhibits a small birefringence on the order of  $10^{-5}$ - $10^{-4}$  during fabrication. Our measurement shows that there is about 5-ps delay between the fast and slow axes. By adjusting the PC before the pump laser, the input polarization of the pump is  $45^\circ$  to the principal axis of the fiber, thus realizing the polarization-insensitive operation. Finally, the converted signal is filtered out using an OBPF with 1-nm 3-dB bandwidth.

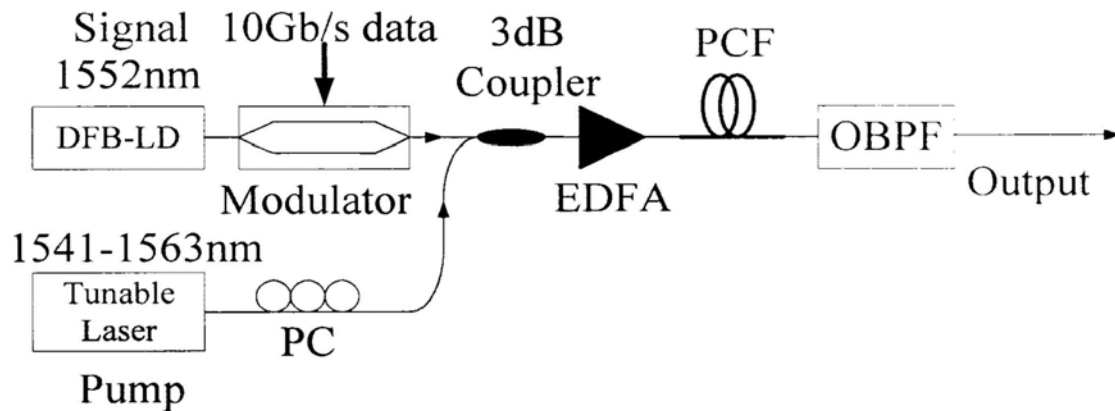


Fig 3.24 Experimental setup

At first, the signal wavelength (S) is fixed at 1552 nm and the CW pump wavelength (P) is tuned to 1546 nm. The up-converted signal (C) appears at 1540 nm. The spectrum obtained after PCF is shown in Fig 3.25. The OSNR of the converted signal is 30 dB, and the conversion efficiency is about -15 dB. To demonstrate the polarization-independent operation of the wavelength converter, Fig 3.26 plots the relative converted signal power against different input signal polarization state. The power variation of the output is less than 0.9 dB. Fig 3.27 (a) and (b) show the obtained eye diagrams (after preamplifier before photodetector) corresponding to the largest and smallest output power, respectively. Clear eye diagrams are shown in both cases, and no modulation instability induced amplitude noise is observed due to the normal dispersion of the PCF over the

1550-nm range. It also indicates that the small birefringence of the PCF did not cause significant distortion to the signals.

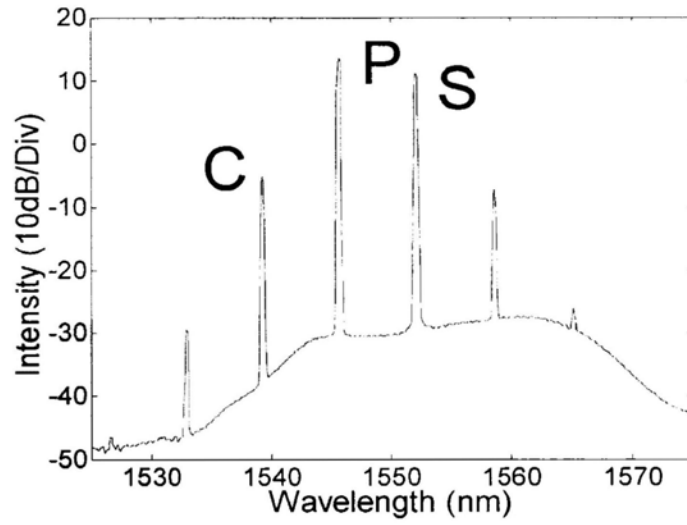


Fig 3.25 Output spectrum of 12-nm up-conversion

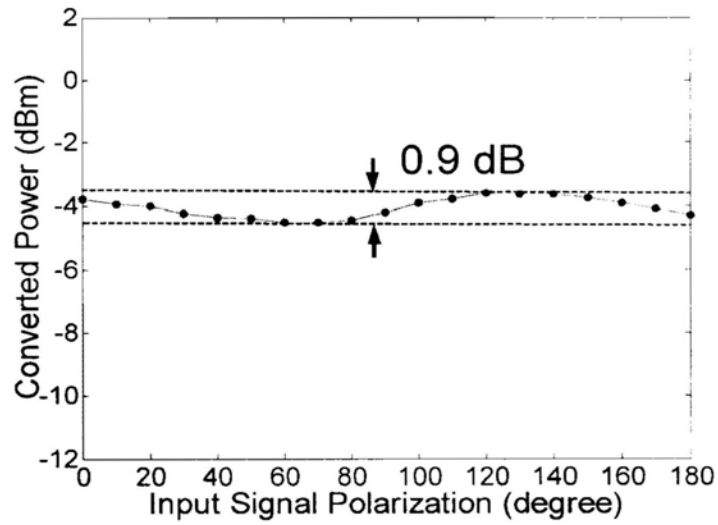


Fig 3.26 Converted signal power vs. the input signal polarization

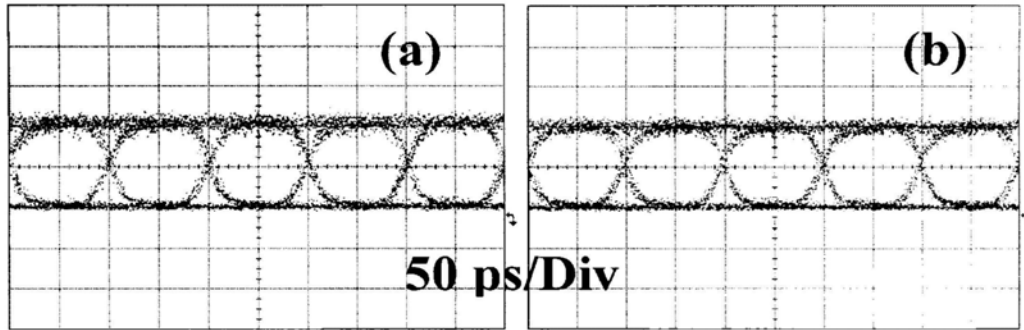


Fig 3.27 Eye diagrams (after preamplifier before the photodetector) corresponding to (a) the largest and (b) the smallest output power when the input signal polarization is changed

The relationship between the conversion efficiency and the converted output wavelength is shown in Fig 3.28. In this measurement, we fix the signal wavelength and tune the pump wavelength (from 1541 nm to 1563 nm with 1-nm spacing) to obtain different outputs. A 3-dB tuning range of 32 nm is achieved where the peak conversion efficiency is -15 dB.

When this scheme is applied in a higher bit-rate wavelength conversion, such as 40 Gb/s or above, the birefringence-induced delay will be significant with respect to the bit period, thus compensation of the birefringence may become necessary. Further reducing the birefringence might be a solution. However, too small a birefringence might increase the polarization-sensitivity. So, optimization of this birefringence value for higher bit-rate system requires further investigation.

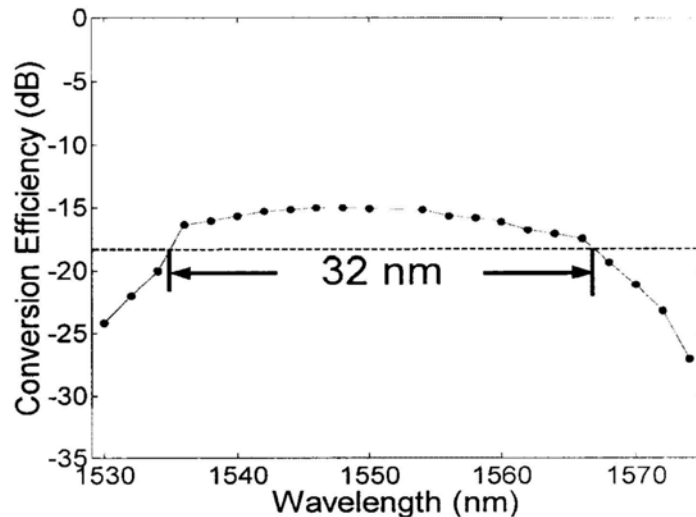


Fig 3.28 Output conversion efficiency vs. the converted wavelength

### **3.2.3.4 Summary**

Utilizing the small birefringence of a nonlinear PCF, we achieve the polarization-insensitive wavelength converter in a simple straight-line configuration with less than 0.9-dB polarization sensitivity. A wide wavelength tuning range of 32 nm is realized due to the dispersion-flattened property of this PCF. The results show that such wavelength converters are promising for wide-band wavelength conversion applications in future all-optical networks.

## **3.3 Summary**

This chapter discussed several new all-optical nonlinear signal processing techniques. In the first half of this chapter, the focus is on the novel NOLM structure design to realize some special functions. In the second half, we discuss the applications of high-nonlinearity photonic crystal fiber in the nonlinear signal processing systems, demonstrating its advantages over the conventional fiber.

# Chapter 4 Summary and Conclusion

## 4.1 Summary of the Thesis

This thesis covers two topics in the area of optical fiber communications. One topic is on the study of WDM-based broadband optical fiber access networks, with the emphasis on the novel network architecture design to improve the network reliability and functionality as well as the reduction of system complexity. A system demonstration to show the potential of WDM technologies in the broadband optical access networks is also described. The other topic is related to the all-optical nonlinear signal processing with the aim at improving the performance of current optical signal processing subsystem via newly-emerging devices and newly-designed configurations.

Chapter 2 is about the broadband optical fiber access network technologies. In the first section, we briefly review the current broadband optical fiber access network technologies including TDM-PON and WDM-PON and their deployments in industry with several representative examples in United States and Japan.

Then, in the second section, several novel network architecture designs are proposed to improve the network reliability and reduce the system complexity and cost. Here we consider two optical network architectures: tree topology and ring topology. For the tree topology, a centrally controlled protection scheme is proposed and experimentally characterized in the AWG-based WDM-PON, which greatly simplifies the ONU structure and is beneficial to the system management. The optical layer survivability of the "Broadcast and Select" WDM-PON has also been studied using the group protection concept. The major advantage of this scheme lies in its flexibility and possibility for smooth and graceful upgrade from the current TDM-PON to future WDM-POM as the broadband service demand increases in the future. For the ring topology, a simple and effective CWDM metro/access network architecture with commercially available unidirectional OADM for automatic optical protection in a Hub/Access Node single-fiber ring has been proposed and demonstrated. This physical-ring/logical star architecture greatly simplifies the design compared with the previous works requiring bidirectional OADM.

In the third section, an in-service fault-surveillance scheme in the current TDM-PON is proposed and experimentally demonstrated. Identification tags in the form of external cavity modes with unique mode spacing are generated optically using FP-lasers with external fiber cavity. By constantly examining the intensities of all the identifying tags in the FFT output waveform at the monitoring receiver, the link quality of all fiber branches can be monitored without interrupting the existing data channels.

At last, one system testbed demonstration of the WDM-based optical broadband access network is presented. Based on this testbed, three kinds of real-life emerging broadband services, including HD video streaming, 3D video streaming and real-time video streaming, are successfully operated over this system testbed, demonstrating the power of WDM-based optical fiber broadband access network in future broadband services delivery.

Chapter 3 discusses the all-optical nonlinear signal processing technologies. In the first section, we focus on the novel NOLM structure designs. After a brief introduction on the existing NOLM technologies, two research works on new structures and applications of NOLM are presented. The first work proposes and experimentally demonstrates a new polarization-independent OTDM demultiplexing scheme by incorporating a polarization-diversity loop into a conventional NOLM. 40-Gb/s to 10-Gb/s demultiplexing is successfully achieved with 0.6-dB polarization dependence. This scheme offers stable operation using the conventional components without sacrificing the operation speed or structural simplicity. The second work is the design and demonstration of a novel OFSK transmitter based on a phase-modulator-embedded NOLM, which features data-rate transparent, continuous tuning of the wavelength spacing and stable operation. The transmitter performance has been experimentally demonstrated, showing its flexibility in transmitter design and potential in high-speed optical fiber communication systems.

The second section is related to the new applications of high nonlinearity PCF in the nonlinear signal processing systems. In the first experiment, a DILM is constructed from a relatively short-length of dispersion-flattened high-nonlinearity PCF and used as a nonlinear intensity discriminator for optical signal regeneration. Specifically, this work experimentally demonstrates its application in the nonlinear suppression of the incoherent interferometric crosstalk, which is one of the major impairments in a transparent optical network resulting in severe degradation of the signal. The special characteristics of the PCF ensure a broadband signal quality improvement and make the DILM more compact and stable. In the second work, utilizing the small birefringence of nonlinear PCF, we achieve the polarization-insensitive operation of a FWM-based wavelength converter in a simple straight-line configuration with less than 0.9-dB polarization sensitivity. A wide wavelength tuning range of 32 nm is realized due to the

dispersion-flattened property of this PCF. These works demonstrate the advantages of PCF over the conventional fiber for such nonlinear signal processing applications.

## 4.2 Conclusion

The 40-year research and development of optical fiber communications technologies has witnessed a series of breakthroughs. Nowadays, optical fiber communications has gradually become a mature industry. This thesis addresses the two remaining challenges in this field: the bottleneck between high-capacity LANs and the backbone network and the bottleneck of low-speed electrical signal processing in high-capacity optical networks, to propose some possible novel solutions and discuss their feasibilities in practice from the research perspective.

From a more practical perspective, the further advancement in this field relies on two aspects. One is the boost of broadband “killer application” to increase the demand on bandwidth. Our trial in this aspect is shown in our testbed demonstration of the WDM-based optical broadband access network, where three kinds of real-life emerging broadband services, including HD video streaming, 3D video streaming and real time video conferencing are successfully running over the network testbed. Among them, HD video streaming is a very promising application, which surely will step into our daily lives in the very near future. Real time video communications will find application in video conferencing and video phone, whose main initial customers may be the commercial companies. With the cost reduction of this technology, the average family customers may also be able to enjoy this service in the predictable future.

The other aspect is the photonic devices. In the access region, especially for the WDM-based broadband access network, the cost reduction of the optical components is an important issue for optical technology to compete with other technologies. Currently, much effort has been put on this issue in optical communication industry. To make current optics smarter, all-optical signal processing is a possible direction. The further improvement in this area strongly depends on the development of newly-emerging photonic devices. Our trial in this aspect is shown in our works related to PCF. One of the purposes of these works is to demonstrate the power of new photonic devices when they are combined with the established photonic technologies. However, this is surely not the final solution. Recall the role of transistor in electronic industry. Where is the “transistor” in optics industry? For integrated OEIC, we still have a long way to go.

## **4.3 Suggestions for Future Work**

For future work regarding the broadband access networks, it is interesting to explore how to extend the capability of CWDM technology in this region. In the current work, only 8 CWDM standard wavelengths are used and the data rate is limited to 1.25 Gb/s (GbE standard). In the future work, the entire 18 CWDM wavelengths can be incorporated into to network and some of the channels can be extended for applications in 10 GbE networks, considering that nowadays the 10 GbE transceivers are commercially available in the market. Another possible region for upgrading is the integrating the wireless broadband technologies at the edge of the optical fiber access network to show a more complete broadband access to end users with more flexibility and mobility.

In topics regarding the all-optical nonlinear signal process technologies, the future work can focus on studies at higher data rates. For instance, the polarization-independent NOLM based OTDM demultiplexer can probably operate at higher data rate, such as 80 Gb/s  $\rightarrow$  10 Gb/s, and deserves further experimental studies. The OFSK transmitter can perform a similar extension from 10 Gb/s to 40 Gb/s when the corresponding electronics are available. For the work of polarization-insensitive FWM-based wavelength converter using the small birefringence of PCF, our present experiment proved that it can work on the data rate of 10 Gb/s. However, whether this scheme can work on 40 Gb/s or above has not been addressed yet. It is interesting to confirm this point with more experiments in the future work.

# Bibliography

- [1] K. C. Kao and G. A. Hockham, "Dielectric-fibre surface waveguides for optical frequencies," *Proc. IEE*, vol. 113, pp. 1151-1158, 1966
- [2] F. P. Kapron, D. B. Keck and R. D. Maurer, "Radiation losses in glass optical waveguides," *Appl. Phys. Lett.*, vol. 17, pp. 423-425, 1970
- [3] R. J. Mears, L. Reekie, I. M. Jauncey, and D. N. Payne, "Low-noise Erbium-doped fiber amplifier operating at 1.54  $\mu\text{m}$ ," *Electron. Lett.*, vol. 23, pp. 1026-1028, 1987
- [4] Chinlon Lin and K. L. Deng, "Broadband optical access networks." *IEEE/OSA CLEO-Pacific Rim '01*, Tokyo, 2001, pp. II576-II577
- [5] "Broadband optical access systems based on passive optical networks (PON)," *ITU-T Recommendation G.983.1*, 1998
- [6] "Gigabit-capable Passive Optical Networks (G-PON)," *ITU-T Recommendation G.984*, 2003
- [7] "Ethernet in the first mile," *IEEE Standard 802.3ah*, 2004
- [8] S. Wagner, H. Kobrinski, T. Robe, H. Lemberg, and L. Smoot, "Experimental demonstration of a passive optical subscriber loop architecture," *Electron. Lett.*, vol. 24, pp. 344-346, 1988
- [9] S. Wagner and H. Lemberg, "Technology and system issues for the WDM-based fiber loop architecture," *IEEE J. Lightwave. Technology*, vol. 7, pp. 1759-1768, 1989
- [10] M. Laha, "Coarse WDM opens the road beyond very-short-reach markets," *WDM Solutions*, vol. 3, pp. 37-43, 2001
- [11] P. St. J. Russell, J. C. Knight, T. A. Birks, B. J. Mangan and W. J. Wadsworth, "Photonic Crystal Fibres," *Science*, vol. 299, pp. 358-362, 2003
- [12] N. J. Doran and D. Wood, "Nonlinear-optical loop mirror," *Opt. Lett.*, vol. 13, pp. 56-58, 1988
- [13] G. Kramer and G. Pesavento, "Ethernet Passive Optical Network (EPON): Building a Next-Generation Optical Access Network," *IEEE Communications Magazine*, pp. 66-73, 2000
- [14] C. Su, L. K. Chen and K. W. Cheung, "Theory of burst-mode receiver and its applications on optical multiaccess networks," *IEEE J. Lightwave. Technology*, vol. 15, pp. 590-606, 1997
- [15] M. Zirngibl, C. R. Doerr and L. W. Stulz, "Study of spectral slicing for local access applications," *IEEE Photon. Technol. Lett.*, vol. 8, pp. 721-723, 1996
- [16] D. K. Jung, S. K. Shin, C. H. Lee and Y. C. Chung, "Wavelength-division-multiplexed passive optical network based on spectrum-slicing techniques," *IEEE Photon. Technol. Lett.*, vol. 10, pp. 1334-1336, 1996

- [17] R. D. Feldman, E. E. Harstead, S. Jiang, T. H. Wood and M. Zirngibl, "An evaluation of architectures incorporating wavelength division multiplexing for broad-band fiber access," *IEEE J. Lightwave. Technology*, vol. 16, pp. 1546-1559, 1998
- [18] "Spectral grids for WDM applications: CWDM wavelength grid," *ITU-T Recommendation G.694.2*, 2002
- [19] J. Campbell, "Coarse WDM makes waves in metro/access markets," *Laser Focus World Supplement*, Nov. 2000
- [20] B. R. Eichenbaum, S. K. Das, "Economics for choosing a coarse WDM wavelength grid," *NFOEC '01*, pp. 1444-1448, 2001
- [21] K. Iwatsuki, J. Kani, H. Suzuki and M. Fujiwara, "Access and metro networks based on WDM technologies," *IEEE J. Lightwave. Technology*, vol. 22, pp. 2623-2630, 2004
- [22] K. Iwatsuki and K. Nakagawa, "Suppression of mode partition noise by laser diode light injection," *IEEE J. Quantum Electron.*, vol. 18, pp. 1669-1674, 1982
- [23] N. Frigo, P. P. Iannone, P. D. Magill, T. E. Darcie, M. M. Downs, B. N. Sesai, U. Koren, T. L. Koch, C. Dragone, H. M. Presby, and G. E. Bodeep, "A wavelength-division multiplexed passive optical network with cost-shared components," *IEEE Photon. Technol. Lett.*, vol. 6, pp. 1365-1367, 1994
- [24] M. D. Feur, et al., "Single-port laser-amplifier modulators for local access," *IEEE Photon. Technol. Lett.*, vol. 8, pp. 1175-1177, 1996
- [25] W. Hung, C.K. Chan, L.K. Chen, and F. Tong, "An optical network unit for WDM access networks with downstream DPSK and upstream re-modulated OOK data using injection-locked FP laser," *IEEE Photonic Technol. Lett.*, vol. 15, pp. 1476-1478, 2003.
- [26] W. Hung, N. Deng, C. K. Chan and L. K. Chen, "A novel wavelength shift keying transmitter based on optical phase modulation," *IEEE Photon. Technol. Lett.*, vol. 16, pp. 1739-1741, 2004
- [27] H. D. Kim, S. G. Kang and C. H. Lee, "A low cost WDM source with an ASE injected Fabry-Perot semiconductor laser," *IEEE Photon. Technol. Lett.*, vol. 12, 1067-1069, 2000
- [28] B. Zhang, Chinlon Lin, L. Huo, Z.X. Wang and C.K. Chan; "A simple high-speed WDM-PON utilizing a centralized supercontinuum broadband light source for colorless ONUs," *OFC '06*, Anaheim, 2006, Paper OTuC6
- [29] [http://lw.pennnet.com/Articles/ArticleDisplay.cfm?ARTICLE\\_ID=224875&p=13&pc=ENL](http://lw.pennnet.com/Articles/ArticleDisplay.cfm?ARTICLE_ID=224875&p=13&pc=ENL)
- [30] V. O'Byrne, "Verizon's fiber to the premises: lessons learned", *OFC '05*, Anaheim, 2005, OWP6
- [31] "Today's broadband fiber access technologies and deployment considerations at SBC," Chapter 2, in *Broadband Optical Access Networks and Fiber-to-the-Home*. Chinlon Lin (ed.), John Wiley and Sons, U. K., June 2006.
- [32] H. Shinohara, "Broadband expansion in Japan," *OFC '05*, Anaheim, 2005, Plenary Talk

- [33] T. J. Chan, C. K. Chan, L. K. Chen and F. Tong, "A self-protected architecture for wavelength-division-multiplexed passive optical networks," *IEEE Photon. Technol. Lett.*, vol. 15, pp. 1660-1662, 2003
- [34] C. M. Lee, T. J. Chan, C. K. Chan, L. K. Chen and C. Lin, "A group protection architecture (GPA) for traffic restoration in multi-wavelength passive optical network," *ECOC '03*, Rimini, 2003, paper Th2.4.2
- [35] Chinlon Lin, H. Kobrinski, A. Frenkel and C. A. Brackett, "A tunable 16 optical channel transmission/distribution experiment at 2 Gb/s and 600 Mb/s for broadband subscriber distribution", *ECOC '88*, vol. 1, pp. 251 – 254, 1988
- [36] J. Grubor, M. Schlosser and K. D. Langer, "Protected ring network in optical access domain", *NOC '04*, Eindhoven, 2004
- [37] T. Zami, F. Dorgeuille, L. Noirie, N. Sauze and A. Jourdan, "Optical metro-access ring featuring a flexible color management", *OFC '04*, Los Angeles, 2004, Paper WG6
- [38] Y. Shen, X. Wu, C. Lu, T. H. Cheng, and M. K. Rao, "A novel single-fiber bidirectional optical add/drop multiplexer for distribution networks", *OFC '01*, Anaheim, 2001, paper WY5
- [39] S. B. Park, C. H. Lee, S. G. Kang, and S. B. Lee, "Bidirectional WDM self-healing ring network for Hub/Remote nodes", *IEEE Photon. Technol. Lett.*, vol.15, pp. 1657-1659, 2003
- [40] I. Sankawa, "Fault location technique for in-service branched optical fiber networks," *IEEE Photon. Technol. Lett.*, vol. 2, pp. 766-768, 1990
- [41] Y. Koyamada, T.K. Horiguchi, and S. Furukawa, "Recent progress in OTDR technologies for maintaining optical fiber networks," in *Tech. Dig., IOOC ' 95*, Hong Kong, 1995, paper FA1-4
- [42] C. K. Chan, F. Tong, L. K. Chen, J. Song and D. Lam, "A practical passive surveillance scheme for optically amplified passive branched optical networks," *IEEE Photon. Technol. Lett.*, vol. 9, pp. 526-528, 1997
- [43] K. Chan, C. K. Chan, F. Tong and L. K. Chen, "Performance supervision for multiple optical amplifiers in WDM Transmission systems using spectral analysis," *IEEE Photon. Technol. Lett.*, vol. 14, pp. 705-707, 2002
- [44] M. E. Fermann, F. Haberl, M. Hofer and H. Hochreiter, "Nonlinear amplifying loop mirror." *Opt. Lett.*, vol. 15, pp. 752-754, 1990
- [45] W. S. Wong, S. Namiki, M. Margalit, H. A. Haus, and E. P. Ippen, "Self-switching of optical pulses in dispersion-imbalanced nonlinear loop mirrors," *Opt. Lett.*, vol. 22, pp. 1150-1152, 1997
- [46] M. N. Islam, E. R. Sunderman, R. H. Stolen, W. Pleibel and J. R. Simpson. "Soliton switching in a fiber nonlinear loop mirror," *Opt. Lett.*, vol. 14, pp. 811-813, 1989
- [47] B. E. Olsson and P. A. Andrekson, "Noise filtering with the nonlinear optical loop mirror," *IEEE J. Lightwave. Technology*, vol. 13, pp. 213-215, 1995

- [48] A. Bogoni, P. Ghelfi, M. Scaffardi and L. Poti, "All-optical regeneration and demultiplexing for 160-gb/s transmission systems using a NOLM-based three-stage scheme," *IEEE J. Selected Topics in Quantum. Electron.*, vol. 10, pp. 192-196, 2004
- [49] K. Smith, N. J. Doran and P. G. J. Wigley, "Pulse shaping, compression, and pedestal suppression employing a nonlinear-optical loop mirror," *Opt. Lett.*, vol. 15, pp. 1294-1296, 1990
- [50] I. N. Duling III, "All-fiber ring soliton laser mode locked with a nonlinear mirror," *Opt. Lett.*, vol. 16, pp. 539-541, 1991
- [51] K. J. Blow, N. J. Doran, B. K. Nayar and B. P. Nelson, "Two-wavelength operation of the nonlinear fiber loop mirror," *Opt. Lett.*, vol. 15, pp. 248-251, 1990
- [52] P. A. Andrekson, N. A. Olsson, J. R. Simpson, D. J. Digiovanni, P. A. Morton, T. Tanbun-Ek, R. A. Logan and K. W. Wecht, "64 Gb/s all-optical demultiplexing with the nonlinear optical-loop mirror," *IEEE Photon. Technol. Lett.*, vol. 4, pp. 644-647, 1992
- [53] T. Sakamoto, F. Futami, K. Kikuchi, S. Takeda, Y. Sugaya and S. Watanabe, "All-optical wavelength conversion of 500-fs pulse trains by using a nonlinear-optical loop mirror composed of a highly nonlinear DSF," *IEEE Photon. Technol. Lett.*, vol. 13, pp. 502-504, 2001
- [54] S. Bigo, E. Desurvire and B. Desruelle, "All-optical RZ-to-NRZ format conversion at 10Gbit/s with nonlinear optical loop mirror," *Electron. Lett.*, vol. 30, pp. 1868-1870, 1994
- [55] G. R. Williams, M. Vaziri, K. H. Ahn, B. C. Barnett, M. N. Islam, K. O. Hill and B. Malo, "Soliton logic gate using low-birefringence fiber in a nonlinear loop mirror," *Opt. Lett.*, vol. 20, pp. 1671-1673, 1995
- [56] A. Bogoni, L. Poti, R. Proietti, G. Meloni, F. Ponzini and P. Ghelfi, "Regenerative and reconfigurable all-optical logic gates for ultra-fast applications," *Electron. Lett.*, vol. 41, pp. 435-436, 2005
- [57] J. P. Sokoloff, P. R. Prucnal, I. Glesk and M. Kane, "A terahertz optical asymmetric demultiplexer (TOAD)," *IEEE Photon. Technol. Lett.*, vol. 5, pp. 787-790, 1993
- [58] K. Uchiyama, H. Takara, S. Kawanishi, T. Morioka and M. Saruwatari, "Ultrafast polarisation-independent all-optical switching using a polarisation diversity scheme in the nonlinear optical loop mirror," *Electron. Lett.*, vol. 28, pp. 1864-1866, 1992
- [59] J. W. Lou, J. K. Andersen, J. C. Stocker, M. N. Islam and D. A. Nolan, "Polarization insensitive demultiplexing of 100-Gbs words using a twisted fiber nonlinear optical loop mirror," *IEEE Photon. Technol. Lett.*, vol. 11, pp. 1602-1604, 1999
- [60] B. E. Olsson and P. A. Andrekson, "Polarization independent demultiplexing in a polarization diversity nonlinear optical loop mirror," *IEEE Photon. Technol. Lett.*, vol. 9, pp. 764-766, 1997

- [61] H. C. Lim, T. Sakamoto and K. Kikuchi, "Polarization-independent optical demultiplexing by conventional nonlinear optical loop mirror in a polarization-diversity loop configuration," *IEEE Photon. Technol. Lett.*, vol. 12, pp. 1704-1706, 2000
- [62] T. Sakamoto, H. C. Lim and K. Kikuchi, "All-optical polarization-insensitive time-division demultiplexer using a nonlinear optical loop mirror with a pair of short polarization-maintaining fibers," *IEEE Photon. Technol. Lett.*, vol. 14, pp. 1737-1739, 2002
- [63] J. Mo, Y. Dong, Y. Wen, S. Takahashi, Y. Wang and C. Lu, "Optical minimum-shift keying modulator for high spectral efficiency WDM systems", *ECOC '05*, Glasgow, UK, 2005, paper 1. 2. 3
- [64] J. Zhang, N. Chi, P. Holm-Nielson, C. Peucheret and P. Jeppeson, "A novel optical labeling scheme using a FSK modulated DFB laser integrated with an EA modulator," *OFC '03*, Atlanta, 2003, paper TuQ5
- [65] W. Hung, N. Deng, C. K. Chan and L. K. Chen, "A novel wavelength shift keying transmitter based on optical phase modulation," *IEEE Photon. Technol. Lett.*, Vol. 16, pp. 1739-1741, 2004
- [66] S. S. Pun, C. K. Chan and L. K. Chen, "A novel optical frequency shift keying transmitter based on polarization modulation," *IEEE Photon. Technol. Lett.*, Vol. 17, pp. 1528-1530, 2005
- [67] A. Klekamp, W. Idler and R. Dischler, "Comparison of FSK by directly modulated DFB laser with DPSK, NRZ and RZ modulation formats at 10 Gb/s," *ECOC '03*, Rimini, Italy, 2003, paper We4. P. 118
- [68] E. Yablonovitch, "Inhibited spontaneous emission in solid-state physics and electronics," *Physical Rev. Lett.*, vol. 58, pp. 2059-2062, 1987
- [69] J. C. Knight, T. A. Birks, P. St. J. Russell and D. M. Atkin, "All-silica single-mode optical fiber with photonic crystal cladding," *Opt. Lett.*, vol. 21, pp. 1547-1549, 1996
- [70] T. A. Birks, J. C. Knight and P. St. J. Russell, "Endlessly single-mode photonic crystal fiber," *Opt. Lett.*, vol. 22, pp. 961-963, 1997
- [71] <http://www.crystal-fibre.com/>
- [72] M. J. Gander, R. McBride, J. D. C. Jones, D. Mogilevtsev, T. A. Birks, J. C. Knight and P. St. J. Russell, "Experimental measurement of group velocity dispersion in photonic crystal fiber," *Electron. Lett.*, vol. 35, pp. 63-64, 1999
- [73] P. Petropoulos, T. M. Monro, W. Belardi, K. Furusawa, J. H. Lee and D. J. Richardson, "2R-regenerative all-optical switch based on a highly nonlinear holey fiber," *Opt. Lett.*, vol. 26, pp. 1233-1235, 2001
- [74] J. H. Lee, Z. Yusoff, W. Belardi, M. Ibsen, T. M. Monro and D. J. Richardson. "A tunable WDM wavelength converter based on cross-phase modulation effects in normal dispersion holey fiber," *IEEE Photon. Technol. Lett.*, Vol. 15, pp. 437-439, 2003
- [75] J. H. Lee, W. Belardi, K. Furusawa, P. Petropoulos, Z. Yusoff, T. M. Monro and D. J.

- Richardson, "Four-wave mixing based 10-gb/s tunable wavelength conversion using a holey fiber with a high SBS threshold," *IEEE Photon. Technol. Lett.*, Vol. 15, pp. 440-442, 2003
- [76] J. K. Ranka, R. S. Windeler and A. J. Stentz, "Visible continuum generation in air-silica microstructure optical fibers with anomalous dispersion at 800 nm," *Opt. Lett.*, vol. 25, pp. 25-27, 2000
- [77] J. C. Knight, J. Broeng, T. A. Birks and P. St. J. Russell, "Photonic band gap guidance in optical fibers," *Science*, vol. 282, pp. 1476-1478, 1998
- [78] R. F. Cregan, B. J. Mangan, J. C. Knight, T. A. Birks, P. St. J. Russell, P. J. Roberts and D. C. Allan, "Single-mode photonic band gap guidance of light in air," *Science*, vol. 285, pp. 1537-1539, 1999
- [79] K. Kurokawa, K. Tajima, J. Zhou, K. Nakajima, T. Matsui and I. Sankawa, "Penalty-free dispersion-managed soliton transmission over 100 km low loss PCF," *OFC'05*, Anaheim, 2005, paper PDP21
- [80] E. L. Goldstein, L. Eskildsen and A.F. Elrefaie, "Performance implications of component crosstalk in transparent lightwave networks," *IEEE Photon. Technol. Lett.*, vol. 6, pp. 657-659, 1994
- [81] Y. J. Chai, I. Y. Khrushchev and I. H. White, "Nonlinear suppression of incoherent interferometric crosstalk using dispersion-imbalanced loop mirror," *Electron. Lett.*, vol. 36, pp. 1565-1166, 2000
- [82] Y. J. Chai, I. Y. Khrushchev, R. V. Penty and I. H. White, "Interferometric noise suppression by means of dispersion-imbalanced loop mirror over a wavelength range of 28nm," *IEEE Photon. Technol. Lett.*, vol.14, pp. 417-419, 2002
- [83] B. E. Olsson and D. J. Blumenthal, "Pulse restoration by filtering of self-phase modulation broadened optical spectrum," *IEEE J. Lightwave Technol.*, vol.20, pp. 1113-1117, 2002
- [84] J. Hiroishi, N. Kumano, K. Mukasa, R. Sugizaki, R. Miyabe, S. Matsushita, H. Tobioka, S. Namiki and T. Yagi, "Dispersion slope controlled HNL-DSF with high  $\gamma$  of  $25 \text{ W}^{-1}\text{km}^{-1}$  and band conversion experiment using this fiber," *ECOC'02*, Copenhagen, Denmark. 2002, paper PD1.5
- [85] K. P. Hansen, J. R. Folkenberg, C. Percheret and A. Bjarklev, "Fully dispersion controlled triangular-core nonlinear photonic crystal fiber," *OFC'03*, Atlanta, 2003, paper PD2-1
- [86] W. S. Wong, P. B. Hansen, T. N. Nielsen, M. Margalit, S. Namiki, E. P. Ippen and H. A. Haus, "In-band amplified spontaneous emission noise filtering with a dispersion-imbalanced nonlinear loop mirror," *J. Lightwave. Technology*, vol. 16, pp.1768-1772, 1998
- [87] O. Leclerc, B. Lavigne, E. Balmeffre, P. Brindel, L. Pierre, D. Rouvillain and F. Segueineau, "Optical regeneration at 40Gb/s and beyond (invited)," *J. Lightwave. Technology*, vol. 21, pp.2779-2790, 2003
- [88] C. H. Kwok, S. H. Lee, K. K. Chow, C. Shu, Chinlon Lin and A. Bjarklev, "Widely tunable wavelength conversion with extinction ratio enhancement using PCF-based NOLM," *IEEE*

- Photon.Technol. Lett.*, vol.17, pp. 2655-2657, 2005
- [89] K. K. Chow, C. Shu, Chinlon Lin and A. Bjarklev, "Polarization-insensitive widely tunable wavelength converter based on four-wave mixing in a dispersion-flattened nonlinear photonic crystal fiber," *IEEE Photon.Technol. Lett.*, vol.17, pp. 624-626, 2005
- [90] K. Inoue, "Polarization independent wavelength conversion using fiber four-wave mixing with two orthogonal pump lights of different frequencies," *J. Lightwave. Technology*, vol. 12, pp.1916-1920, 1994
- [91] K. Inoue, "Polarization effect on four-wave mixing efficiency in a single-mode fiber," *J. Quantum. Electronics*, vol. 28, pp.883-894, 1992

# List of Publications

## Journal papers:

- 1 **Z. X. Wang**, Chinlon Lin and C. K. Chan, "Demonstration of a Single-Fiber Self-Healing CWDM Metro Access Ring Network with Uni-directional OADM"; *Photonics Technology Letters*, vol. 18, no. 1, pp. 163-165, Jan. 2006.
- 2 **Z. X. Wang**, Chinlon Lin, K. K. Chow, Y. C. Ku and A. Bjarklev, "Wavelength-Tunable Dispersion-Imbalanced Loop Mirror Based on Dispersion-Flattened High-Nonlinearity Photonic Crystal Fiber and Its Application in Suppression of the Incoherent Interferometric Crosstalk", *Photonics Technology Letters*, vol. 17, no. 9, Sep. 2005.
- 3 **Z. X. Wang**, X. F. Sun, Chinlon Lin, C. K. Chan and L. K. Chen, "A Novel Centrally Controlled Protection Scheme for Traffic Restoration in WDM Passive Optical Networks". *Photonics Technology Letters*, vol. 17, pp. 717-719, 2005.

## Conference papers:

- 1 **Z. X. Wang**, N. Deng, Chinlon Lin, C. K. Chan, "Polarization-Insensitive Widely Tunable Wavelength Conversion Based on Four-Wave Mixing Using Dispersion-Flattened High-Nonlinearity Photonic Crystal Fiber with Residual Birefringence", *ECOC 2006*, We3.P.18, Cannes, France, Sep. 2006.
- 2 **Z. X. Wang**, Chinlon Lin and C. K. Chan, "A Single-Fiber Self-Healing CWDM Metro Access Ring Network for Broadcast and Dedicated Broadband Services", *OECC 2006*, Paper 5E3-1, Kaohsiung, Taiwan, Jul. 2006.
- 3 **Z. X. Wang**, C. K. Chan and Chinlon Lin, "A Novel Optical Frequency-Shift-Keying Transmitter Using Phase Modulator-Embedded Optical Loop Mirror", *CLEO 2006*, Paper JThC80, Long Beach, California, United States, May. 2006.
- 4 **Z. X. Wang**, L. Huo, Chinlon Lin and C. K. Chan, "Polarization-Independent OTDM Demultiplexer Based on a NOLM with a Polarization Diversity Loop", *OFC 2006*, Paper OWI14, Anaheim, California, United States, Mar. 2006.
- 5 **Z. X. Wang**, B. Zhang, Chinlon Lin and C. K. Chan, "A Broadcast and Select WDM-PON and its Protection", *ECOC 2005*, Paper We4.P.24, Glasgow, United Kingdom, Sep. 2005.
- 6 **Z. X. Wang**, Chinlon Lin, K. K. Chow, Y. C. Ku and A. Bjarklev, "Nonlinear Suppression of Incoherent Interferometric Crosstalk with Dispersion Imbalanced Loop Mirror Using Dispersion-Flattened High-Nonlinearity Photonic Crystal Fiber", *CLEO 2005*, JThE43, Baltimore, Maryland, United States, May. 2005.
- 7 **Z. X. Wang**, Chinlon Lin and C. K. Chan, "A Simple Single-Fiber CWDM Metro/Access Ring Network with Unidirectional OADM and Automatic Protection", *OFC 2005*, OFA2, Anaheim, California, United States, Mar. 2005.

- 8 **Z. X. Wang**, X. F. Sun, Chinlon Lin, C. K. Chan and L. K. Chen, "A Novel Centrally Controlled Protection Architecture for Bidirectional WDM Passive Optical Network", *ECOC 2004*, Tu1.6.2, Stockholm, Sweden, Sep. 2004.
- 9 **Z. X. Wang**, X. F. Sun, Chinlon Lin, C. K. Chan and L. K. Chen, "A Novel Surveillance Scheme for Passive Optical Networks Using Spectral Analysis", *ECOC 2004*, We4.P.142, Stockholm, Sweden, Sep. 2004.
- 10 L. Huo, J. Zhao, Chinlon Lin, C. K. Chan and **Z. X. Wang**, "Demonstration of an Optical Frequency-Hopping Scheme for Secure Communications", *CLEO 2006*, Paper CWQ4, Long Beach, California, United States, May. 2006.
- 11 B. Zhang, Chinlon Lin, L. Huo, **Z. X. Wang** and C.K. Chan, "A Simple High-Speed WDM PON Utilizing a Centralized Supercontinuum Broadband Light Source for Colorless ONUs". *OFC 2006*, Paper OTuC6, Anaheim, California, United States, Mar. 2006.
- 12 X. F. Sun, **Z. X. Wang**, C. K. Chan, Chinlon Lin, L. K. Chen, "A Single-Fiber Bi-directional Self-Healing WDM Metro-Ring Network with Bi-directional OADM", *ECOC 2005*, Paper We4.P.41, Glasgow, United Kingdom, Sep. 2005.

# Appendix – Testbed Equipments and Results

## A. Building Blocks Demonstration

### 1. Hub

Fig A.1 shows the setup at the Hub, which includes one rack, two projectors and one specially designed screen for 3D display. Fig A.2 shows the configuration inside the rack.

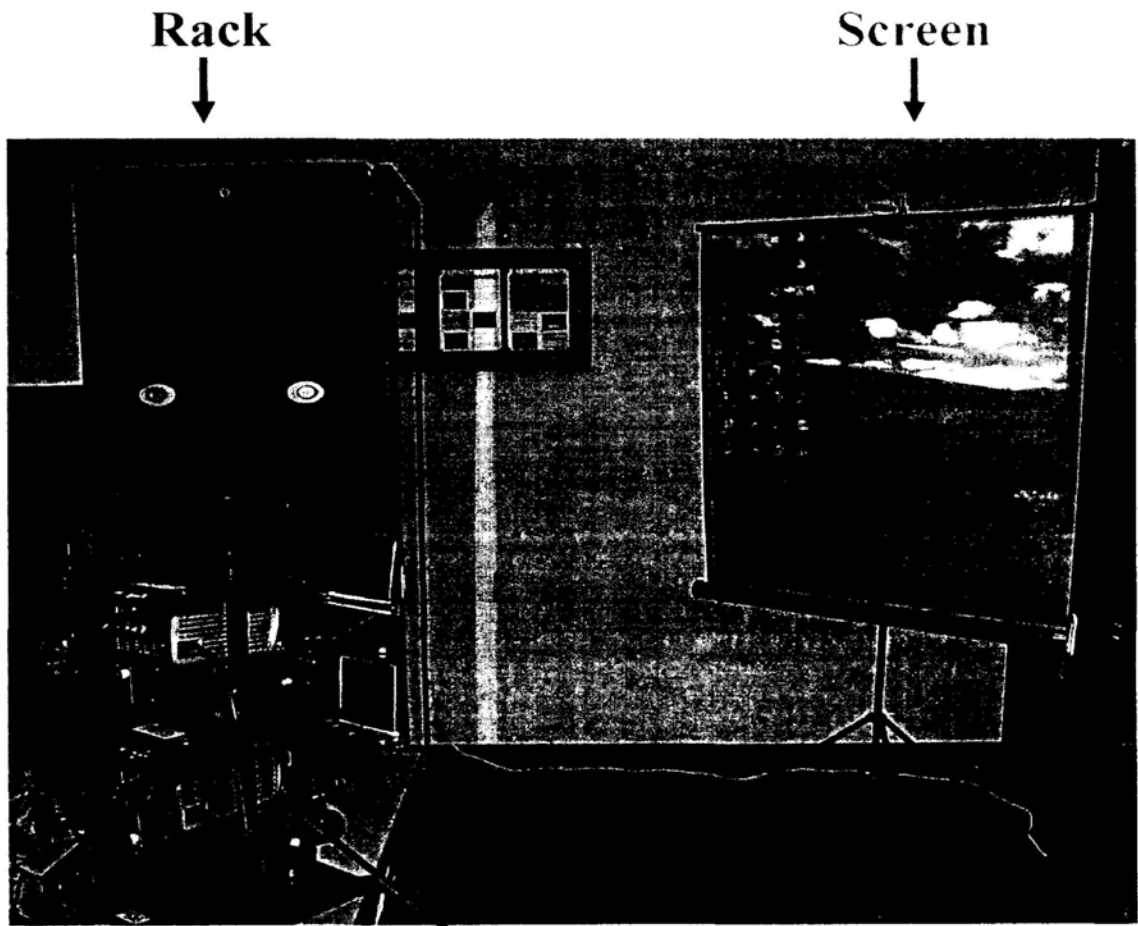
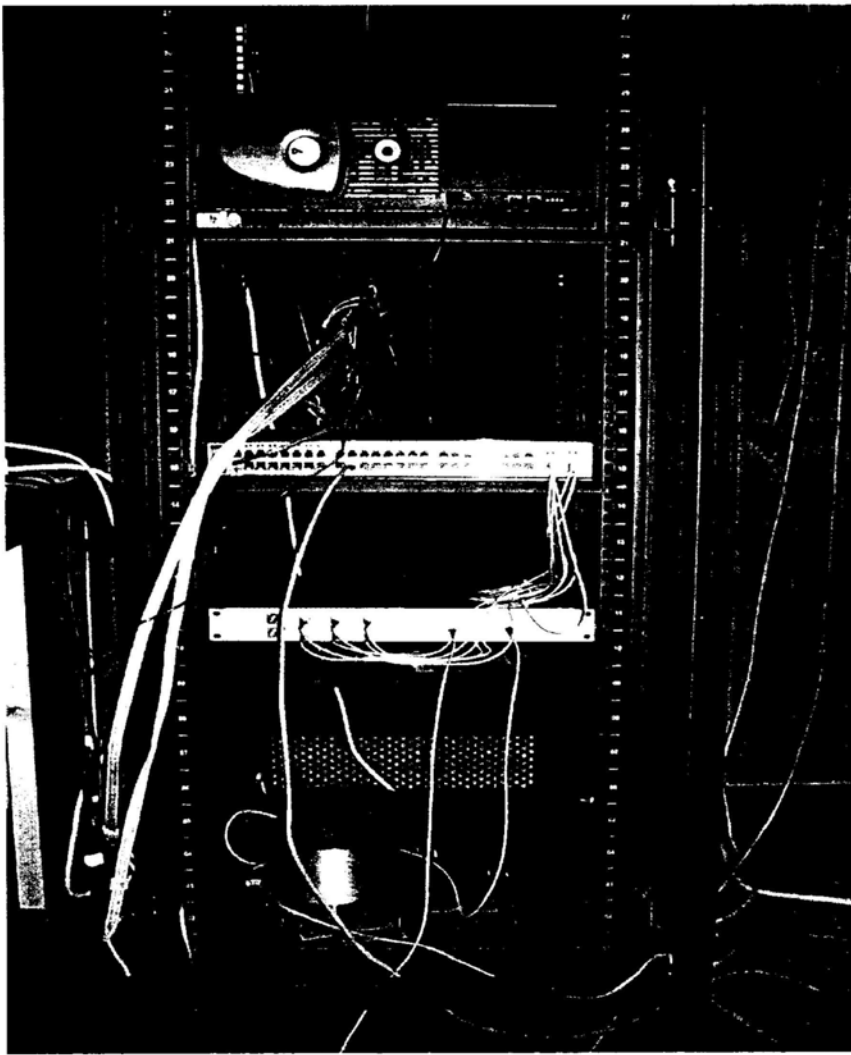


Fig A.1 Setup at the Hub

Projectors



**Work Station**

**Cisco Switch**

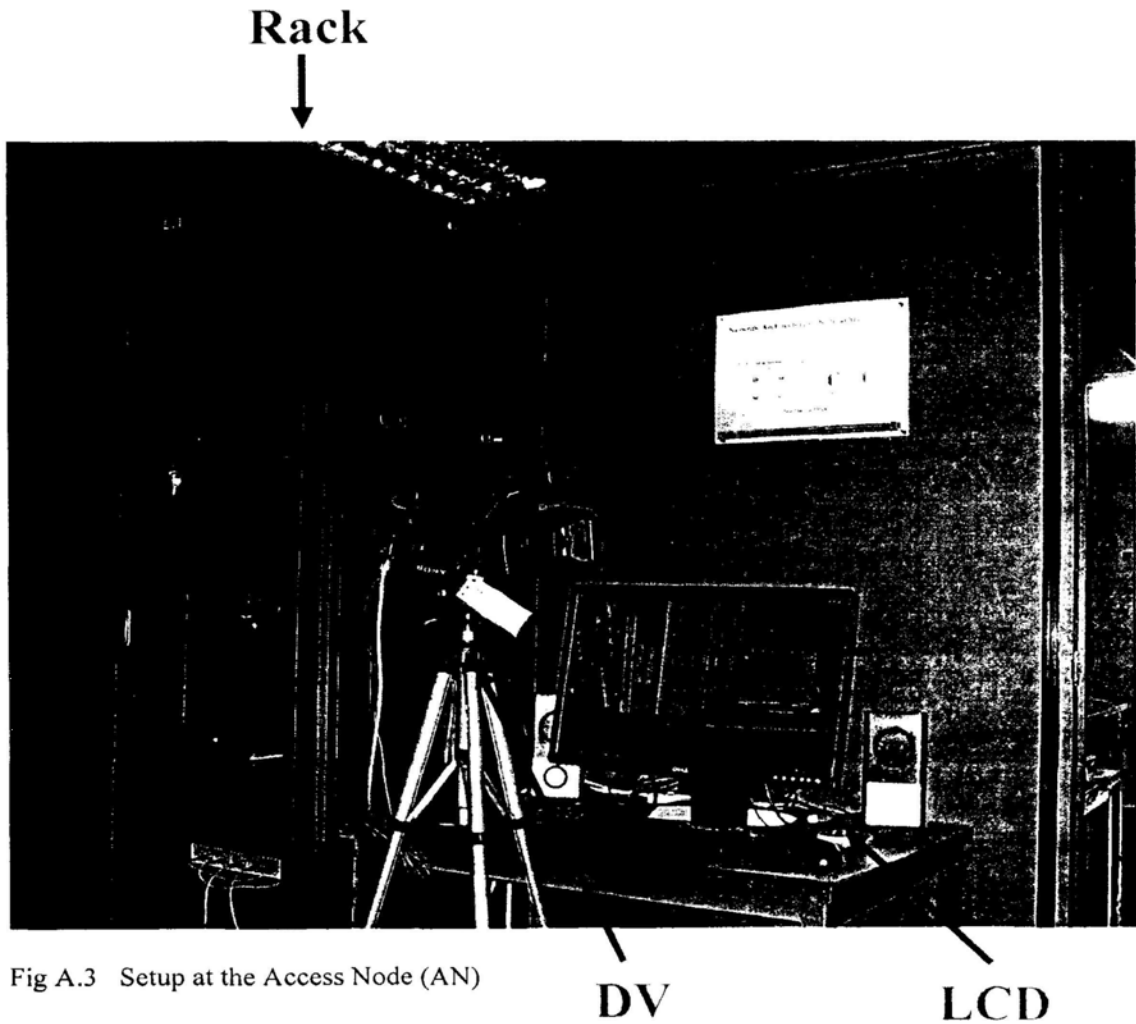
**Self-made Package**

**Fiber**

Fig A.2 Configuration inside the rack at the Hub

2. Access Node (AN)

Fig A.3 shows the setup of the Access Node (AN), which includes one rack, one 24" wide screen LCD and digital video camera. Fig A.4 shows the configuration inside the rack.



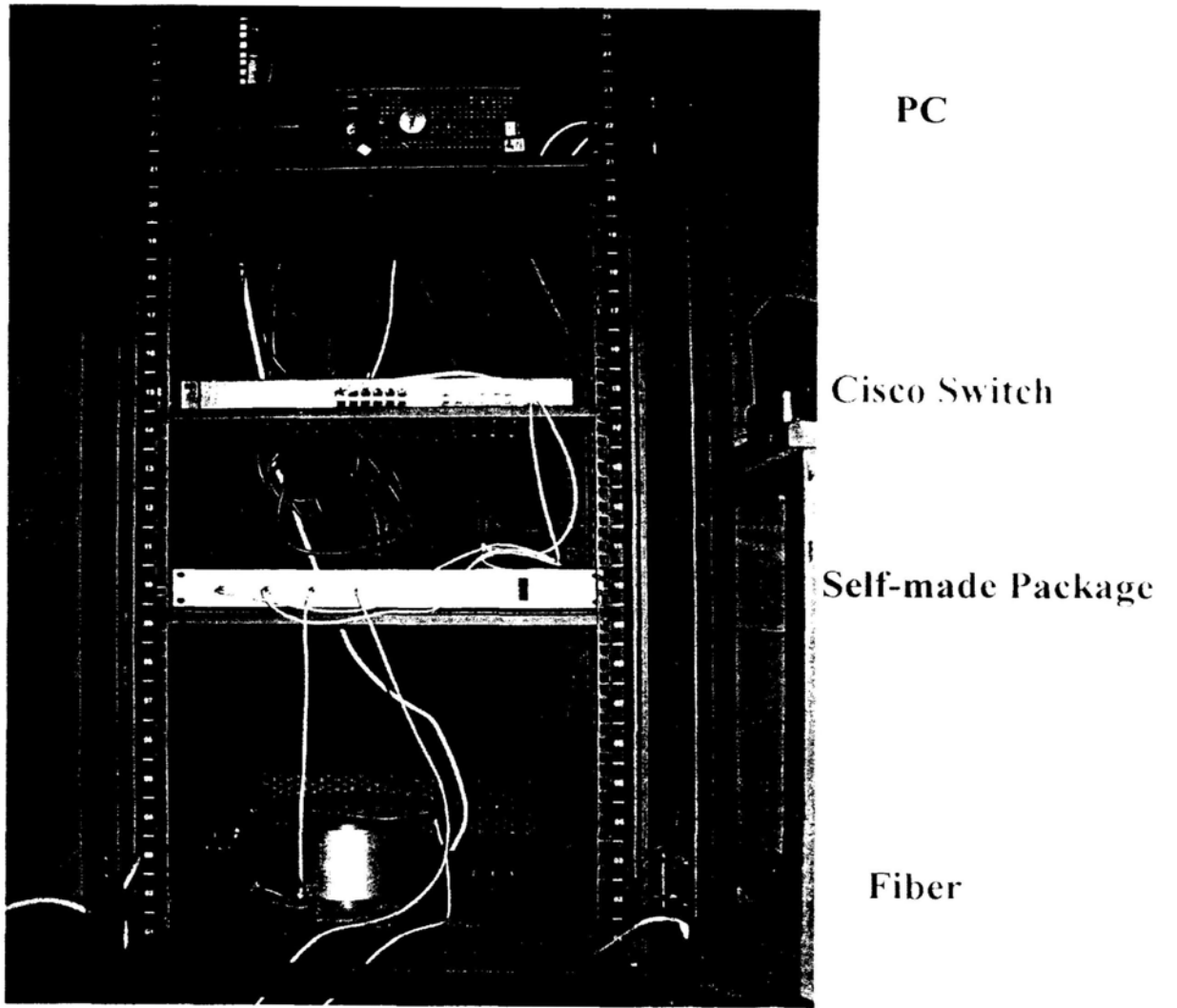


Fig A.4 Configuration inside the rack at the Hub

## B. Broadband Service Demonstration

1. HD video streaming (Fig A.5)

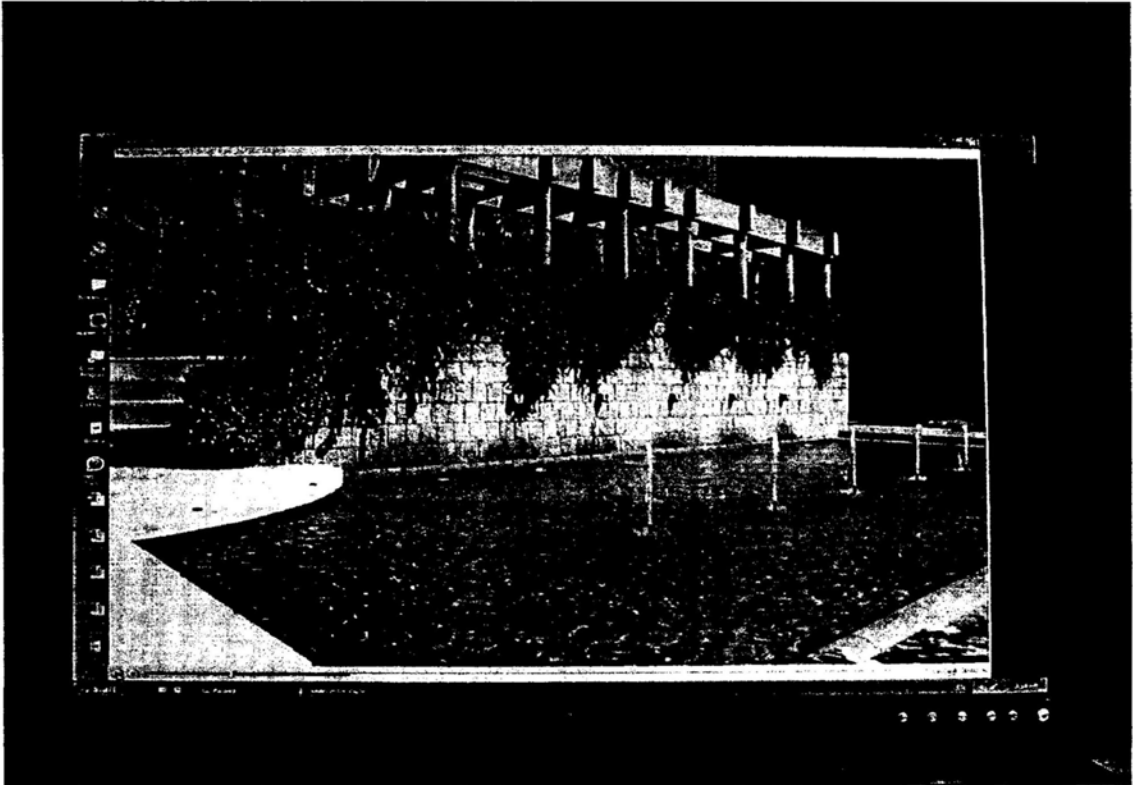


Fig A.5 Screen display of the HD video streaming

2. 3D video streaming(Fig A.6)

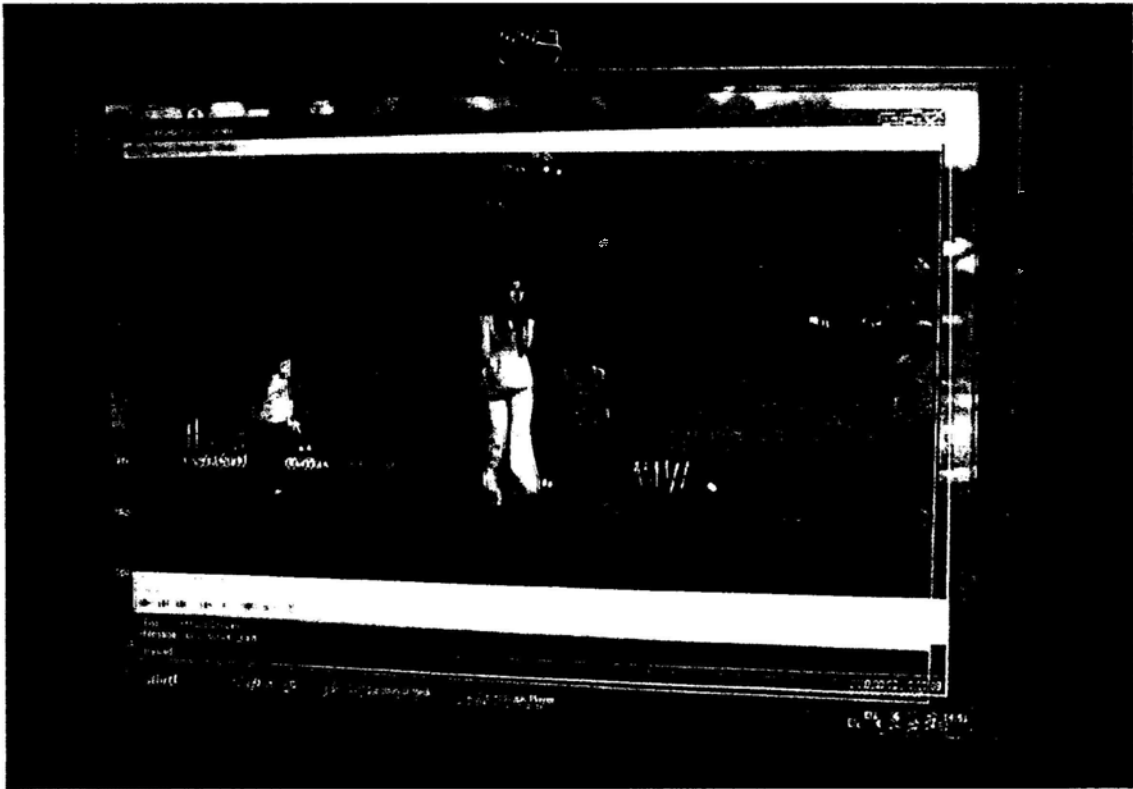


Fig A.6 Screen display of the 3D video streaming

3. Real-time video conferencing (Fig A.7)

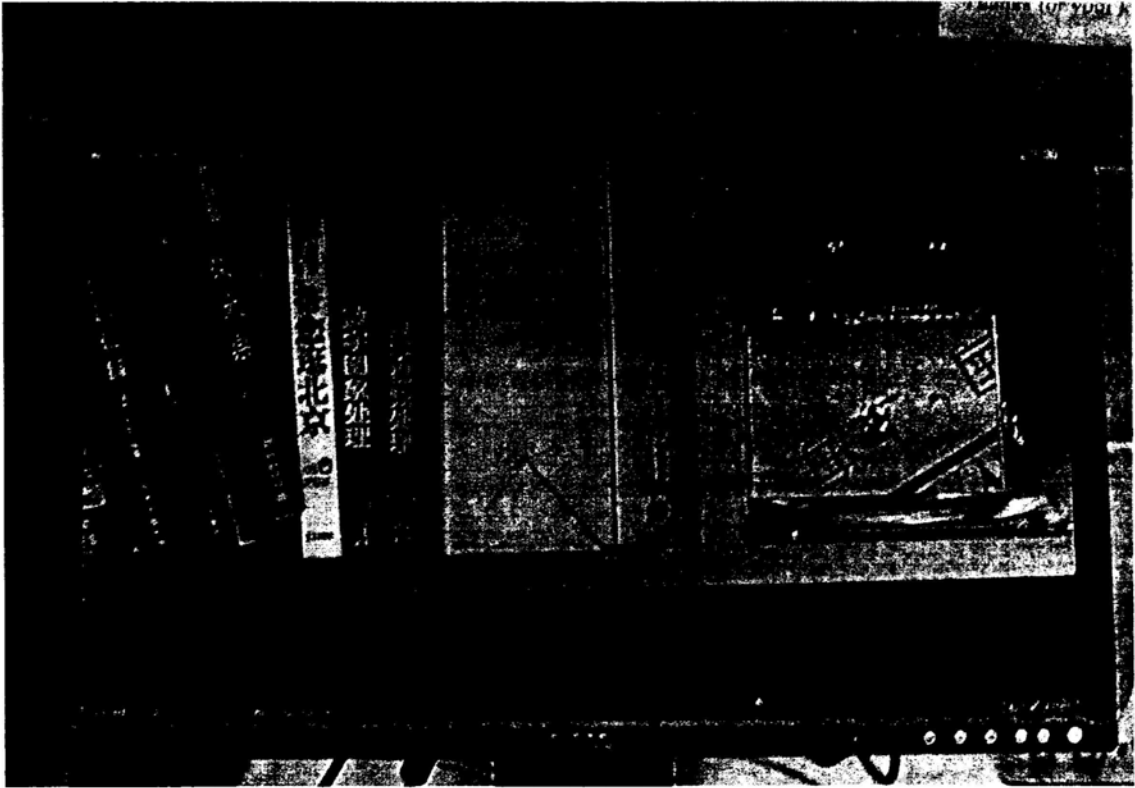


Fig A.7 Screen display of the real-time video streaming